Hall of Fame Article



# A Review of Femtosecond-Laser-Induced Underwater **Superoleophobic Surfaces**

Jiale Yong, Feng Chen,\* Qing Yang, Zhuangde Jiang, and Xun Hou

Underwater superoleophobic surfaces have attracted increasing interest because of their remarkable antioil ability and wide range of promising applications. In the meantime, femtosecond laser microfabrication becomes a rising star in the field of micro/nanomanufacturing based on the advantages of negligible heat-affected zone, no-contact process, precise ablation threshold, and high resolution. The collision of femtosecond laser microfabrication and achieving underwater superoleophobicity finally produces some colorful fireworks. In this review, the recent progress of femtosecond-laser-induced underwater superoleophobic surfaces, mainly including materials, fabrication, properties, multifunctions, and applications, is summarized. The related background is first introduced to show the principle for creating an underwater superoleophobic surface and the unique features of femtosecond laser. Based on the principle of "from in-air superhydrophilicity to underwater superoleophobicity," underwater superoleophobicity is achieved on different kinds of materials surfaces by simple femtosecond laser ablation. Furthermore, the femtosecond-laserinduced underwater superoleophobic surfaces can also be endowed with some additional properties such as controllable oil adhesion, underwater anisotropic oil wettability, good transparency, and durability, leading to the resultant surfaces that have various practical applications. The development of underwater superoleophobicity is still in its "toddler stage," so the existing challenges and future prospects of this growing field are discussed finally.

1. Introduction

Wettability is one of the most basic properties of solid surfaces, mainly depending on the surface chemical composition and structures.[1-12] Particularly, the materials showing superwettability are most captivating for their significance in bionics, fundamental research, and practical applications.<sup>[1-5]</sup> Superhydrophobic surface is the earliest and the most widely studied interface in the field of superwettability because of its

repellence.[1,9,13-18] remarkable water Inspired by the superhydrophobicity of lotus leaf, thousands of artificial superhydrophobic surfaces have been fabricated, and those surfaces are wildly applied in self-cleaning coatings, [13,19–21] microdroplets manipulation, [22–25] oil/water separation, [26–30] anticorrosion, [31] antifog/ ice/snow,[32-35] drag reduction,[36-39] antifouling,<sup>[40]</sup> cell engineering,<sup>[21,41–43]</sup> water collection. [44–46] microfluidics. [47–50] lab chips,[51-54] etc. After more than 20 years of development, both the basic theory and the fabrication technologies for superhydrophobic surfaces have reached a high level. Thus, in recent years, the interests of researchers are gradually shifting to the liquid object of oil which is another common liquid in our daily life.[2,6,55] Following the same principle of superhydrophobicity, superoleophobicity can be defined as a small oil droplet showing an oil contact angle (OCA) larger than 150° on a substrate surface. [2,6,55,56] Superoleophobic surfaces that cannot be wetted by organic liquids are harder to be fabricated than superhydrophobic surfaces, mainly because the surface tensions of oils are much lower than that of water.<sup>[57–62]</sup> In 2007, Tuteja et al. revealed that the reentrant microstructure

is very important for preparing a superoleophobic surface in air, beyond the sufficient roughness and the rigorous chemical modification with ultralow surface-free-energy materials. [63] The reentrant surface curvature generally refers to the overhang, mushroom-like, inverted trapezoid microstructures, and so on. [6,61,63-72] Although the development of the superoleophobicity has been accelerated by the concept of reentrant texture, the fabrication of in-air superoleophobic surfaces is still restricted by the difficulty of creating reentrant microstructures until now.<sup>[2,55]</sup>

Dr. J. Yong, Prof. F. Chen, Prof. X. Hou State Key Laboratory for Manufacturing System Engineering and Key Laboratory of Photonics Technology for Information of Shaanxi Province School of Electronics and Information Engineering Xi'an Jiaotong University Xi'an 710049, P. R. China E-mail: chenfeng@mail.xjtu.edu.cn

The ORCID identification number(s) for the author(s) of this article can be found under https://doi.org/10.1002/admi.201701370.

Dr. J. Yong, Prof. F. Chen, Prof. Q. Yang, Prof. Z. Jiang The International Joint Research Center for Micro/Nano Manufacturing and Measurement Technologies Xi'an Jiaotong University Xi'an 710049, P. R. China Prof. Q. Yang, Prof. Z. Jiang School of Mechanical Engineering Xi'an Jiaotong University Xi'an 710049, P. R. China

DOI: 10.1002/admi.201701370

www.advancedsciencenews.com



www.advmatinterfaces.de

Fish can swim freely even in oil-polluted water without any contamination on its skin. In 2009, Jiang and co-workers revealed that such antioil-pollution ability is caused by the unique underwater superoleophobicity of fish scales.<sup>[73]</sup> In addition, the underwater superoleophobicity is ascribed to the synergy between the hydrophilic chemistry and the hierarchical rough surface microstructures of the fish scales. This finding has opened up an important alternative path to prepare underwater superoleophobic surfaces. Inspired by the underwater superoleophobicity of fish scales, various technologies have been developed to fabricate underwater superoleophobic surfaces following the design principle of "from in-air superhydrophilicity to underwater superoleophobicity," such as lithography,<sup>[73–75]</sup> templating,<sup>[73,76,77]</sup> chemical etching,<sup>[75,78–82]</sup> hydrothermal method, [83] self-assembly, [60,84,85] electrochemical deposition, [86-91] electrochemical anodization, [92] and spray/ dip coating. [93-97] The same as the superhydrophobic surfaces, the artificial underwater superoleophobic surfaces have also attracted much attention recently owning to their significant applications in antioil coatings, [73,82,98] oil/water separation, [26-30] manipulation of oil microdroplets, [84,88,98-101] selfcleaning, [74,88] bioadhesion, [102] antiblocking, [74,103] guiding the movement of oil droplets,[101,104] floating on oil,[79] and oil droplets patterning. [105] Underwater superoleophobic surfaces can be successfully prepared by the above-mentioned traditional methods, but those methods, more or less, have to face their inherent limitations, such as complex fabrication process, tight restriction on special materials, and lack flexibility. The fabrication of underwater superoleophobic surfaces through a versatile and simple way is still the major trend in this research field.

In recent years, the technology of femtosecond laser microfabrication has been successfully applied in the interface science to control the liquid wettability of material surfaces. [8,10,65,99,103,106–110] Such micromachining technology has many unique features, including negligible heat-affected zone, no-contact process, precise ablation threshold, and high resolution. [111–114] Furthermore, this technology can process a very wide range of materials, e.g., semiconductors, glasses, metals, polymers, ceramics, and even biological tissues. [111–114] Based on the above advantages, this technology has also been a great success in achieving basic and functional underwater superoleophobicity.

This review will focus on the recent developments in underwater superoleophobic surfaces that are prepared by femtosecond laser micro/nanofabrication. The article starts with a presentation of the related background including the organisms with underwater superoleophobicity, the theoretical basis of wettability, and a brief introduction of femtosecond laser microfabrication (Section 2). Then, different femtosecond-laserinduced underwater superoleophobic surfaces are summarized, grouped by material categories (Section 3). The underwater superoleophobic surfaces with additional properties (e.g., controllable oil adhesion, underwater anisotropic oil wettability, high transparency, and durability) are also introduced following various underwater superoleophobic materials (Section 3). The next section illustrates with some examples about the practical applications of the artificial underwater superoleophobic surfaces (Section 4). Finally, the existing challenges and future prospects of the femtosecond laser creating underwater superoleophobic surfaces are discussed (Section 5).



Jiale Yong is currently a lecturer of electronic science and Technology at Xi'an Jiaotong University. He received his B.S. degree from Xi'an Jiaotong University in 2011. After that, he joined Prof. Chen's research group and received a Ph.D. in electronic science and technology from Xi'an Jiaotong University in 2016. His research inter-

ests include femtosecond laser microfabrication, controlling wettability of solid surfaces, and bioinspired designing superhydrophobic and superoleophobic interfaces.



Feng Chen is a Full
Professor of the School of
Electronics and Information
Engineering at Xi'an Jiaotong
University, where he directs
the Femtosecond Laser
Laboratory. He received a
B.S. degree in physics from
Sichuan University, China,
in 1991, and then began to
work for the Chinese Academy
of Science (1991–2002),

where he was promoted to a Full Professor in 1999. He received a Ph.D. in optics from the Chinese Academy of Science in 1997. In 2002, he joined Xi'an Jiaotong University, where he became a group leader. His current research interests are femtosecond laser microfabrication and bionic microfabrication.

## 2. Background

## 2.1. Underwater Superoleophobicity in Nature

After millions years of slow evolution and natural selection, the majority of organisms have developed perfect multifunctional surfaces to adapt to their living environment. In nature, some animals and plants have the surface with special wettability.[115-118] For example, lotus leaves grow in the silt but not imbrued because of their self-cleaning property (Figure 1a);[119,120] water strider is able to walk and jump on water (Figure 1b);[121,122] red rose petals show high adhesive force to water droplet and can capture droplets (Figure 1c);<sup>[123]</sup> the raindrops and dew are inclined to slide along the leaf vein and finally toward the root of a rice leaf, helping the rice to survive (Figure 1d);<sup>[124,125]</sup> butterfly can even fly in the rain because the directional adhesion of the butterfly wing allows it to shake raindrops off (Figure 1e);[126] mosquito eyes have antifog ability, ensuring an unimpaired view in humid conditions where the mosquitoes usually live (Figure 1f);<sup>[32]</sup> desert beetle can harvest fog by its shell in the arid desert (Figure 1g); [46] and gecko feet have multifunctions of superhydrophobicity, high adhesion, and reversible adhesion

21967330, 2018, 7, Downloaded from https://advanced.onlinelibrary.wiley.com/doi/10.1002/admi.201701370 by CAS-XIAN INSTITUTION OPTICS PRECISION MECHANICS, Wiley Online Library on [09/11/2025]. See the Terms and Conditions (https://onlinelibrary.wiley.com/

onditions) on Wiley Online Library for rules of use; OA articles are governed by the applicable Creative Commons

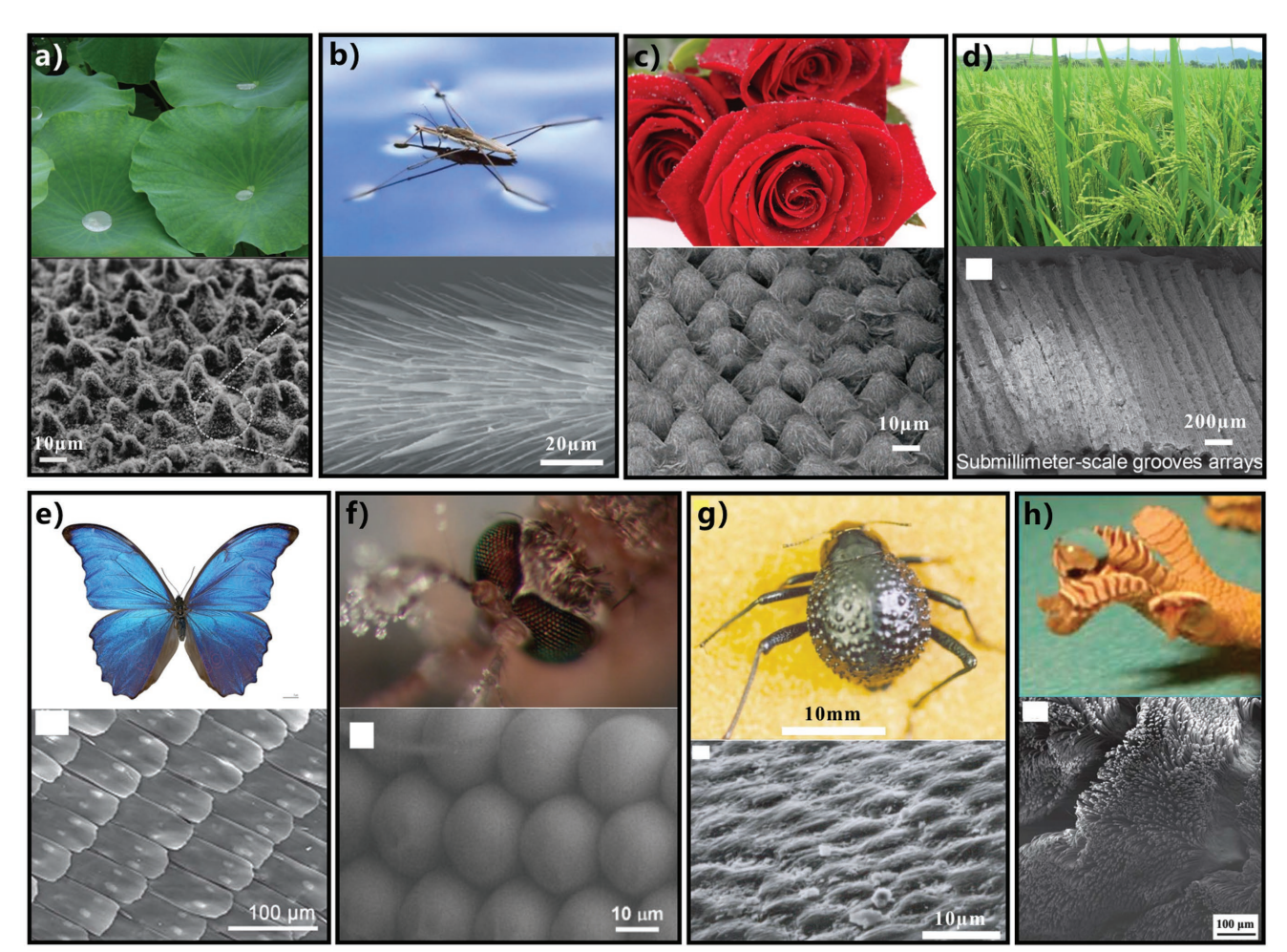


Figure 1. Photographs and surface microstructures of the organisms with special wettability. a) Lotus leaves. Reproduced with permission. [120] b) Water strider. Reproduced with permission. [121] Copyright 2004, Nature. c) Red rose petals. Reproduced with permission. [123] Copyright 2008, American Chemical Society. d) Rice leaves. Reproduced with permission. [125] e) Butterfly wings. Reproduced with permission. [126] Copyright 2007, Royal Society of Chemistry. f) Mosquito eyes. Reproduced with permission. [127] Copyright 2012, Royal Society of Chemistry.

(Figure 1h).<sup>[127]</sup> It is found that all of these unique wettabilities are caused by the combined effect of both different hierarchical surface microstructures and chemical compositions, verifying the unification and coordination of structure and performance. Inspired by the above phenomena, a high amount of artificial functional surfaces with special wettability has been designed and prepared, and those surfaces have been widely used in our lives.<sup>[3–5,10–12]</sup> In fact, the study of underwater superoleophobicity was also originated from the revelation of the antioil function of fish scales.<sup>[73]</sup>

Compared to the seabirds that are endangered by oil pollution during a spill accident, fish can keep their body clean in the same oil-polluted water. In 2009, Jiang and co-workers discovered the underlying mechanism of the antioil ability of fish body, which comes from the underwater superoleophobicity of the fish scales.<sup>[73]</sup> The fish body is completely covered by well-aligned fan-like scales (**Figure 2**a). Fish scale is made up of hydrophilic calcium protein, phosphate, and a thin layer of mucus. Figure 2b–d shows the scanning electron microscopy (SEM) images of a fish scale. There are many oriented

micropapillae with 100-300 µm in length and 30-40 µm in width on the fish scale surface (Figure 2b). These micropapillae arrange in the radial direction. The surface of every micropapilla also shows fine-scale roughness (Figure 2c,d). Such multiscale hierarchical microstructure makes the fish scale have both superhydrophilicity and superoleophilicity (Figure 2e) in air. The contact angles to water or oil droplets on the fish scale are close to 0°. However, when the fish scale is immersed in water where fish generally live, it will become superoleophobic with an OCA of 156.4  $\pm$  3.0° to a 1,2-dichloroethane droplet (Figure 2f). It is the surrounding water medium that results in the wettability transition from in-air superoleophilicity to underwater superoleophobicity for the fish scales. The rough surface microstructures can be fully wetted when the fish scales are immersed in water. After placing oil droplets on the fish scale, the trapped water layer in the rough microstructures will become an oil-repellent water cushion underneath the oil droplet, forming a solid/water/oil three-phase system. As a result, the fish scales are endowed with excellent superoleophobicity and antioil ability in water. The fish scale inspires us

2196733.0 2018. 7, Downholded from https://adatroced.onlinelibrary.wiley.com/doi/10.1002/admi.201701.370 by CAS-XIAN INSTITUTION OPTICS PRECISION MECHANICS, Wiley Online Library on [0911] 2025]. See the Terms and Conditions (https://conhelibrary.wiley.com/herms-and-conditions) on Wiley Online Library for rules of use; OA articles are governed by the applicable Celevier Commons.

www.advmatinterfaces.de

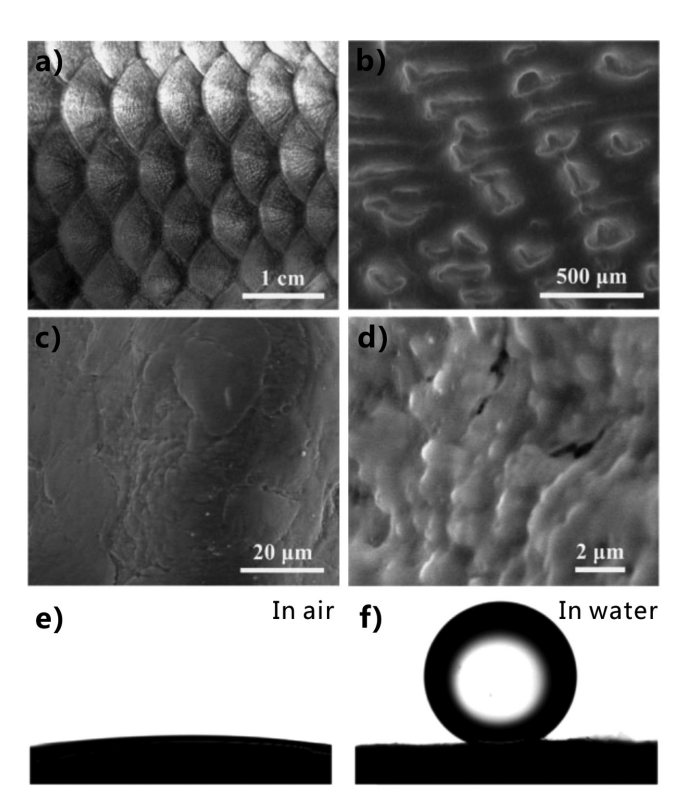


**Figure 2.** Underwater superoleophobicity of fish scale surface. a) Photograph of well-aligned fan-like scales on a fish skin. b–d) Microstructure on the fish scale surface. An oil droplet on fish scale e) in air and f) in water, respectively, exhibiting in-air superoleophilicity and underwater superoleophobicity of the fish scales. Reproduced with permission.<sup>[73]</sup>

to fabricate underwater superoleophobic surfaces by the cooperation of rough microstructures and hydrophilic chemical composition.

The underwater oil-repellent materials usually face a big stable challenge for applications, especially in the water with high salinity. It is found that seaweed (Saccharina japonica) can still maintain superoleophobicity in the saturated NaCl solution (Figure 3a).[128] Figure 3b shows the surface microstructure of the seaweed. Abundant micropores can be observed. There are also many reticular structures and microfibers covering on the seaweed surface. Furthermore, seaweed is rich in natural polysaccharides (e.g., alginate, carrageenan, and agar). The polysaccharide molecules are easy to bond water molecules, even in a high salinity solution. As far as an underwater oil droplet on a piece of seaweed surface (Figure 3c), the measured OCA reaches up to  $160.7 \pm 5.0^{\circ}$  (Figure 3d), and the oil droplet can roll away at a small tilted angle of ≈2° (Figure 3e), showing underwater superoleophobicity and ultralow oil adhesion. Surprisingly, the seaweed surface still shows ultralow oil-adhesive underwater superoleophobicity in NaCl solutions with the concentration increasing from 0.5 mol L<sup>-1</sup> to fully saturated water, revealing that underwater oil droplets are repelled by seaweed even under the condition of the high ion strength and salinity. Such salt-tolerant underwater superoleophobicity of seaweed surface is mainly ascribed to the combined effect of the saltinsensitive polysaccharide compositions and the porous surface microstructures.

Except for the underwater superoleophobicity, the skin of filefish (Navodon septentrionalis) also exhibits anisotropic oil wettability in water (Figure 3f).<sup>[76]</sup> The filefish skin is covered by high-surface-energy-oriented hook-like spines rather than common fan-shaped scales (Figure 3g,h). The height of each spine is about 383.7 μm and the width is about 51.6 μm. The tips of every spine are curved toward the filefish's tail. In a water medium, a small oil droplet on the filefish skin shows an OCA of 156.1  $\pm$  1.8° (Figure 3i). The oil droplet will roll off the filefish skin along the head-to-tail (HT) direction as long as the surface is tilted 13.4°, whereas the oil droplet can roll until the surface is tilted 22.5° along the opposite direction (TH direction), as shown in Figure 3j. The result indicates that oil droplets are inclined to roll away along HT direction, but to be pinned in the TH direction, showing an anisotropic oil wettability of the filefish skin. The close hydrophilic hook-like spines result in the underwater superoleophobicity and antioil function of filefish skin because of high surface roughness. Meanwhile, the spines' curved tips lead to the unidirectional sliding trend of oil droplets. Such anisotropic oil repellence means that filefish has directional self-cleaning capacity in oil-polluted seawater because the accumulation of oils is avoided at its head.

Many other organisms also have underwater superoleophobic property, such as the shell of clam and the bottom surface of lotus leaf.<sup>[77,82]</sup> Inspired by these creatures, we can prepare an underwater superoleophobic surface by combining the suitable surface microstructures and the high surface-free-energy chemistry. An effective route that can also be concluded is "from in-air superhydrophilicity to underwater superoleophobicity."<sup>[60,73-75,79,80,87,129,130]</sup>

## 2.2. Theoretical Basis about Wettability

When a small liquid droplet is dripped onto a solid surface, a three-phase contact line (TPCL) will form after just touch. As the liquid further wets the surface, the TPCL expands outward until reaches a certain diameter, resulting in a spherical crownshaped droplet staying on the substrate surface, as shown in Figure 4a. At this moment, the formed angle between the liquid/solid interface and the tangent to the air/liquid curved surface at the TPCL is named contact angle (CA), which is usually used to assess the static wettability of the solid surface.<sup>[40]</sup> Regarding the dynamic wettability, it can be investigated by measuring the sliding angle (SA).[1,17] The sample is tilted until the droplet on its surface can just roll away. This tilted angle of the substrate is SA (Figure 4b). In general, the value of the SA can reflect the degree of the adhesion between the solid substrate and the liquid droplets.[23,84,88,131-133] A higher liquid adhesion usually gives rise to a larger SA value.

For the droplet on a flat substrate, its wetting state can be described by the Young's model (Figure 4a).<sup>[2,40]</sup> The CA ( $\theta$ ) of the droplet is expressed as

$$\cos\theta = \frac{\gamma_{\rm SV} - \gamma_{\rm SL}}{\gamma_{\rm LV}} \tag{1}$$

where  $\gamma_{SV}$ ,  $\gamma_{SL}$ , and  $\gamma_{LV}$  are the surface free energies of solid-vapor, solid-liquid, and liquid-vapor interfaces.

21967350, 2018, 7, Downloaded from https://advanced.onlinelibrary.wiley.com/doi/10.1002/admi.201701370 by CAS-XIAN INSTITUTION OPTICS PRECISION MECHANICS, Wiley Online Library on (09/11/2025). See the Terms and Conditions (https://onlinelibrary.wiley.com/doi/10.1002/admi.201701370 by CAS-XIAN INSTITUTION OPTICS PRECISION MECHANICS, Wiley Online Library on (09/11/2025). See the Terms and Conditions (https://onlinelibrary.wiley.com/doi/10.1002/admi.201701370 by CAS-XIAN INSTITUTION OPTICS PRECISION MECHANICS, Wiley Online Library on (09/11/2025). See the Terms and Conditions (https://onlinelibrary.wiley.com/doi/10.1002/admi.201701370 by CAS-XIAN INSTITUTION OPTICS PRECISION MECHANICS, Wiley Online Library on (09/11/2025). See the Terms and Conditions (https://onlinelibrary.wiley.com/doi/10.1002/admi.201701370 by CAS-XIAN INSTITUTION OPTICS PRECISION MECHANICS, Wiley Online Library on (09/11/2025). See the Terms and Conditions (https://onlinelibrary.wiley.com/doi/10.1002/admi.201701370 by CAS-XIAN INSTITUTION OPTICS PRECISION MECHANICS, wiley Online Library on (09/11/2025). See the Terms and Conditions (https://onlinelibrary.wiley.com/doi/10.1002/admi.201701370 by CAS-XIAN INSTITUTION OPTICS PRECISION MECHANICS, wiley Online Library on (09/11/2025). See the Terms and Condition of the Condition of

onditions) on Wiley Online Library for rules of use; OA articles are governed by the applicable Creative Commons

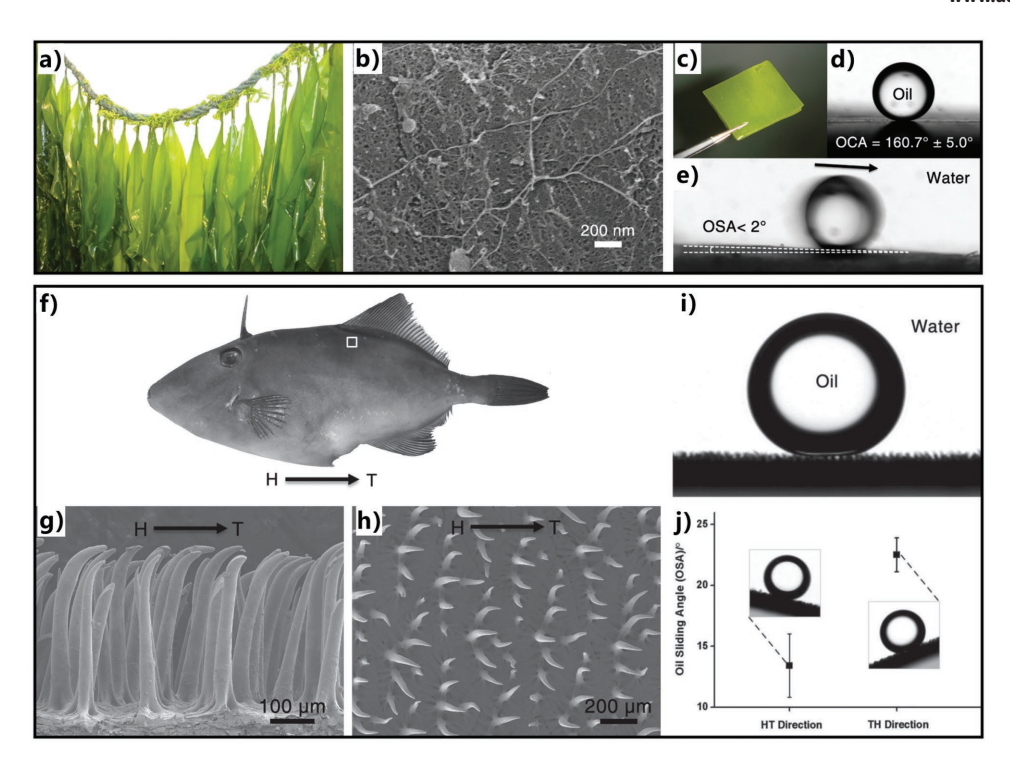


Figure 3. Underwater superoleophobicity of seaweed surface and filefish skin. a) Photograph of seaweed. b) Surface microstructure of seaweed. c) Picture of a piece of seaweed used in measurement. d) Underwater oil droplet on the seaweed surface. e) Underwater oil droplet rolling off the seaweed surface. a-e) Reproduced with permission. [128] f) Picture of a filefish. SEM images of the oriented hook-like spines on the filefish skin: g) side view and h) top view. i) Underwater oil droplet on the filefish skin. j) Anisotropic oil sliding angles on the filefish skin along the HT direction and the TH direction, respectively. f-j) Reproduced with permission. [76]

This equation is only valid for the ideal smooth substrate, but most real surfaces are usually rough. The surface roughness also has a crucial influence on the wetting behavior of a substrate surface. To explain the impact of the surface microstructures on the wettability, two classical wetting models (i.e., the Wenzel state and the Cassie state) have been extracted from various experimental data. [2,9,16,17,134,135] Wenzel pointed out that the actual surface area is larger than the apparent surface area for a rough solid surface. [136] Considering the surface roughness, he modified the Young's equation as bellow

$$\cos \theta^* = \frac{r(\gamma_{SV} - \gamma_{SL})}{\gamma_{LV}} = r \cos \theta \tag{2}$$

where  $\theta^*$  and  $\theta$  are the apparent CAs of a liquid droplet on the rough substrate and its corresponding flat substrate, respectively. The roughness factor, r, is defined as the ratio of the actual surface area to the projected area. The liquid completely fills the valleys of the surface microstructures (Figure 4c). It can be deduced from this equation that rough microstructures can amplify the intrinsic wetting nature of the surface, that is, the surface roughness makes the hydrophilic materials become more hydrophilic while the hydrophobic materials become more hydrophobic.<sup>[2,9]</sup>

In contrast, for Cassie's wetting state, the liquid droplet is assumed to sit on a heterogeneous surface with air pockets trapped between the surface microstructures and the liquid droplet (Figure 4e). [137] In other words, the cavities of the surface microstructures are difficult to be penetrated by the liquid droplet and then are filled with air. The apparent CA,  $\theta^*$ , of a small droplet on such heterogeneous surface is given as follows

$$\cos \theta^* = f \cos \theta + f - 1 \tag{3}$$

where  $\theta$  is the Young's contact angle and f is the area fraction of the surface that contacts with the liquid.

In the case of Wenzel state, there is usually a very high adhesion between the droplet and the substrate. By contrast, the adhesion is relatively ultralow if the droplet is at the Cassie state. Apart from the above-mentioned wetting states, there is also a transition state between the Wenzel state and the Cassie state.[2,134,138] The droplet can partly penetrate into the rough microstructures of the substrate surface, resulting in a transitional liquid adhesion between the Wenzel state and the Cassie state (Figure 4d). This adhesion can be controlled from low to high according to the level of the droplet penetrating into the rough microstructures.[25,139-142]

If an in-air superhydrophilic surface is dipped into water, the whole surface microstructures will be wetted and filled by water, like the water being trapped by the rough microstructures. When an oil droplet is further put on such prewetted surface, a trapped water cushion can form underneath the oil droplet (Figure 4f). Oil droplet sitting on a solid-water composite surface can only touch the top of the surface protrusions. This underwater oil droplet is at a version of underwater Cassie state.<sup>[73]</sup> The inherent oil repellence of the trapped water layer

and-conditions) on Wiley Online Library for rules of use; OA articles are governed by the applicable Creative Commons

www.advancedsciencenews.com



www.advmatinterfaces.de

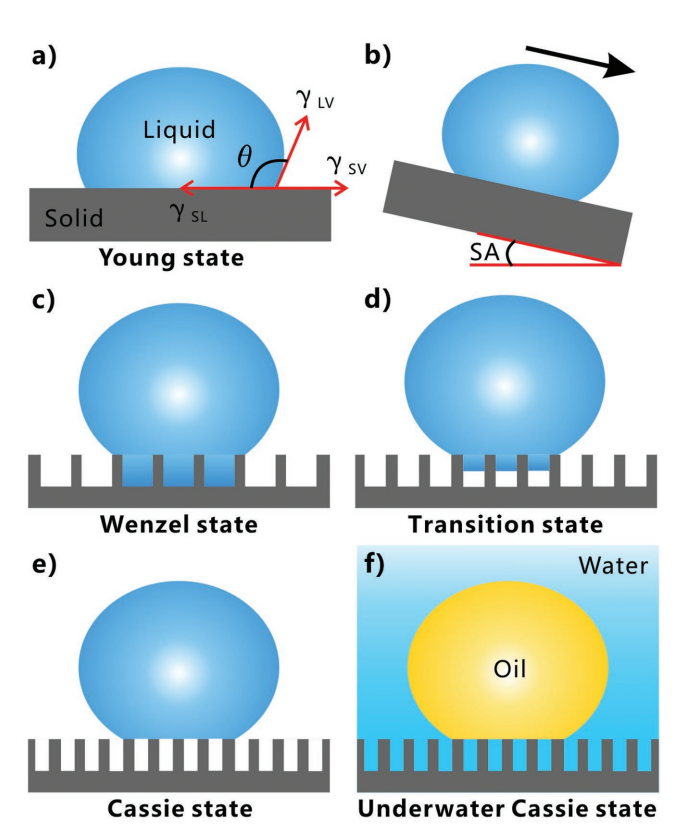


**Figure 4.** Wetting states of liquid droplet on various substrates. a) Droplet on a flat substrate: Young state. b) Definition of the sliding angle: the tilted angle for the droplet just rolling away. Droplet on a rough substrate: c) Wenzel sate, d) transition state, and e) Cassie state. f) Underwater Cassie state for an oil droplet on a textured substrate in water.

results in an ultrahigh OCA. For the underwater Cassie's case, the apparent OCA,  $\theta_{\text{ow}}^*$ , is described by the underwater Cassie's equation

$$\cos \theta_{\text{ow}}^* = f \cos \theta_{\text{ow}} + f - 1 \tag{4}$$

where f is the area fraction of the oil–solid interface,  $\theta_{\rm OW}$  is the underwater Young's OCA which is defined as the CA of a small oil droplet on a flat solid surface in a water medium. In this solid/water/oil three-phase system,  $\theta_{\rm OW}$  of an oil droplet in underwater Young state meets Equation (5)[2,73]

$$\cos \theta_{\text{OW}} = \frac{\gamma_{\text{OV}} \cos \theta_{\text{O}} - \gamma_{\text{WV}} \cos \theta_{\text{W}}}{\gamma_{\text{OW}}}$$
 (5)

where  $\gamma_{\rm OV}$ ,  $\gamma_{\rm WV}$ , and  $\gamma_{\rm OW}$  are the interfacial tensions of oilvapor, water-vapor, and oil-water interfaces, respectively.  $\theta_{\rm O}$  is the intrinsic CA of an oil droplet on such flat solid surface in air and  $\theta_{\rm W}$  is the intrinsic CA of a water droplet on this flat substrate.

## 2.3. Femtosecond Laser Microfabrication

Femtosecond laser has been proven to be an effective and powerful tool in advanced microfabrication and

nanofabrication.[111-114,143] Because of the unique features of ultrashort pulse width and extremely high peak intensity, femto second laser microfabrication has many definite advantages against the traditional laser processing techniques that are based on the longer pulse or continuous wave lasers, such as a very small heat-affected zone formation around the ablated area, noncontact manufacturing, high spatial resolution, and versatility in terms of the materials that can be processed.[111-114] In addition, the femtosecond laser beam can also interact with transparent materials by a nonlinear process, such as multiphoton absorption or tunneling ionization, because of the high peak intensity of femtosecond laser.[111,112] Thus, the femtosecond laser can ablated a wide range of materials, no matter the opaque or the transparent materials, including semiconductors, brittle materials (e.g., glasses), metals, polymers, ceramics, biomaterials (e.g., biotissues), and so on.[111-113,144-164] Taking silicon surface as an example, when the fluence of incoming femtosecond laser pulses is exceeded the damage threshold of silicon material, part of the laser energy will be instantaneously absorbed by electrons through the nonlinear effects (i.e., multiphoton and avalanche ionization).[111,145] Then, some energy is further transferred from electrons to the lattice. After reaching thermal equilibrium of the electrons and ions, high-pressure and high-temperature plasmas are formed above the substrate surface. As the plasmas expand and burst out of the focal spot, the ablated materials are removed from the surface, resulting in a textured surface with various rough microstructures. In general, the laser-induced microstructures are also covered with abundant self-assembly nanometer-sized protrusions coming from the recrystallization of ejected particles.[145]

Femtosecond laser microfabrication has already been successfully applied in high-quality, high-precision surface micro/ nanomachining, such as drilling, cutting, nanograting, surface patterning and texturing, and micro/nanostructuring.[111-114] Figure 5 shows a typical setup of femtosecond laser microfabrication system.[165] The sample is fixed on a 3D processing platform in advance. The Gaussian laser beam coming from a femtosecond laser is then focused on the sample surface by an objective lens. Of course, some other lenses such as medium optical convex lens, plane-convex lens, and cylindrical lens can also be used to focus the laser beam. The movement of the 3D platform can be precisely controlled by computer program. The pulse energy is adjusted by a variable attenuator. An electromechanical shutter is used to turn on/off the laser beam. The micromachining process is monitored by a charge-coupled device (CCD) camera in real time. In the experiment, the typical line-by-line (serial) scanning manner is usually adopted, as shown in the lower right inset of Figure 5.

Femtosecond laser microfabrication has also been successfully applied in the field of surface science to design and change the surface wettability of solid materials in the past decade. [8,10,65,99,103,106–110] Various micro/nanoscale hierarchical structures can be directly created on the surfaces of a wide range of materials by using simple one-step femtosecond laser scanning manner. [10,65,103,107,108,110,166–169] Since the laser processing position, the scanning speed, and the scanning track are precisely controlled by computer program, different predesigned 2D patterns and 3D microstructures can easily be fabricated without the need of expensive masks, as shown in **Figure 6**. [107,168] Because surface wettability is mainly determined by both the

www.advancedsciencenews.com

21967350, 2018, 7, Downloaded from https://advanced.onlinelibrary.wiley.com/doi/10.1002/admi.20701370 by CA-SX-IAIA INSTITUTION OPTICS PRECISION MECHANICS, Wiley Online Library on [09/11/2025]. See the Terms and Conditions (https://oinelibrary.wiley.com/doi/10.1002/admi.20701370 by CA-SX-IAIA INSTITUTION OPTICS PRECISION MECHANICS, Wiley Online Library on [09/11/2025]. See the Terms and Conditions (https://oinelibrary.wiley.com/doi/10.1002/admi.20701370 by CA-SX-IAIA INSTITUTION OPTICS PRECISION MECHANICS, Wiley Online Library on [09/11/2025]. See the Terms and Conditions (https://oinelibrary.wiley.com/doi/10.1002/admi.20701370).

conditions) on Wiley Online Library for rules of use; OA articles are governed by the applicable Creative Commons License

www.advmatinterfaces.de

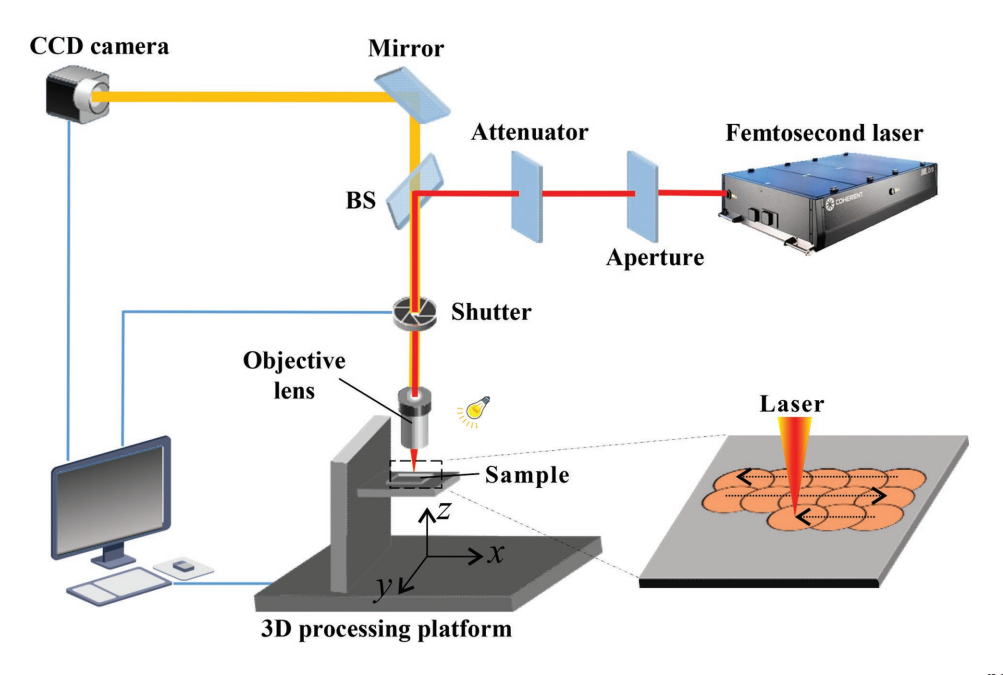
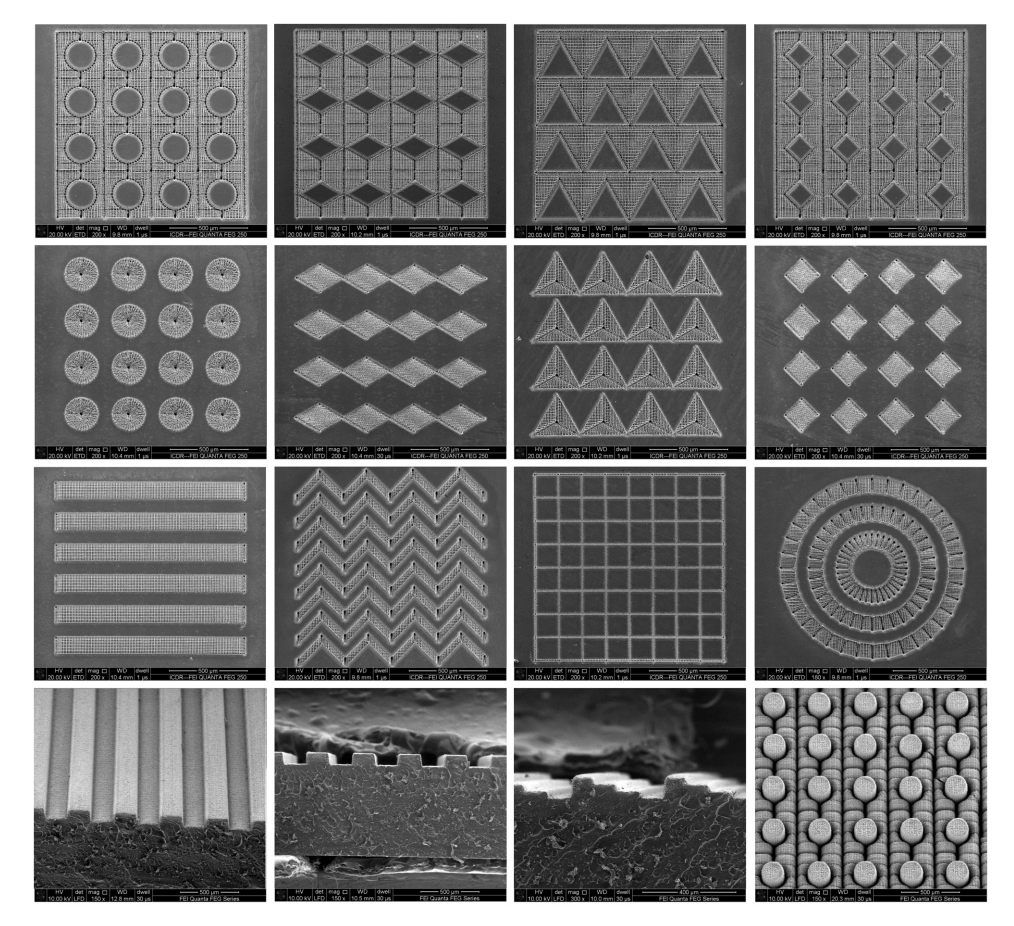


Figure 5. Schematic diagram of a typical experimental setup for femtosecond laser microfabrication. Reproduced with permission. [165] Copyright 2017, Royal Society of Chemistry.



**Figure 6.** Various 2D patterns (the first to third lines) and 3D microstructures (the fourth line) fabricated by femtosecond laser ablation. (the first to third lines) Reproduced with permission. [107] Copyright 2015, Royal Society of Chemistry. (the fourth line) Reproduced with permission. [168] Copyright 2014, Elsevier.

and-conditions) on Wiley Online Library for rules of use; OA articles are governed by the applicable Creative Commons

www.advancedsciencenews.com



www.advmatinterfaces.de

surface topography and chemical composition, these patterned microstructures usually show various unique wetting properties. Compared to the common methods that are used to prepare different wetting surfaces, what is particularly special about the femtosecond laser microfabrication is that it is more good at achieving sophisticated and heterogeneous wettability, and this technology can apply to most of the materials.

# 3. Femtosecond Laser-Induced Underwater Superoleophobicity

Inspired by fish scales, a new strategy to fabricated superoleophobic surfaces in an aqueous environment was proposed.<sup>[73]</sup> The underwater superoleophobicity of fish scales is ascribed to the combined effect of the inherently hydrophilic chemical composition and the hierarchical rough surface microstructure. It has been demonstrated that an in-air superhydrophilic surface generally exhibits superoleophobicity after the immersion of the sample surface in water. Therefore, there are two main routes for creating underwater superoleophobic surfaces based on the design principle of "from superhydrophilicity to underwater superoleophobicity." For an intrinsically hydrophilic substrate, underwater superoleophobicity can be directly obtained by building proper micro/nanoscale structure on this substrate surface. Regarding a hydrophobic substrate, the surface needs to be roughed first and further modified with hydrophilic molecular layer. Since femtosecond laser is able to directly generate various micro/nanoscale hierarchical structures on the surfaces of a wide range of materials by simple one-step ablation manner, femtosecond laser microfabrication has great success in designing and achieving underwater superoleophobicity on various substrates, including basic and complex superoleophobicity.

### 3.1. Underwater Superoleophobic Materials

#### 3.1.1. Silicon Surface

Microstructured silicon surface is the first example of achieving underwater superoleophobicity by using femtosecond laser ablation.[103] Silicon wafer is a typical intrinsically hydrophilic material. Yong et al. easily prepared a hierarchical rough microstructure on the silicon surface by femtosecond laser ablation.[103] The laser pulse beam with the energy of 20 µJ was focused onto the silicon surface by an objective lens with NA of 0.45. The used scanning speed was 2 mm s<sup>-1</sup> and the interval of the adjacent laser scanning lines was 2 µm. Figure 7a,b shows the SEM images of the as-prepared silicon surface after femtosecond laser ablation. There is a self-organized micromountains array on the resultant surface (Figure 7a). The micromountains are about 6 µm in diameter and 2.9 µm in height, and are arranged in a square array with the period of 10 µm. The surface of every micromountain is further decorated with abundant nanoscale protrusions (Figure 7b). Microscale holes form between four adjacent micromountains. The average diameter of the holes is  $8 \, \mu m$  and its depth reaches to  $4.6 \, \mu m$ . The surface roughness of such micro/nanoscale hierarchical structure is

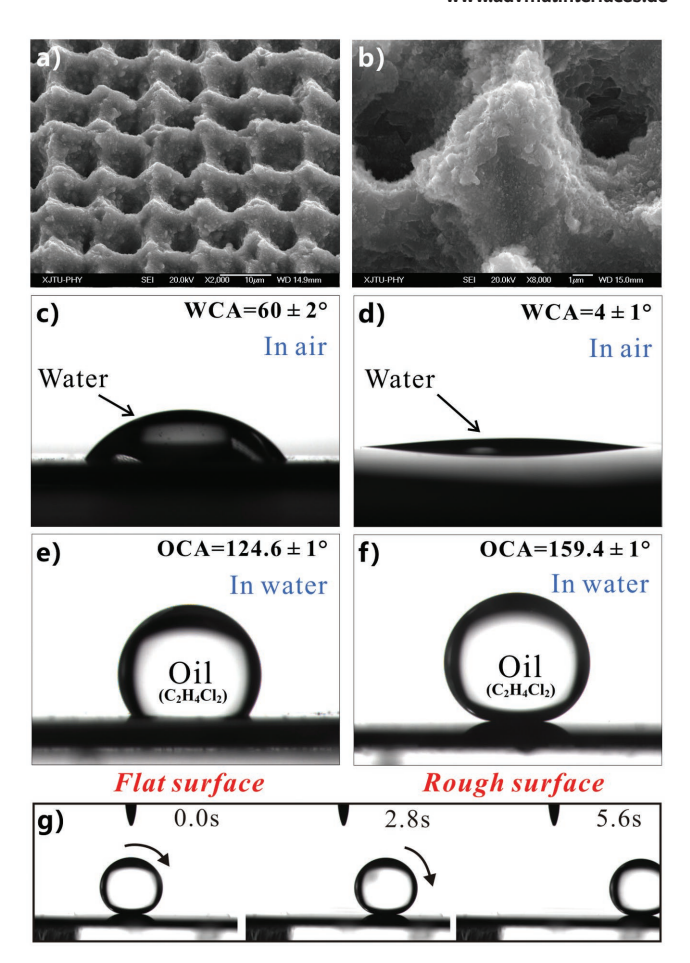


**Figure 7.** Microstructure and underwater superoleophobicity of the silicon surface after femtosecond laser ablation. a,b) SEM images of the structured silicon surface. c) Shape of a water droplet on a flat silicon surface in air. d) Shape of a water droplet on the rough silicon surface in air. e) Shape of an oil (1,2-dichloroethane) droplet on a flat silicon surface in water. f) Shape of an oil droplet on the rough silicon surface in water. g) Underwater oil droplet rolling on the 0.5° tilted rough silicon surface. Reproduced with permission. [103] Copyright 2014, Royal Society of Chemistry.

measured to be 2.46  $\mu m.$  A small water droplet on a flat silicon surface shows a water contact angle (WCA) of  ${\approx}60^{\circ}$  (Figure 7c). The hydrophilicity of the silicon surface can be greatly enhanced by the formation of the hierarchical microstructures. When a water droplet is dripped onto the laser-ablated surface, it will rapidly spread out and fully wet the structured area (Figure 7d). The WCA is only  $4\pm1^{\circ}$  in this case.

Regarding the underwater oil wettability, the flat silicon surface shows common oleophobicity in a water medium. Underwater oil droplet (1,2-dichloroethane) on such surface usually has a spherical crown shape with the OCA of 124.6  $\pm$  1° (Figure 7e). Compared to the small oil droplet on a flat silicon surface, it on the femtosecond laser-ablated rough surface is approximately spherical in shape, and its OCA is increased to 159.4  $\pm$  1° (Figure 7f). Such high OCA value indicates that the silicon surface becomes underwater superoleophobic after femtosecond laser ablation. If the needle of a syringe is inserted into the oil droplet and drags the droplet, the underwater oil droplet can move forward along the rough silicon surface freely,

www.advancedsciencenews.com



www.advmatinterfaces.de

without any trailing adhesion behind. Similarly, the oil droplet that is previously placed on the sample surface can roll away easily as long as the femtosecond laser structured surface is slightly tilted at  $0.5^{\circ}$  or shaken (Figure 7g). Such low oil sliding angle (OSA) value of  $0.5^{\circ}$  means that the adhesion between the oil droplet and the underwater superoleophobic substrate is ultralow. With the scanning speed increasing from 2 to  $25~\rm mm~s^{-1}$  and the interval of the scanning lines increasing from 2 to  $25~\rm \mu m$  during femtosecond ablation, the underwater superoleophobicity is still presented by the resultant surface because all the measured OCA values of underwater oil droplets on those structured surfaces are higher than  $150^{\circ}$ . This result reveals that femtosecond laser can endow silicon surface with underwater superoleophobicity over a wide range in machining parameters.

The formation mechanism of the underwater superoleophobicity of the femtosecond laser-ablated silicon surface is the same as that of fish scales. The superoleophobicity and ultralow adhesion of the hierarchical rough silicon surface to an underwater oil droplet can be explained by the underwater version of the Cassie wetting state (Figure 4f). The femtosecond-laser-induced rough silicon surface will be completely wetted by water owning to its in-air superhydrophilicity if the sample is immersed in water. As a result, the valley of the micro/nanoscale hierarchical structures is filled by water. When a small oil droplet is further dripped onto the sample surface, the water in the hierarchical microstructures will form a trapped water cushion underneath the oil droplet. The trapped water

cushion is able to prevent oil droplet from penetrating into the microstructures because of the natural repulsive force between water (polar molecule) and oils (nonpolar molecule). Since the underwater oil droplet can only contact with the top of the micromountains array, the contact area between the oil droplet and the silicon substrate is remarkably decreased, thereby resulting in the underwater superoleophobicity and very low oil adhesion of the femtosecond laser structured silicon surface.

The above-mentioned results reveal that the in-air hydrophilicity of the flat silicon surface will turn into oleophobicity after the immersion of the sample in water, and the oleophobicity can be further amplified to underwater superoleophobicity by the femtosecond-laser-induced hierarchical microstructures.

Li et al. obtained micro/nanostructured silicon surfaces by liquid-assisted femto-second laser ablation. When the silicon substrate was ablated by femtosecond laser in an ethanol solution, a kind of microcones with the average height of 3.3  $\mu$ m was formed on the silicon surface. These microcones are regularly distributed. For the sample that was ablated in a sucrose solution, its surface was covered by a layer of micromolars. The height of the micromolars reaches up to 5.9  $\mu$ m. Both the above-mentioned samples were ablated at the pulse energy of 60  $\mu$ J, the scanning speed of 1 mm s<sup>-1</sup>, and the scanning space

of 50  $\mu m.$  The size such as the height of the femtosecond-laserinduced microcones and micromolars can be simply adjusted by changing the solutions and the pulse energy. Because of the same machining parameters, the difference of the resultant surface microstructures prepared in ethanol and sucrose solutions, respectively, are mainly caused by the different physical properties for the two solutions. Compared to the high density (99.3%), low boiling point (78.4 °C), and low viscosity of ethanol, the sucrose solution has a higher boiling point of >100 °C and a higher viscosity. The microcone/micromolar-like rough microstructures endow the as-prepared silicon surfaces with tunable superhydrophilicity, superoleophilicity, and underwater superoleophobicity. In a water medium, the maximal OCA values of an oil droplet on the structured surface even reach  $157.76^{\circ}$  for the silicon surface (with microcone structure) ablated in ethanol solution and 169.21° for the silicon surface (with micromolar structure) ablated in sucrose solution.

#### 3.1.2. Glass

Silica glass is a very common optical material. It is widely applied in optical components and devices. Many microfabrication technologies are difficult to generate microstructures on the silica glass surface due to its high hardness, but femtosecond laser can easily ablate the silica glass surface. [111] Figure 8 shows the photograph and the SEM images of the silica glass

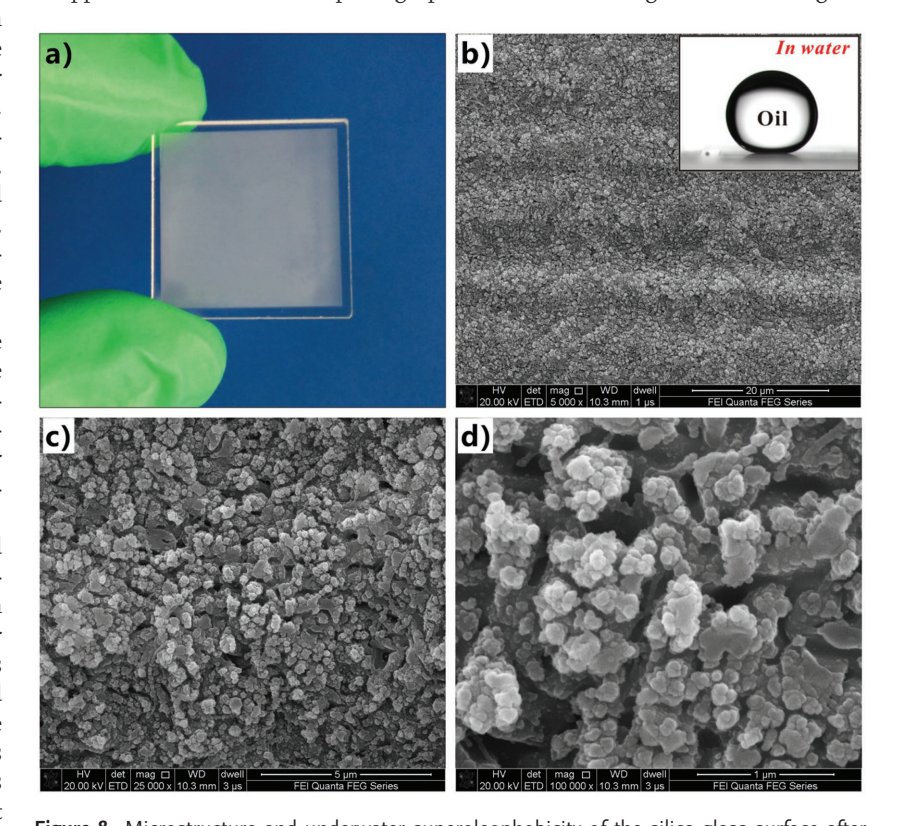


**Figure 8.** Microstructure and underwater superoleophobicity of the silica glass surface after femtosecond laser ablation. a) Photography of a piece of laser-ablated silica glass with the size of  $2 \times 2$  cm². b–d) SEM images of the structured silica glass surface at different magnification. The inset shows an oil droplet on the rough silica glass surface in water. Reproduced with permission. [108] Copyright 2015, Royal Society of Chemistry.

and-conditions) on Wiley Online Library for rules of use; OA articles are governed by the applicable Creative Commons



www.advmatinterfaces.de

surface after femtosecond laser ablation.<sup>[108]</sup> The used laser pulse energy is 20 µJ, the scanning speed is 4 mm s<sup>-1</sup>, and the interval of the adjacent laser scanning lines is 4 µm. There are a large number of irregular particles with the size ranging from several tens to several hundreds of nanometers covering on the resultant surface (Figure 8b-d). Some particles pile up, leading to abundant nanoholes and nanogrooves. During the interaction between the femtosecond laser pulse and the silica glass, the plasma with ultrahigh temperature and high pressure forms above the sample surface.[145,170,171] At the same time, the plasma expands and bursts out of the laser focused area, taking the ablated materials away from the surface. High temperature allows those ejected particles to keep in a molten state in the air. Once the ejected particles fall back to the substrate surface, they will cool down instantly. The resolidification makes the particles firmly adhere to the silica glass surface. Therefore, the laser-pulse-induced ablation and the resolidification of the ejected particles jointly create such irregular nanoscale surface structure.

Water droplet can easily spread out once it touches the femtosecond-laser-ablated silica glass surface. The final WCA is as low as near 0°. After the immersion of the rough sample in water, its surface wettability will change from in-air superhydrophilicity to superoleophobicity. The measured OCA of a small oil droplet (1,2-dichloroethane) placed on the rough silica glass surface in a water medium is  $160.2 \pm 1^{\circ}$  (inset of Figure 8b). Compared to the femtosecond-laser-ablated surface, the flat silica glass surface before laser treatment is just weakly oleophobic with the intrinsic OCA of 125.5  $\pm$  2°. In addition to the underwater superoleophobicity, the resultant surface also exhibits ultralow adhesion to underwater oil droplet as the OSA is no more than 1°. Besides the 1,2-dichloroethane droplet, the underwater superoleophobicity and ultralow oil adhesion of the laser-ablated silica glass surface are also valid for a wide range of other oils, such as hexadecane, petroleum ether, paraffin liquid, crude oil, sesame oil, chloroform, and so on (Figure 9).

The underwater superoleophobicity was also achieved on other more common glass surfaces such as glass slide by femtosecond laser ablation besides the silica glass surface. [98,105,172]

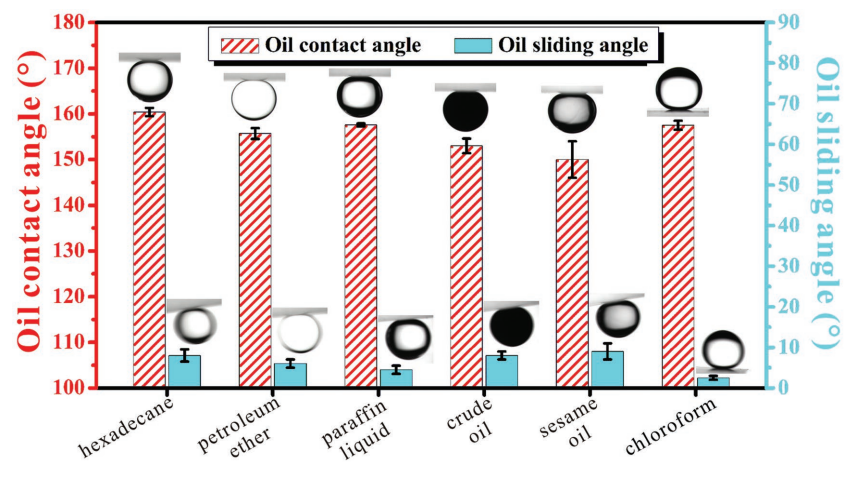


**Figure 9.** Underwater superoleophobicity and ultralow oil adhesion for a wide range of oil droplets on the femtosecond-laser-ablated silica glass surface. Reproduced with permission. [108] Copyright 2015, Royal Society of Chemistry.

#### 3.1.3. Metals

Figure 10a-d shows the microstructure of the titanium (Ti) surface after being ablated by femtosecond laser.[107] The sample was ablated at the laser pulse energy of 15 µJ, the scanning speed of 2 mm  $\rm s^{-1}$ , and the interval of the scanning lines of 2  $\mu m$ , by using a microscope objective lens with NA of 0.45. The formed microstructure is very similar to that of the femtosecond-laserablated silicon surface (Figure 7a). A uniform rough micromountains array is created on the pure Ti surface during the femtosecond laser ablation (Figure 10a,b). The energy dispersive X-ray spectroscopy result reveals that the laser-treated surface is composed of 51.81% titanium and 48.19% oxygen (by atomic proportion). It also reveals that the microstructure formation and the oxidization happen concurrently during femtosecond laser ablation, forming a thin stratum of rough TiO2 layer covering on the original pure Ti substrate. Although the just laserablated surface shows underwater superoleophilicity with OCA of 4° (Figure 10e), the sample can be switched to underwater superoleophobic as long as it is irradiated by UV light for an enough time before immersing in water (Figure 10f). In this case, the underwater oil droplet can keep a spherical shape on the resultant surface and can roll away freely once the substrate is tilted 1°. The measured OCA can reach up to  $160.5 \pm 2^{\circ}$ (Figure 10f). The underwater superoleophobicity can always be maintained unless it is stored in dark for several days.

Similarly, Wu and co-workers fabricated a kind of three-level cobblestone-like anatase TiO $_2$  microcones array on Ti sheets by femtosecond laser-induced self-assembly.  $^{[173]}$  The microcones are 15–25  $\mu m$  in height and 20–35  $\mu m$  in diameter. The surfaces of the microscale cones are fully covered by a lot of ripple-like features with a width of  $\approx\!460$  nm and smaller particles with a size of 10–500 nm. The TiO $_2$  surfaces display dual-responsive water/oil reversible wettability between underwater superoleophobicity and superoleophilicity via heat treatment and selective UV irradiation without fluorination.

Nickel is an important ferromagnetic metal and is widely applied in electronic devices, chemical catalysts, nickel-batteries, etc. Li et al. prepared self-organized hierarchical micro-

cones on a nickel surface by sucrose solutionassisted femtosecond laser irradiation.[104] After the nickel sheet being ablated by femtosecond laser (laser pulse =  $190 \mu J$ ) in sucrose solution (sucrose:water = 55:100 by mass), it turned to gray color (Figure 11a). The laserablated area is characterized by uniform hierarchical cones with the bottom radius of 3 µm (Figure 11b). The surface of every microcone is completely covered by nanovillus structures with a size of only 10–30 nm. The X-ray diffraction (XRD) measurement also reveals that the chemistry of the nickel sample is not changed after femtosecond laser ablation (Figure 11c). Nickel is an inherently hydrophilic material with intrinsic WCA of 58.26°. After the formation of rough microcone structure by laser ablation, it becomes superhydrophilicity. The water droplet can spread out rapidly as long as it contacts with the

21967350, 2018. 7, Downloaded from https://advanced.onlinelibrary.wiley.com/doi/10.1002/admi.201701370 by CAS-XIAN INSTITUTION OPTICS PRECISION MECHANICS, Wiley Online Library on [09/11/2025]. See the Terms and Conditions (https://onlinelibrary.com/doi/10.1002/admi.201701370 by CAS-XIAN INSTITUTION OPTICS PRECISION MECHANICS, Wiley Online Library on [09/11/2025]. See the Terms and Conditions (https://onlinelibrary.com/doi/10.1002/admi.201701370 by CAS-XIAN INSTITUTION OPTICS PRECISION MECHANICS, Wiley Online Library on [09/11/2025]. See the Terms and Conditions (https://onlinelibrary.com/doi/10.1002/admi.201701370 by CAS-XIAN INSTITUTION OPTICS PRECISION MECHANICS, Wiley Online Library on [09/11/2025]. See the Terms and Conditions (https://onlinelibrary.com/doi/10.1002/admi.201701370 by CAS-XIAN INSTITUTION OPTICS PRECISION MECHANICS, Wiley Online Library on [09/11/2025]. See the Terms and Conditions (https://onlinelibrary.com/doi/10.1002/admi.201701370 by CAS-XIAN INSTITUTION OPTICS PRECISION MECHANICS, Wiley Online Library on [09/11/2025]. See the Terms and Conditions (https://onlinelibrary.com/doi/10.1002/admi.201701370 by CAS-XIAN INSTITUTION OPTICS PRECISION MECHANICS, Wiley Online Library on [09/11/2025]. See the Terms and Conditions (https://onlinelibrary.com/doi/10.1002/admi.201701370 by CAS-XIAN INSTITUTION OPTICS PRECISION MECHANICS.

nditions) on Wiley Online Library for rules of use; OA articles are governed by the applicable Creative Commons

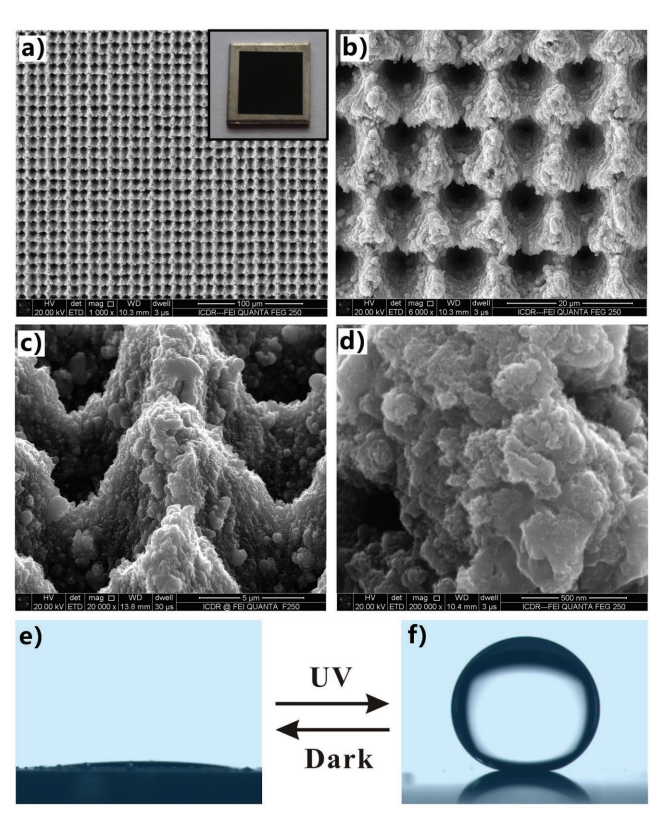


Figure 10. Microstructure and underwater superoleophobicity of the femtosecond-laser-ablated Ti surface. a-d) SEM images of the resultant surface at different magnification. The inset shows the photography of a piece of the laser-ablated Ti sheet. e) Oil droplet on the just laserablated surface in a water medium, showing underwater superoleophilicity. f) Underwater oil droplet on the resultant surface after UV irradiation, showing underwater superoleophobicity. Reproduced with permission. [107] Copyright 2015, Royal Society of Chemistry.

sample surface, resulting in a WCA less than 5° (Figure 11a). It happens because the in-air hydrophilicity is enhanced by the femtosecond-laser-induced roughness. The resultant surface also shows superoleophilicity in air besides the superhydrophilicity. The oil droplet can spread out much faster than water because the surface tension of oil is smaller than that of water. However, when the oil droplet is dripped onto the structured nickel surface which is put in water in advance, superoleophobicity will be exhibited. The measured OCA and OSA are 166° (Figure 11a) and 2.2°, respectively. The underwater superoleophobicity and ultralow oil adhesion are ascribed to the formation of underwater Cassie wetting state between the oil droplet and the femtosecond-laser-induced microcone structure. [2,73,103] Compared to the case of laser ablation in sucrose solution, if the nickel sample is ablated by femtosecond laser in an ethanol medium, the resultant surface microstructure is self-organized 3D porous nickel micro/nanocages (Figure 11e). The structured nickel surface shows a black color (Figure 11d). Its surface wettability is very different from the sample that is ablated in sucrose because the nickel is also oxidized apart from the formation of rough microstructures during femtosecond laser ablation (Figure 11f). Such surface shows hydrophobicity in air and superoleophilicity in water (Figure 11d).

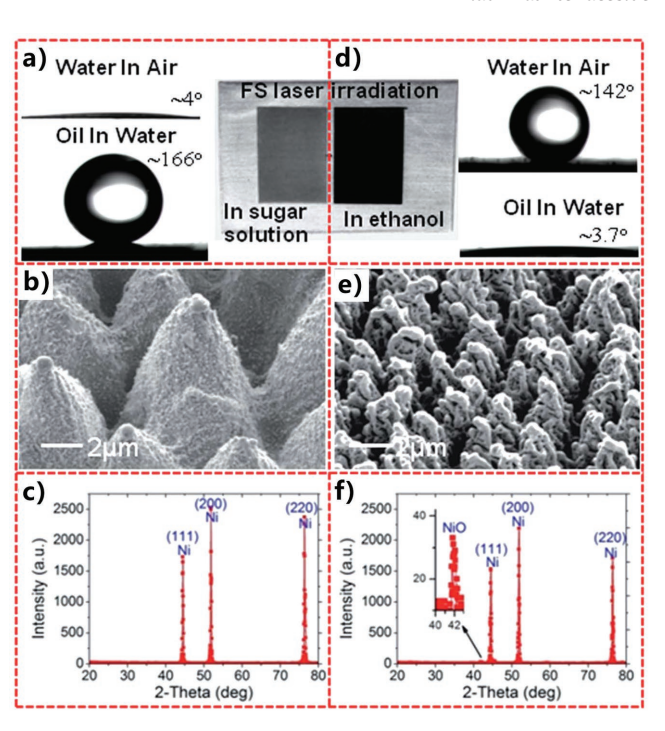


Figure 11. Wettability, microstructure, and chemical change of the nickel surfaces that are ablated by femtosecond laser a-c) in a sucrose solution and d-f) in an ethanol solution. a,d) Photography, in-air water wettability, and underwater oil wettability of the laser-ablated nickel surfaces. b,e) SEM images of the femtosecond-laser-induced microstructure. c,f) XRD analysis of the nickel surfaces after laser ablation. Reproduced with permission.<sup>[104]</sup> Copyright 2015, Royal Society of Chemistry.

Zhang et al. created hierarchical rough microstructure composed of many microholes and nanoparticles on the aluminum substrate by the in-air one-step femtosecond laser ablation.<sup>[174]</sup> The laser-induced rough aluminum surface shows underwater superoleophobicity and ultralow oil adhesion. The OCA on the structured aluminum surface reaches up to 157° while the OSA is only 7° to an underwater 1,2-dichloroethane droplet. By using the same processing procedure, they further demonstrates that femtosecond laser ablation can also endow other metals such as iron, copper, molybdenum, and stainless steel surfaces with excellent underwater superoleophobicity with OCAs of  $157 \pm 1^{\circ}$ ,  $155 \pm 0.5^{\circ}$ ,  $152 \pm 0.5^{\circ}$ , and  $155.5 \pm 0.5^{\circ}$ , respectively. Underwater oil droplets on these surfaces can easily roll away by microvibration. The underwater superoleophobicity with ultralow oil adhesion is resulted from the formation of rough microstructures caused by femtosecond laser ablation and the inherent high surface free energy of these metals. The above results mean that such a method to achieve underwater superoleophobicity is valid for a wide range of metals.

## 3.1.4. Polymer

Because of the inherent hydrophobicity, most polymer materials are deemed not suitable for obtaining underwater superoleophobicity. [23,106,131,167,168,175] Polymer materials owning to their advantages such as low price, flexibility, thermal stability, fine thermoplasticity, biocompatibility, and nontoxicity are widely

on Wiley Online Library for rules of use; OA articles are governed by the applicable Creative Commons

www.advmatinterfaces.de

used in our daily life. Endowing the polymer surface with antioil property in a water medium is still a difficult thing compared to other kinds of substrate materials. Recently, Yong et al. successfully achieved underwater superoleophobicity on polydimethylsiloxane (PDMS) surface by femtosecond laser ablation and further oxygen plasma treatment.[165] The PDMS substrate was first ablated by femtosecond laser to form a hierarchical surface microstructure. The laser beam with the pulse energy of 40 µJ was focused on the sample surface by an objective lens with NA of 0.40. The scanning speed and the shift of scanning lines were set at 5 mm s<sup>-1</sup> and 5  $\mu$ m, respectively. Figure 12a,b shows the microstructure of the femtosecond-laser-ablated PDMS surface. The surface is fully covered by coral-like microstructures with the size of several micrometers. There are abundant nanoscale protrusions decorating on the surface of the microscale corals. Such micro/nanoscale hierarchical rough structure amplifies the hydrophobicity of a flat PDMS surface to superhydrophobicity for the structured rough surface. The measured CA is  $155.5^{\circ} \pm 1.5^{\circ}$  (Figure 12c) and SA is  $2^{\circ}$  for a small water droplet on the rough PDMS surface. Therefore, the PDMS surface after laser ablation shows superhydrophobicity and ultralow adhesion to water droplets. After the immersion of the rough superhydrophobic PDMS sample in water, a trapped air layer will form between the surface microstructures

and the surrounding water according to the Cassie wetting model.  $^{[2,134]}$  The existence of this trapped air layer is also verified by that a silver mirror like reflectance appears.  $^{[176,177]}$  When an oil droplet is placed on the rough PDMS surface in a water medium, the oil will enter into the trapped air layer and spreads out along this gas gap under the capillary action and pressure, leading to a very small OCA of  $6.5 \pm 1.5^{\circ}$  (Figure 12d). So, the original femtosecond-laser-induced rough PDMS surface is superoleophilic in water.

To switch the femtosecond-laser-ablated PDMS surface from superhydrophobic to superhydrophilic and also from underwater superoleophobic, the rough PDMS sample just needs to be irradiated by oxygen plasma for a short time. [74,76,178,179] Short-time oxygen plasma irradiation is the most common method to activate PDMS substrate, which can introduce a large number of radical silanol groups (—SiOH) on the PDMS surface, as shown in Figure 12h. [74,76,178,179] The original —CH<sub>3</sub> of the PDMS substrate is converted into the hydrophilic group of —OH under the plasma irradiation. When the femtosecond-laser-ablated rough PDMS surface is further treated by oxygen plasma for 30 s (55 W), the water droplet that is placed on the resultant surface can fully wet the structured area. The measured WCA is only 4.5 ± 0.5°, indicating that the PDMS surface shows

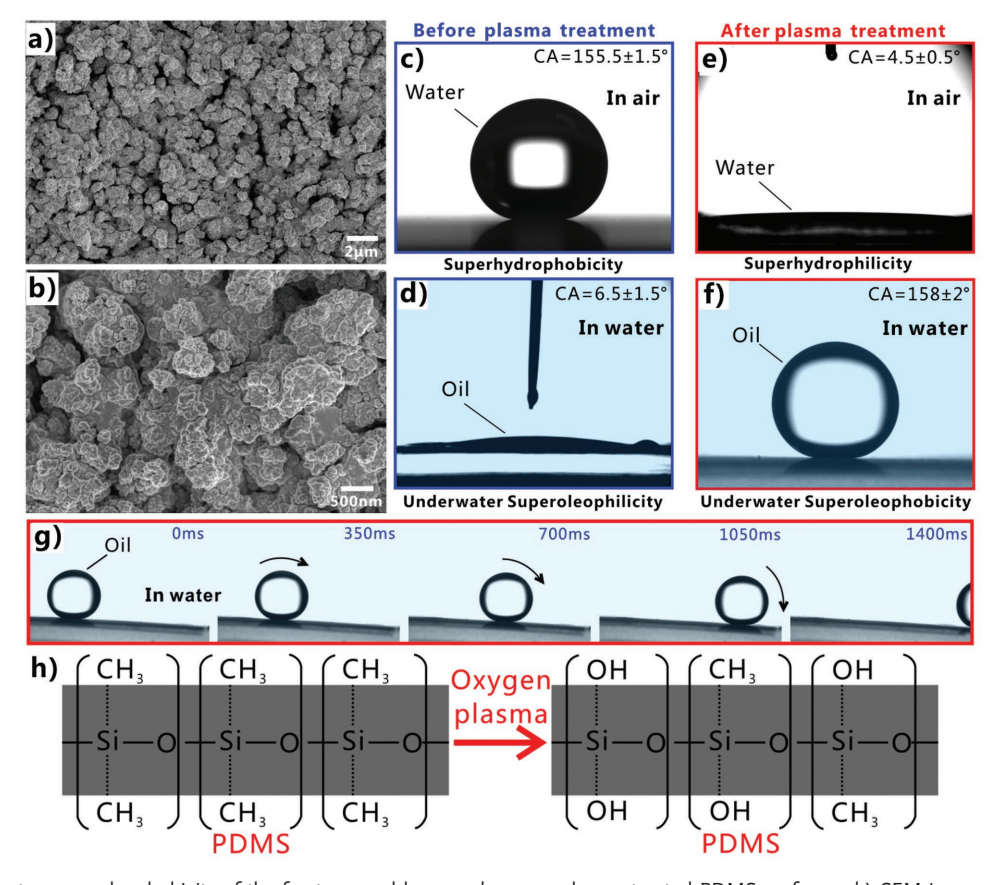


Figure 12. Underwater superoleophobicity of the femtosecond laser and oxygen plasma treated PDMS surface. a,b) SEM images of the PDMS after femtosecond laser ablation. c,d) In-air water wettability and underwater oil wettability of the original femtosecond laser structured PDMS surface. e,f) In-air water wettability and underwater oil wettability of the PDMS surface after femtosecond laser ablation and further oxygen plasma treatment. g) Underwater oil droplet rolling off on the resultant surface. a–g) Reproduced with permission. [165] Copyright 2017, Royal Society of Chemistry. h) Chemical change of the PDMS substrate after oxygen plasma treatment. Reproduced with permission. [178] Copyright 2018, Royal Society of Chemistry.

nditions) on Wiley Online Library for rules of use; OA articles are governed by the applicable Creative Commons

www.advmatinterfaces.de

superhydrophilicity at this moment (Figure 12e). Instead of the superoleophilicity of the original laser-ablated PDMS surface, the plasma-treated rough surface exhibits superoleophobicity and great oil-repellent ability in water. Underwater oil droplet can keep an approximately spherical shape on the plasma-treated rough PDMS surface, with the OCA of 158  $\pm$  2° (Figure 12f). Furthermore, the resultant underwater superoleophobic surface also shows ultralow oil adhesion because the oil droplet can roll away freely as the substrate is tilted 3° (Figure 12g).

#### 3.2. Controllable Oil Adhesion

The superoleophobic surface like fish scales that show both a very large OCA and an ultralow adhesion to an oil droplet generally has great antioil ability. There also exists some surfaces that show a very large CA but very high adhesion to the liquid droplet. [22,23,25,88,118,132,139,169,180] For example, red rose petal is superhydrophobic, whereas water the droplet can firmly adhere

to the rose petal.<sup>[123]</sup> Contrary to the fish scales, if the oil adhesion of a superoleophobic surface is very high rather than ultralow, the oil droplet will be able to stick to the surface no matter the substrate is tilted at any angle. Such high adhesive surface can be used to transport small oil droplet without any volume loss.<sup>[60,84,87,88,98]</sup> Because of the important applications in manipulating oil droplets on the target materials, the multifunctional superoleophobic surfaces showing controllable adhesion (from low to high) to oil droplet have attracted growing interest among the researchers.<sup>[60,84,88,98]</sup>

Yong et al. prepared various underwater superoleophobic surfaces with different oil adhesion by ablating glass slide surfaces through femtosecond laser at different laser scanning speed and the shift of scanning lines, as shown in **Figure 13**. [98] For the sample that is ablated at scanning speed of 2 mm s<sup>-1</sup> and the shift of scanning lines of 2  $\mu$ m, its surface is made up of self-organized and periodic microislands (Figure 13a). Every microisland is further decorated with a large number of nanoscale porous structures and protrusions (Figure 13b,c).

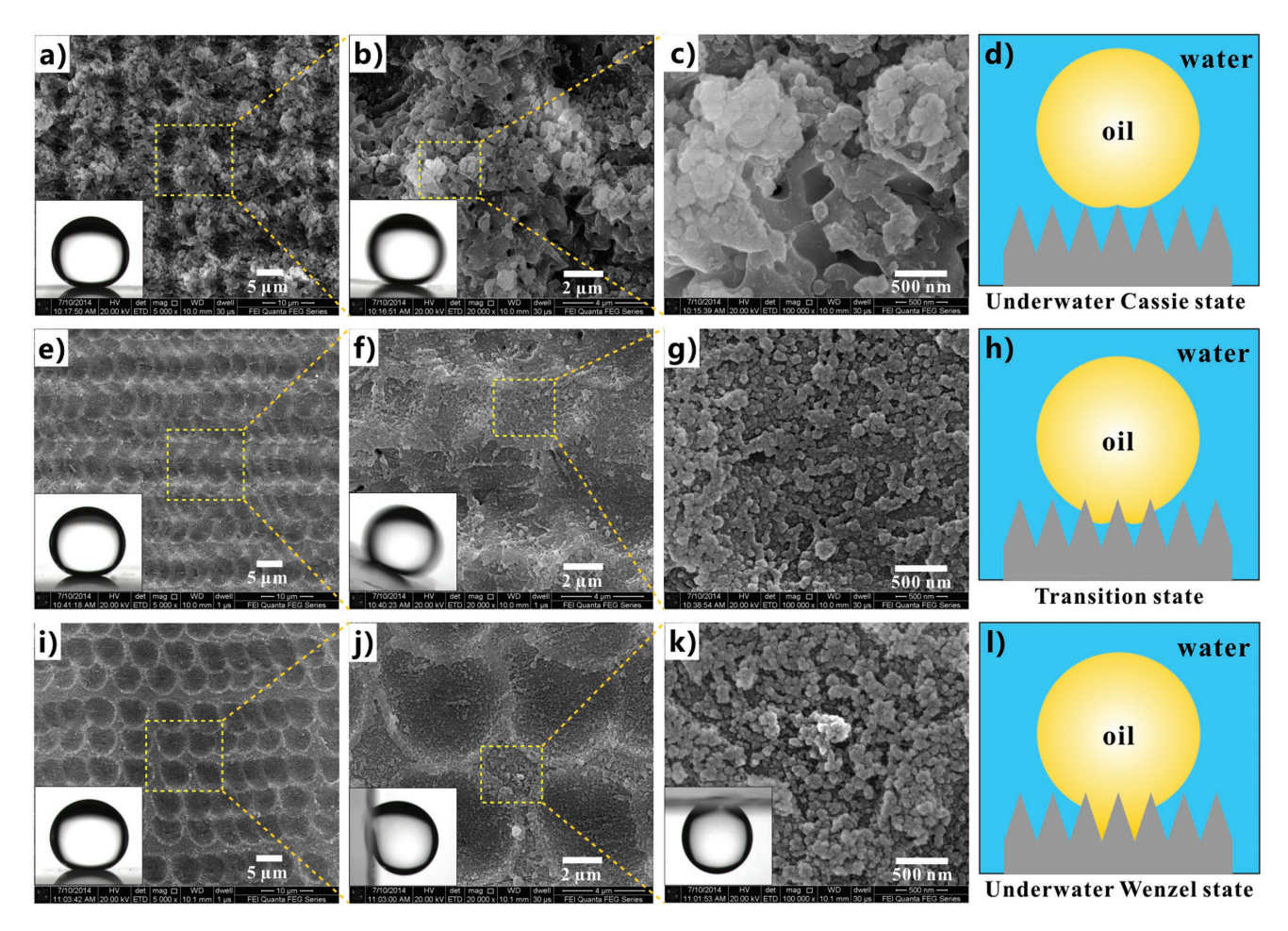


Figure 13. Surface microstructures and underwater superoleophobicity of the femtosecond-laser-ablated glass slide surface. a–c) SEM images of the surface that is ablated at the laser scanning speed of 2 mm s<sup>-1</sup> and the shift of scanning lines of 2  $\mu$ m. e–g) SEM images of the surface that is ablated at the laser scanning speed of 4 mm s<sup>-1</sup> and the shift of scanning lines of 4  $\mu$ m. i–k) SEM images of the surface that is ablated at the laser scanning speed of 6 mm s<sup>-1</sup> and the shift of scanning lines of 6  $\mu$ m. Three different wetting states of a small oil droplet on the rough surface microstructures (in water medium): d) underwater Cassie state, h) transition state, and l) underwater Wenzel state. Insets in (a,e,i): shapes of an underwater oil droplet on the corresponding substrate. Insets in (b,f,j,k): underwater oil droplet rolling away or being pinned on the corresponding substrate. Reproduced with permission.<sup>[98]</sup> Copyright 2015, Springer.



www.advancedsciencenews.com



www.advmatinterfaces.de

This micro/nanoscale hierarchical structure is different from the typical laser-pulse-induced microcrater-like structures because the adjacent areas ablated by every laser pulse overlap strongly. The oil droplet on the as-prepared surface presents almost spherical shape in a water medium with the OCA of  $160.5 \pm 2^{\circ}$  (inset of Figure 13a). Therefore, the surface shows underwater superoleophobicity. In addition, the adhesion between the underwater oil droplet and the substrate is very low. The measured OSA is only 3.5° (inset of Figure 13b). As the laser scanning speed increases to 4 mm s<sup>-1</sup> and the shift of the scanning lines increases to 4 µm during laser ablation, the resultant surface is characterized by a wave-like pattern (Figure 13e,f). Such micropattern is resulted from the partly overlap and the interconnection of the laser pulses-induced craters. Meanwhile, the whole surface is also uniformly covered with a layer of nanoparticles with a few tens of nanometers in diameter (Figure 13g). This surface also shows underwater superoleophobicity with the OCA of 158  $\pm$  2.5° (inset of Figure 13e). However, only for the substrate that is tilted at 25.5° the underwater oil droplet on the superoleophobic surface can roll off, that is, the OSA is 25.5° (inset of Figure 13f). When the scanning speed and the shift of scanning lines reach to 6 mm s<sup>-1</sup> and 6 µm, respectively, the obtained surface is covered by nearly complete microcraters (Figure 13i,j). There are abundant irregular nanoscale particles randomly decorating on the inside and the outer rim of the microcraters (Figure 13k). The OCA of an oil droplet on the resultant surface is as high as  $154 \pm 1.5^{\circ}$  in water (inset of Figure 13i). Regarding the dynamic aspect, the oil droplet can tightly pin on such surface even though the sample is vertical or turned upside down (insets of Figure 13j,k). The result indicates that such surface in water shows not only superoleophobicity but also ultrahigh adhesion to oil droplet. Therefore, the oil adhesion of the femtosecond-laserablated surfaces can be adjusted from ultralow to very high by increasing the scanning speed and the shift of scanning lines.

The adhesion between the underwater oil droplet and the solid substrate is primarily determined by the wetting state of the droplet. [60,84,88,126,181,182] The hierarchical periodic microislands fabricated at the scanning speed of 2 mm s<sup>-1</sup> and the shift of scanning lines of 2 µm are rough enough. There are a large number of pores and valleys on the resultant surface. These pores and valleys can be filled with water after the immersion of the sample in water, thereby a trapped water cushion will form between the oil droplet and the rough microstructure once an oil droplet is placed onto the sample surface. Such oil droplet is at the underwater Cassie wetting state (Figure 13d). Because the effective contact between the oil droplet and the rough substrate is hindered by the tapped water cushion, the oil droplet only contacts with the top of the microstructures, resulting in a discrete TPCL. Both the small contact area and the discontinuous TPCL endow the surface with ultralow underwater oil adhesion. There is no obvious microscale structure on the surface that is ablated at the relatively high scanning speed and the large shift of scanning lines (e.g., 6 mm  $\rm s^{-1}$  and 6  $\mu m$ , respectively). The interspaces between the microstructures are so limited that they cannot trap water firmly. In water, when an oil droplet is dripped onto the sample surface, it will tend to wet the nanoscale particles on the sample surface, forming a stable and continuous TPCL. The wetting state of the oil droplet and the substrate

belongs to underwater Wenzel state (Figure 131). A very high oil adhesion is exhibited by this surface because the oil droplet can pin the surface microstructures tightly. The wave-like patterned microstructure is intermediate between the periodic microislands and the nanoparticles coated complete microcraters. As a result, the underwater oil droplet on such surface is also at a transitional state between the underwater Cassie state and Wenzel state (Figure 13h). The oil droplet partly penetrates into the interspaces between the surface microstructures, so the surface shows an adhesion to oil droplet between the Cassie state (ultralow) and the Wenzel state (ultrahigh). The low oil-adhesive superoleophobic surfaces have strong oil-resistance ability in water, while the underwater superoleophobic surface with ultrahigh oil adhesion can be used to transfer small oil droplets.

Huo et al. proposed a simple method to obtain underwater superoleophobic patterned glass slide surfaces with tunable adhesion to oil droplet.[172] The resultant patterned microstructure comprises two different domains: untreated flat bare circles and the femtosecond-laser-induced rough microstructures around the circles, as shown in Figure 14a-d. Some special areas are ablated by femtosecond laser to generate a kind of hierarchical rough microstructure (inset of Figure 14b). The rough surface is made up of periodical microislands with the size of  $\approx 10 \mu m$ . Abundant accumulated or sporadic nanograins are further covered on the surface of the microisland, making the microislands look loose and porous. The rest domain which is not ablated by laser finally forms a periodic center circles array. In water, an oil (1,2-dichloroethane) droplet on a flat glass slide surface shows an OCA of 100° and very high oil adhesion, which reveals an ordinary oleophobicity. The oil droplet is completely in contact with the glass substrate. This contact is at the underwater Young state. By contrast, femtosecond-laser-ablated glass slide surface is underwater superoleophobic. The OCA of an underwater oil droplet on the laser-induced hierarchical rough microstructure is measured to be 160  $\pm$  1°, and its OSA is just 1°. The underwater superoleophobicity and the ultralow oil adhesion indicate that the oil droplet on the femtosecond-laser-ablated surface is at the underwater Cassie wetting state. Therefore, when an oil droplet is placed on the as-prepared patterned surface, a hybrid contact that is composed of partial underwater Young wetting state and partial Cassie wetting state will form at the interface between the oil droplet and the solid substrate (Figure 14f). As the area proportion of the untreated flat region to the laser-induced rough region increases, all of the patterned surfaces show superoleophobicity in water, while the OSA of an oil droplet on the sample surfaces increases from below  $2^{\circ}$  to  $48^{\circ}$  and then to  $90^{\circ}/180^{\circ}$  (oil droplet can pin on the substrate firmly), as shown in Figure 14e. The result reveals that the underwater oil adhesion of the superoleophobic patterned glass surface can be controlled from ultralow to ultrahigh. The practical applications such as no-loss oil droplet transportation, fusion of oil droplets, and oil droplet capture were also achieved by using the as-prepared superoleophobic glass surfaces with different oil adhesion. [98,172]

## 3.3. Underwater Anisotropic Oil Wettability

Liquid droplet on a textured surface with obvious anisotropic microstructures usually has unequal CAs and SAs along different

21967536, 2018, 7, Downloaded from https://advanced.onlinelibrary.wiely.com/doi/10.1002/admi.201701370 by CAS-XIAN INSTITUTION OPTICS PRECISION MECHANICS, Wiley Online Library on [09/11/2025]. See the Terms and Conditions (https://onlinelibrary.

ditions) on Wiley Online Library for rules of use; OA articles are governed by the applicable Creative Commons

www.advmatinterfaces.de

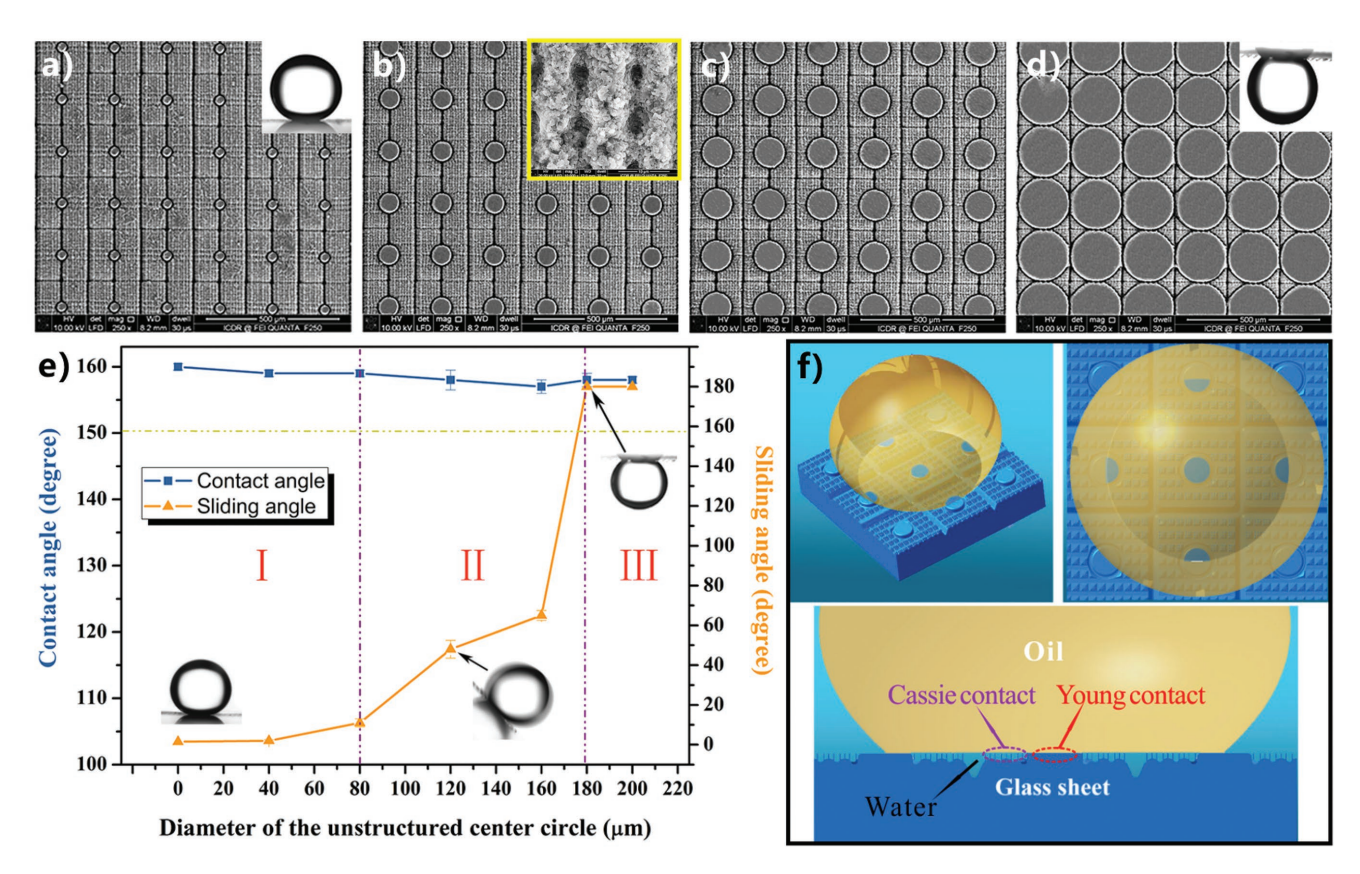


Figure 14. Controllable oil adhesion of the femtosecond-laser-induced center circle array patterns. SEM images of the center circle array patterns. The side of every unit is set at 200 μm, and the diameters of the untreated flat circles are a) 40 μm, b) 80 μm, c) 160 μm, and d) 200 μm, respectively. e) Variation of the OCA and OSA of the underwater oil droplet on the resultant surfaces with the diameter of the untreated flat center circles. f) Schematic illustration of the wetting state of the underwater oil droplet on the center circle array pattern which is composed of untreated flat circles and surrounding laser-induced hierarchical rough microstructures. Reproduced with permission. [172] Copyright 2017, American Chemical Society.

directions, resulting in an elongated droplet.[124,126,180,183-187] This phenomenon is named anisotropic wettability. The anisotropic wettability has a wide range of applications in selectively self-cleaning, microfluidics, liquid pumps, droplet manipulation, smart devices, etc.[47-50,53,76,188] Although the in-air anisotropic water wettability has been achieved on various textured substrates, the report related to the anisotropic wettability of an oil droplet is still  $\bar{l}$  imited. $^{[76,101,187,189]}$ 

Recently, Yong et al. achieved underwater anisotropic oil wettability on a femtosecond-laser-induced microgroove-structured surface.<sup>[189]</sup> The microgrooves array is generated by a simple line-by-line femtosecond laser scanning process on silicon substrate. Different with the preparation of the above-mentioned uniform microstructures, the shift of the adjacent scanning lines in this experiment is set large enough during laser ablation to make the microgrooves separate with each other. Figure 15a shows the SEM image of the resultant surface. The rough periodic microgrooves are 8 µm in width and 5 µm in depth. Every microgroove is composed of a series of microcraters, and further decorated with abundant irregular nanoparticles on its inner wall and outer rim (inset of Figure 15a). The period (D) of the microgrooves array can easily be changed by the interval of the scanning lines.

The oriented surface micropatterns have obvious influence on the shape of the underwater oil droplet that is placed on the

solid surface. [184–186,190–194] To investigate the anisotropic wetting property of groove-like surfaces, the perpendicular and parallel CAs or SAs are usually measured. [184-186,190] For the underwater oil droplet on the femtosecond-laser-induced microgroove-array surface with the D of 450 µm, the measured OCA perpendicular to the microgrooves, OCA<sub>1</sub>, is 155.5  $\pm$  1.6° (Figure 15b), whereas it is in the parallel direction, OCA<sub>||</sub>, is only  $135.7 \pm 1.5^{\circ}$ (Figure 15c). The degree of the wetting anisotropy (OCAA,  $OCA \triangle = OCA_{\parallel} - OCA_{\parallel}$ ) which is defined as the difference of the OCA values along two directions reaches up to ≈20°. The OCA<sub>II</sub> is much less than the OCA<sub>L</sub>, indicating that the oil droplet prefers to spread along the microgrooves. Figure 15d shows the changes of the OCA and OCA of an underwater oil droplet on the as-prepared surfaces with increasing the value of D. When the microgrooves are very close (e.g., the *D* is smaller than 100  $\mu$ m), the OCA<sub>||</sub> and OCA<sub>||</sub> have very little difference. The anisotropy of the oil wettability is not obvious. By contrast, there is a distinct difference between the OCA<sub>1</sub> and  $OCA_{\parallel}$  for the microgroove-structured surface with D larger than 100 µm. With the increase of D, the OCA decrease slowly in the perpendicular direction but it shows a significant reduction in the parallel direction. The downtrend of the OCA values with increasing D is manly ascribed to an area increase in flat nonstructured domain of the resultant surface which causes the decrease of the average surface roughness. Apart from

21967350, 2018, 7, Downloaded from https://advanced.onlinelibrary.wiley.com/doi/10.1002admi.201701370 by CAS-XIAN INSTITUTION OPTICS PRECISION MECHANICS, Wiley Online Library on [09/11/2025]. See the Terms and Conditions (https://onlinelibrary.wiley

and-conditions) on Wiley Online Library for rules of use; OA articles are governed by the applicable Creative Commons

the laser-ablated microgroove arrays with D less than 250 µm in the parallel direction and with D less than 500 um in the perpendicular direction. underwater The superoleophobicity and the ultralow oil adhesion of the femtosecond-laser-ablated rough silicon surface mean that the oil droplet on the laser

structured area is at the underwater Cassie state.[2,73,103] Therefore, when the microgroove-structured surface is dipped into water, the microgrooves will be wetted and filled with water which is able to prevent the oil droplet from effectively contacting with the rough microstructures. The oil droplet only touches the tips of the microstructures of the microgrooves, whereas it can completely contact with the nonirradiated flat domain between the adjacent microgrooves at the underwater Young wetting state, as shown in Figure 15e,f. There exists an energy barrier at the boundary between two domains with different wettabilities based on the Gibbs' criterion.[106,186,195] As far as the femtosecond-laser-ablated microgrooves array, the energy barrier between trapped water in the microgrooves and the untreated domain can hinder the oil droplet from spreading along the perpendicular direction. Because no energy barrier exists in the parallel direction, so the small oil droplet is more inclined to be elongated along the microgrooves (Figure 15e,f). As a result, the OCAs of an underwater oil droplet on the asprepared surfaces along the parallel direction are smaller than that along the perpendicular direction, showing a controllable anisotropic oil wettability.

The anisotropic underwater oil wetting on the microgroove-structured surface was further verified by Wu's group.[101] They developed a simple way to build microcones or micromolars on silicon surface by ethanol- or sucrose-assisted femtosecond laser irradiation. When the scanning space (D) is large enough, there is some untreated space appearing between the scanning lines (Figure 16a,b). It is found that the scanning lines prepared in sucrose solution are wider than that prepared in ethanol. Figure 16c,d shows the shapes of an oil droplet that is placed on

the resultant microgrooves surface with D of 200 µm in a water medium, viewing along the scanning lines (the parallel direction) and their perpendicular direction, respectively. For the surface prepared in ethanol, the values for  $OCA_{\perp}$  and  $OCA_{\parallel}$  are 138.08° and 124.36°, so the  $OCA_{\triangle}$  for the two directions is 13.72°, revealing a anisotropic wetting for the two directions (Figure 16c). Similarly, the measured

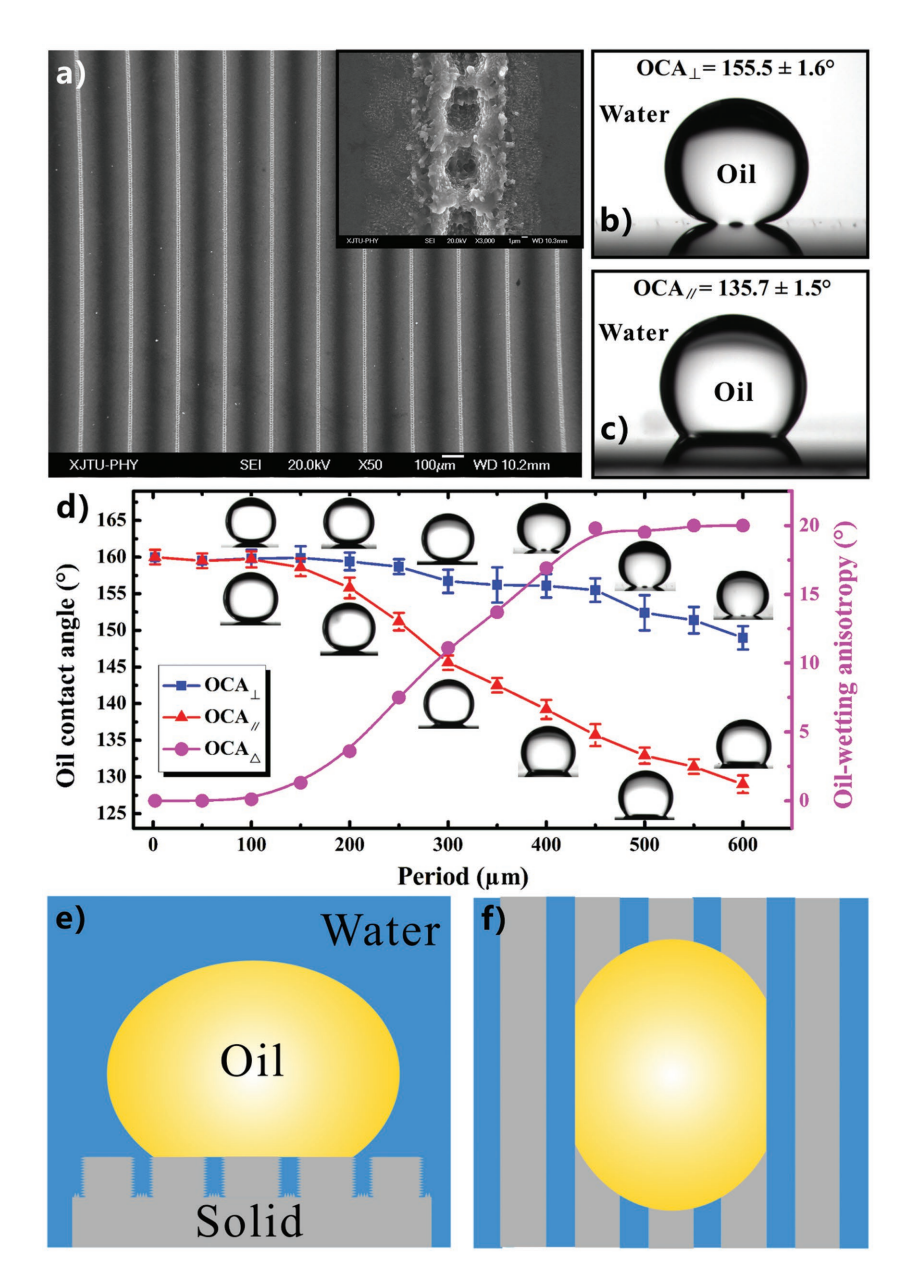
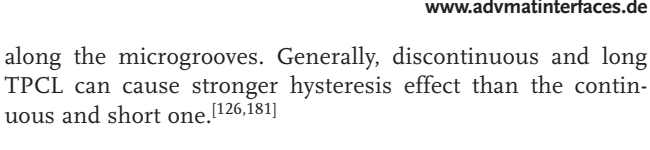


Figure 15. Underwater anisotropic oil wettability of the femtosecond-laser-induced silicon microgrooves array. a) SEM image of the microgrooves array. The inset shows the high-magnification SEM image of a single microgroove. Images of an oil droplet on the microgroove-array silicon surface in a water medium: b) along the perpendicular direction and c) along the parallel direction. d) Oil contact angles and the degree of the anisotropic oil wetting of an underwater oil droplet on the microgroove-array-structured surface with different period. Formation mechanism of the anisotropic oil wettability of the resultant textured surface: e) side view and f) top view. The oil droplet (yellow) is restricted by the energy barrier at the boundary between the untreated flat domains (gray) and the trapped water (blue) in the microgrooves. Reproduced with permission.<sup>[189]</sup> Copyright 2015, American Institute of Physics.

the similar change trend, the OCA1 is always higher than the OCA<sub>II</sub>, demonstrating that underwater anisotropic oil wetting can be achieved in a wide parameter range. Such anisotropic oil wetting can easily be controlled by adjusting the period of the microgroove arrays, and the OCA∆ can be tuned from 0° to 20° (Figure 15d). In addition to the anisotropic oil wettability, underwater superoleophobicity is also exhibited by

21967330, 2018, 7, Downloaded from https://advanced.onlinelibrary.wiely.com/doi/10.1002/admi. 201701370 by CAS-XIAN INSTITUTION OPTICS PRECISION MECHANICS, Wiley Online Library on [09/11/2025]. See the Terms and Conditions (https://onlinelibrary.

conditions) on Wiley Online Library for rules of use; OA articles are governed by the applicable Creative Commons



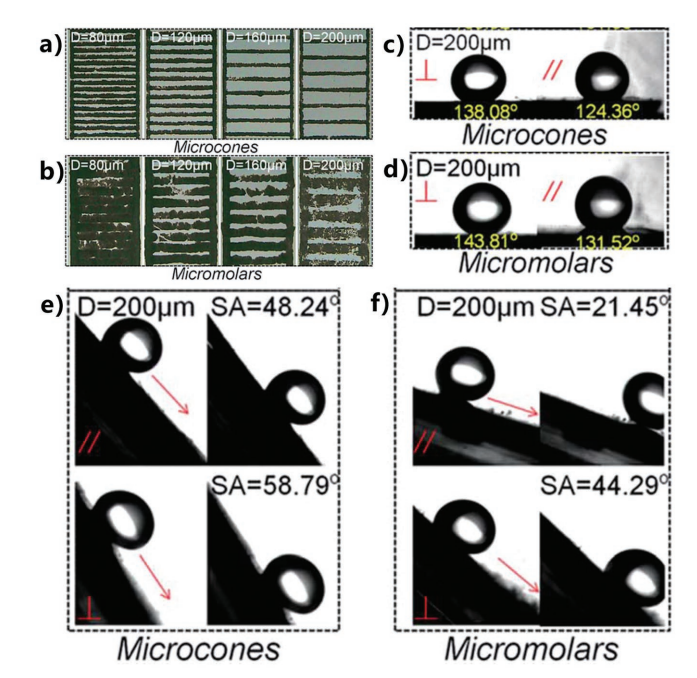


Figure 16. Anisotropic underwater oil wetting and sliding of the linepatterned surfaces fabricated by the liquid-assisted femtosecond laser irradiation. Optical microscope images of the line-patterned silicon surfaces fabricated by laser ablation a) in ethanol and b) in sources solution with different scanning spaces. c,d) Shapes of the underwater oil droplet on the resultant line-patterned surface in the directions of perpendicular and parallel to the scanning lines. e,f) The snapshots of oil droplet rolling on the resultant line-patterned surfaces, along the parallel and perpendicular directions. The silicon surface that is ablated by femtosecond laser in ethanol medium shows a microcone-like structure while the surface ablated in sucrose solution shows micromolarlike structure. Reproduced with permission.[101] Copyright 2016, Royal Society of Chemistry.

 $OCA_{\perp}$ ,  $OCA_{\parallel}$ , and  $OCA_{\triangle}$  are respectively 143.81°, 131.52°, and 12.29° for the microgroove-structured surface that is prepared in sucrose solution (Figure 16d). As the *D* increases, although both the OCA<sub>1</sub> and OCA<sub>1</sub> decrease, it can be noticed that OCA is always larger than OCA, agreeing well with the results reported in Yong's experiment.[189] In addition, dynamic oil wettability of the oil droplets was also investigated by measuring the OSAs perpendicular (OSA1) and parallel (OCA<sub>II</sub>) to the scanning lines. Figure 16e,f shows the snapshots of an underwater oil droplet rolling on the tilted sample surface with D of 200  $\mu m$ . The measured OSA<sub>1</sub> and  $OSA_{\parallel}$  are respectively 58.79° and 48.24° for the surface prepared in ethanol solution (Figure 16e). The sliding anisotropy (OSA $\triangle$ , OSA $\triangle$  = OSA $_{\parallel}$  - OSA $_{\parallel}$ ) which is defined as the difference of the OSA values along two directions is 10.55°. By contrast, the OSA $\triangle$  can reach up to 22.84° (OSA $_{\perp}$  = 44.29°,  $OSA_{\parallel} = 21.45^{\circ}$ ) for the surface that is prepared in sucrose solution (Figure 16f). The anisotropic sliding indicates that the oil droplet on the as-prepared surface is more inclined to roll away along the scanning-lines direction. Such anisotropic oil sliding is ascribed to the different TPCL situation of the underwater oil droplet rolling along the two directions.<sup>[106]</sup> The TPCL is discontinuous and long along the perpendicular direction, while the TPCL is continuous and relatively short

## 3.4. Underwater High Transparency

The formation of underwater superoleophobicity requires building a rough microstructure on the substrate surface. [73,74,80,87,108,129] However, such rough microstructure usually leads to strong light scattering and makes the resultant surface become completely opaque. The poor transparency limits the applications of the as-prepared superoleophobic surface in underwater optics, such as diving goggles, oil-proof windows for underwater cameras, imageable substrates for biologically active cells, etc.

In nature, the petals of *Diphylleia grayi* are white in a sunny day, but they turn to be transparent in the rain, as shown in Figure 17a,b. [108] In fact, the white color of the petals of *D. grayi* in air is not resulted from a natural white pigment. The inner of the petal comprises a large number of lacunae and intercellular spaces. Those lacunae and intercellular spaces are filled with air on a sunny day, causing the diffuse reflection in the interface between the colorless cytolymphs and the trapped air. Therefore, it is the loose cell structure that gives rise to the white color of the plant petals. However, a liquid/liquid (water/cytolymph) interface can replace the original air/liquid (air/cytolymph) interface in the rain because water enters the lacunae and intercellular spaces. The diffuse reflection and scattering is greatly weakened because the refractive indices of cytolymph and water are much close, so the petals become transparent. A simple strategy inspired by this interesting phenomenon for enhancing the transparency of a rough surface is to fill the interspaces of the rough microstructures with

The femtosecond-laser-ablated silica glass surface has not only superoleophobicity (Figure 8) but also good transparency in a water medium (Figure 17).[108] It looks white in air (Figure 8a), like the color of *D. grayi* petals. When a paper with black letters is put behind the laser structured sample, the letters are pretty hard to see (Figure 17c). The surface is easy to be contaminated by oils. If an oil droplet (red color) is dripped onto the laserstructured area, it will spread out quickly once after contacting with the silica glass (Figure 17c). In contrast, when the sample is immersed in water, the dyed oil droplet on the surface can maintain a spherical shape due to the underwater superoleophobicity of the rough silica glass surface (inset of Figure 17d). The letters "XJTU" behind the silica glass can be clearly captured, which indicates that the transparency of the resultant silica glass is very high in water (Figure 17d). Figure 17e shows the UV-vis spectra of the femtosecond-laser-ablated silica glass compared to a flat sheet. At visible wavelengths, the transmittance of the rough silica glass in air is low, but the transmittance in water is very close to that of an in-air bare flat silica glass. For example, the transmittance reaches up to 91.6% for the light at the wavelength of 633 nm. As shown in Figure 17f, the underwater transmittance is always larger than that in air for every femtosecond-laser-treated silica glass which is ablated at different fabrication parameters. The transmittance of the

21967350, 2018. 7, Downloaded from https://advanced.onlinelibrary.wiley.com/doi/10.1002/admi.201701370 by CAS-XIAN INSTITUTION OPTICS PRECISION MECHANICS, Wiley Online Library on [09/11/2025]. See the Terms and Conditions (https://onlinelibrary.com/doi/10.1002/admi.201701370 by CAS-XIAN INSTITUTION OPTICS PRECISION MECHANICS, Wiley Online Library on [09/11/2025]. See the Terms and Conditions (https://onlinelibrary.com/doi/10.1002/admi.201701370 by CAS-XIAN INSTITUTION OPTICS PRECISION MECHANICS, Wiley Online Library on [09/11/2025]. See the Terms and Conditions (https://onlinelibrary.com/doi/10.1002/admi.201701370 by CAS-XIAN INSTITUTION OPTICS PRECISION MECHANICS, Wiley Online Library on [09/11/2025]. See the Terms and Conditions (https://onlinelibrary.com/doi/10.1002/admi.201701370 by CAS-XIAN INSTITUTION OPTICS PRECISION MECHANICS, Wiley Online Library on [09/11/2025]. See the Terms and Conditions (https://onlinelibrary.com/doi/10.1002/admi.201701370 by CAS-XIAN INSTITUTION OPTICS PRECISION MECHANICS, Wiley Online Library on [09/11/2025]. See the Terms and Conditions (https://onlinelibrary.com/doi/10.1002/admi.201701370 by CAS-XIAN INSTITUTION OPTICS PRECISION MECHANICS, Wiley Online Library on [09/11/2025]. See the Terms and Conditions (https://onlinelibrary.com/doi/10.1002/admi.201701370 by CAS-XIAN INSTITUTION OPTICS PRECISION MECHANICS.

nditions) on Wiley Online Library for rules of use; OA articles are governed by the applicable Creative Commons

www.advmatinterfaces.de

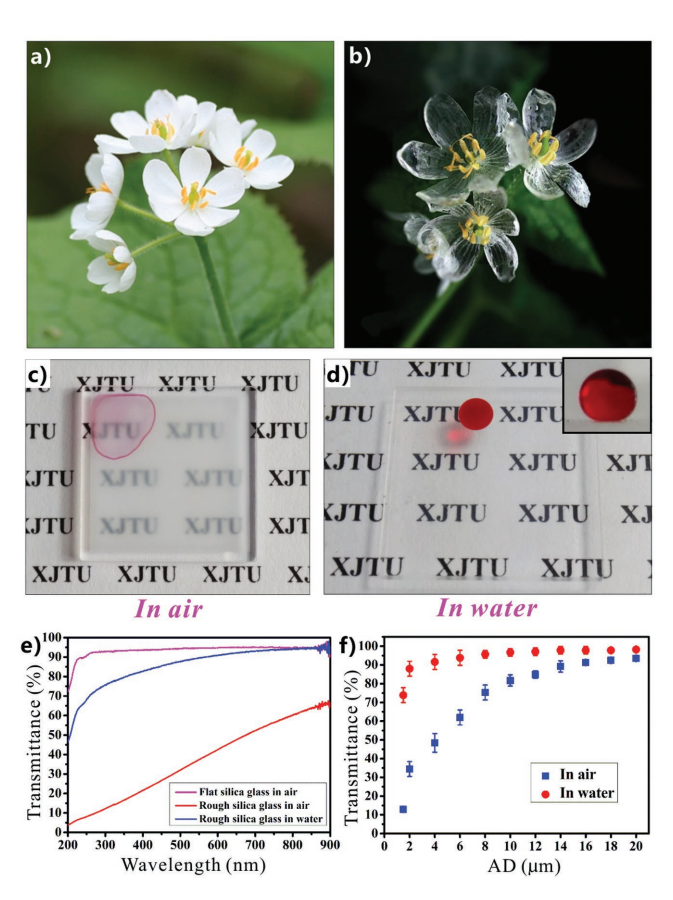


**Figure 17.** Good transparency of the underwater superoleophobic silica glass surface after femtosecond laser ablation. Photos of the petals of *D. grayi*: a) in a sunny day and b) in the rain. Photos of the laser-treated silica glass sheet on a piece of paper in different environment: c) in air and d) in water. e) UV–vis spectra of the rough silica glass in a water medium compared to the in-air rough silica glass and the in-air flat silica glass. f) The transmittance of the silica glass (both in water and in air) after being ablated by the femtosecond laser at different parameters. The increase of AD from 1.5 to 20  $\mu$ m means that the scanning speed increases from 1.5 to 20  $\mu$ m. Reproduced with permission.  $^{[108]}$  Copyright 2015, Royal Society of Chemistry.

silica glass surfaces that are ablated with the scanning speed larger than 4 mm s $^{-1}$  and the shift of the scanning lines larger than 4  $\mu$ m are above 90% in water.

Such excellent transparency is inseparable from the presence of water environment. At the interface of two different medium with the refractive indexes of  $n_1$  and  $n_2$ , respectively, the reflectance,  $R_{12}$ , can be described as<sup>[196]</sup>

$$R_{12} = \left(\frac{n_1 - n_2}{n_1 + n_2}\right)^2 \tag{6}$$

This equation reveals that the smaller reflectance occurs if these two media have closer refractive indices. There are numerous examples of this principle. For example, the ground glass sheet will not be seen and look like "disappear" when it is dipped into water. The femtosecond laser generated nanoscale rough structure of the silica glass surface can be completely wetted by water after the immersion of the sample in water, resulting in that the glass/air interface is replaced by the

glass/water interface. Because of the closer refractive indexes between water (n=1.33) and silica glass ( $n\approx 1.46$ ) than that between air (n=1) and silica glass, the Mie scattering and the reflectance decrease dramatically when the light beams pass through the in-water laser structured silica glass, endowing the rough surface with well transparency. [58,197] In fact, how does the rough superoleophobic silica glass sheet become transparent after being immersed in water is the same as the phenomenon that the D. grayi's petals turn to transparent in the rain.

## 3.5. Durable Underwater Superoleophobicity

Most of the underwater superoleophobic materials easily lose their superwettability in harsh environment because the surface microstructure or the surface chemical composition may be destroyed. Chemical and physical durability is a crucial requirement for the artificial underwater superoleophobic surfaces to be well applied in harsh environments, which will endow the surfaces with many important applications in industrial production and our daily life, such as industrial waste oil cleanup and cell engineering. [89,93,96,108]

Yong et al. found that the femtosecond-laser-ablated silica glass surface also showed underwater superoleophobicity and very low oil adhesion even the sample was dipped into acid or alkaline aqueous solutions. In different aqueous solutions with the pH ranging from 1 to 13, all of the measured OCAs of the oil droplet on the structured surface are maintained above 150°, while all the measured OSAs are no more than 10°. Such chemical stability greatly expands the application scope of the femtosecond-laser-induced underwater superoleophobic surfaces.

Yin et al. generated periodic nanoripple structures on stainless steel mesh surface by femtosecond laser ablation and obtained a superhydrophilic and underwater superoleophobic mesh. [198] The sandpaper abrasion test of the rough mesh was performed by dragging the mesh with a 100 g weight pressing on its upper surface to move forward 10 cm along the horizontal direction and return back on sandpaper. It is found that the femtosecond-laserablated mesh maintains its ultralow oil-adhesive underwater superoleophobicity after 15 abrasion cycles. Even after 30 cycles, the OCA is still higher than 140°, and the OSA is smaller than 20°. Such antiabrasion property is important for the underwater superoleophobic stainless steel mesh to achieve long-term practical service life.

## 4. Functions and Applications

## 4.1. Antioil Contamination

The antioil ability of the ultralow oil-adhesive underwater superoleophobic microstructures can endow the sample surface with excellent antioil-contamination function in a water medium. Figure 18a shows the image of a glass sample whose surface composes two different domains. [98] One is the untreated flat domain and another is the femtosecond-laserablated domain showing underwater superoleophobicity. A contamination experiment was performed by Yong et al. [98] The hybrid glass sheet was first immersed into water.

nditions) on Wiley Online Library for rules of use; OA articles are governed by the applicable Creative Commons

www.advmatinterfaces.de

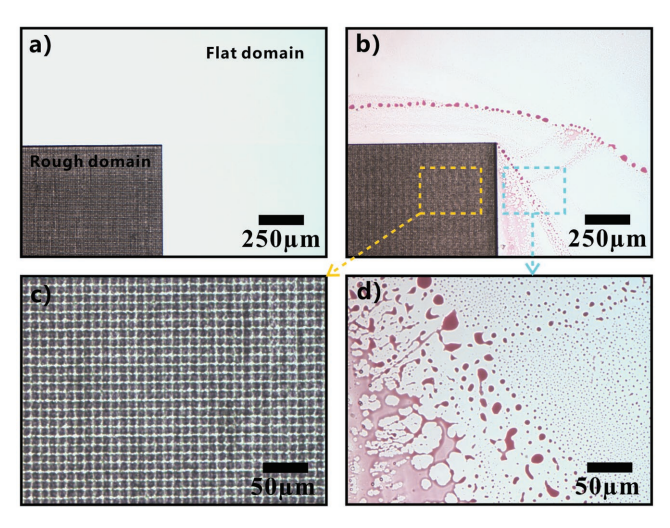


Figure 18. Underwater antioil-contamination ability of the underwater ultralow oil-adhesive superoleophobic surface compared to ordinary surface. a) Optical microscope photograph of the hybrid glass surface that composes two different domains: the flat bare domain and the femtosecond laser-induced rough domain. The laser-treated glass surface shows underwater superoleophobicity and ultralow adhesion to oil droplet. b–d) Optical microscope images of the sample surface after suffered from underwater oil contamination: c) high-magnification image of the laser-treated domain and d) high-magnification image of the flat untreated domain. The oil was dyed with Sudan III and showed red color for observation. Reproduced with permission. [98] Copyright 2015, Springer.

The dyed oil (red color) was used as the pollutant and scattered on the sample surface, covering both the flat and the structured domains. Then, the glass sheet was taken out of water. By investigating through an optical microscopy, it is found that both the flat area and the laser structured region are very clean before being polluted (Figure 18a). After oil contamination, the nonstructured domain is seriously polluted because a high number of red spots and patterns are observed to adhere to this area (Figure 18b,d). By contrast, the laser structured domain is still clean and remains its original color, without any red imprint on it (Figure 18b,c). The comparison result reveals that the femtosecond-laser-induced underwater superoleophobic surfaces with low oil adhesion have great antioil-contamination ability in water. It also should be noticed that the antioil-contamination ability of the underwater superoleophobic surface only occurs in a water medium. If the glass sample is polluted by oil in air, the whole sample (no matter the untreated domain or the laser structured domain) will be contaminated.

Many optical devices working in water are easily contaminated by oils, grease, and microorganism, limiting their use. Yong et al. have taken inspiration from fish scales and skeleton flowers to make a transparent underwater surface that stays clean by repelling oil. By using femtosecond laser ablation to create rough nanostructures on a silica glass surface, the resultant surface combines both properties of transparent and repelling oil when in water. Such underwater transparent superoleophobic surface will have applications in biology and underwater optics, including in diving goggles, oil-proof windows for underwater cameras, and even imageable substrates for biologically active cells or tissues.

#### 4.2. Oil Droplet Manipulation

The technology for manipulating small liquid droplet has a wide range of applications such as liquid transportation, droplet-based microreactors, in-situ analysis, lab on chips, and droplet positioning. [99,100,199-202] However, the use of common precise mechanical microcomponents (e.g., microchannel, micropump, and microvalve) to control and transport microdroplets suffers from high cost, cumbersome equipment, and much reagent droplet loss caused by droplet wetting and pinning. [87] Based on the superhydrophobic/superoleophobic substrate with controllable liquid adhesion, some alternative ways to manipulate microdroplets have been proposed. [23,84,88,98,101,133,203]

After the formation of different hierarchical rough microstructures on glass slide surfaces by femtosecond laser ablation, the resultant surface shows superoleophobicity in water.<sup>[98]</sup> Furthermore, the adhesion of the surface to an oil droplet ranges from very low to ultrahigh. The ability of the ultrahigh oil-adhesive superoleophobic surface for transporting a small underwater oil droplet from an underwater superoleophobic surface to an ordinary oleophobic surface was demonstrated by Yong et al. [98] As shown in Figure 19a, a small oil droplet was placed on an underwater superoleophobic substrate (A-surface) with low oil adhesion in a water medium (Step 1). By used as a "mechanical hand," a sheet (B-surface) showing both underwater superoleophobicity and ultrahigh oil adhesion was lowered down until it just touched this oil droplet (Step 2). Next, when the B-surface was lifted up, the oil droplet would adhere to the B-surface and be picked up by the "mechanical hand" because of the stronger adhesion between the B-surface and the droplet (Step 3). The B-surface was further moved above a weak oleophobic substrate (C-surface) with higher oil adhesion than B-surface (Step 4). After the B-surface was lowered down again to let the hanging oil droplet in contact with the C-surface (Step 5) and then was lifted up, the oil droplet was detached from B-surface and adhered to the C-surface (Step 6). As a result, the underwater oil droplet was transferred from A-surface to C-surface by using B-surface. In addition, there is almost no volume loss of the oil droplet in the whole transportation process because of a very small contact area between the oil droplet and the superoleophobic "mechanical hand." By using the above transporting process, the fusion of two small oil droplets can be further achieved, as shown in Figure 19b. Two different oil droplets were previously placed on A-surface and C-surface, respectively, in a water medium. The B-surface was moved to pick the oil droplet that was on the A-surface up. Then, the oil droplet hanging from the B-surface was transported to touch another oil droplet that was on the C-surface. These two droplets would coalesce to a new bigger one as long as they contacted with each other.

Huo et al. designed a hybrid surface which is composed of half ultralow oil-adhesive area and half ultrahigh oil-adhesive area by selective femtosecond laser ablation.<sup>[172]</sup> When the substrate was slightly tilted and an underwater oil droplet was dripped onto the low oil-adhesive part, the oil droplet would roll off freely. As shown in Figure 19c, the droplet would sharply stop once it is in contact with the ultrahigh oil-adhesive part. Finally, the oil droplet was firmly pinned on the setting area (ultrahigh oil-adhesive part). Therefore, no-loss oil capture on a specific location was achieved by such hybrid underwater superoleophobic surface.

21967350, 2018, 7, Downloaded from https://advanced

com/doi/10.1002/admi.201701370 by CAS-XIAN INSTITUTION OPTICS PRECISION MECHANICS, Wiley Online Library on [09/11/2025]. See the Terms

conditions) on Wiley Online Library for rules of use; OA articles are governed by the applicable Creative Commons

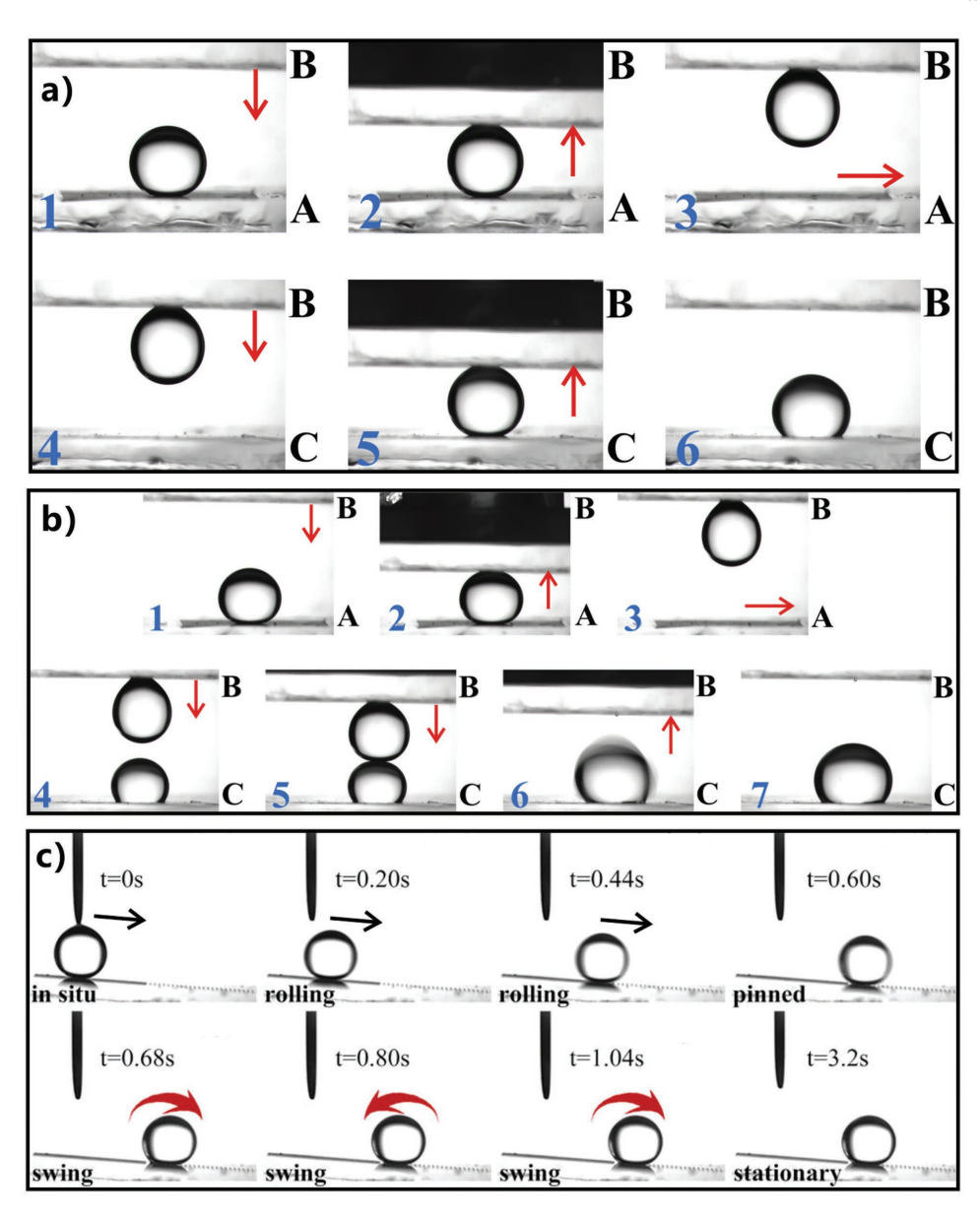


Figure 19. Oil droplet manipulation in a water medium by using the underwater superoleophobic surfaces with different oil adhesion. a) Using an underwater superoleophobic surface (B-surface) with ultrahigh adhesion to transport a small oil droplet from an ultralow oil-adhesive superoleophobic surface (A-surface) to an ordinary underwater oleophobic surface (C-surface). b) Fusion of two small oil droplets by using the similar transporting process in (a). a,b) Reproduced with permission. [98] Copyright 2015, Springer. c) No-loss oil capture based on a hybrid surface which composes half ultralow oil-adhesive area (left part) and half ultrahigh oil-adhesive area (right part). All of the processes were performed in a water medium. Reproduced with permission. [172] Copyright 2017, American Chemical Society.

By using the ultrahigh oil-adhesive superoleophobic sheet as a "mechanical hand," the underwater oil droplet can only be transport from a substrate with ultralow oil adhesion to the target surface with higher oil adhesion. In fact, such transportation process is not reversible, that is, once the oil droplet is picked up, it will not be put back its initial location. Yong et al. further reported a simple way to reversibly transport a small underwater oil droplet between two underwater superoleophobic surfaces by adjusting the density of surrounding water solution.<sup>[99]</sup> As shown in Figure 20a, two paralleled femtosecond-laser-ablated silicon sheets (Figure 7) that show

underwater superoleophobicity are put in a glass container filled with water. The below sheet is fixed but the upper one can be controlled to continuously move up and down. Figure 20b depicts the whole in situ transportation process. A small oil droplet (1,2-dichloroethane, density of 1.26 g cm<sup>-3</sup>) was placed onto the below sheet in advance (Step 1). The underwater superoleophobicity of the rough silicon surface leaded to a spherical shape of this oil droplet. The upper sheet was first lowered down to be just in contact with the top point of this oil droplet (Step 2). Then, the density of the aqueous solution was artificially increased by slowly adding sugar water (density of

www.advmatinterfaces.de

21967350, 2018, 7, Downloaded from https://advanced.onlinelibrary.wiley.com/doi/10.1002/admi.201701370 by CAS-XIAN INSTITUTION OPTICS PRECISION MECHANICS, Wiley Online Library on [09/11/2025]. See the Terms

nditions) on Wiley Online Library for rules of use; OA articles are governed by the applicable Creative Commons

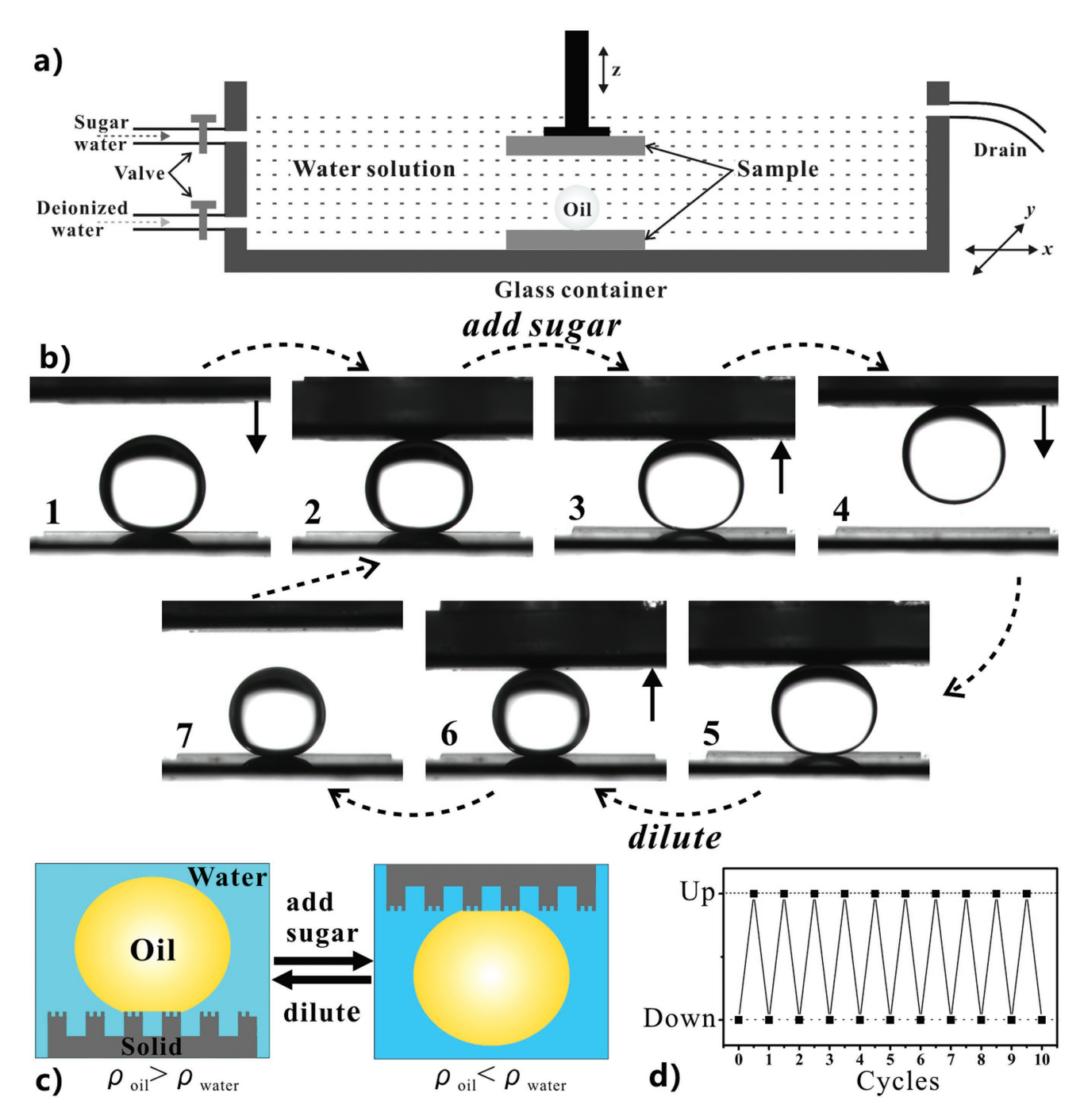


Figure 20. In situ transportation of small oil droplet between two paralleled underwater superoleophobic sheets by switching the density of surrounding water solution. a) Schematic drawing of the setup. b) The process of picking an underwater oil droplet up by the upper sheet (Steps 1–4) and putting it back to the below sheet (Steps 4–7). When the density of aqueous solution was increased to higher than that of oil, underwater oil droplet could be picked up by the upper sheet. By contrast, the oil droplet could be put down when the density of aqueous solution was decreased to lower than that of oil again. c) Schematic diagram of the in situ transportation of oil droplet. d) Repeatability of reversibly transporting an underwater oil droplet. Reproduced with permission. [99]

1.52 g cm<sup>-3</sup>) into the container. This process made the density of surrounding water solution to become higher than that of oil after some time (Step 3). At this moment, the buoyancy force acting on the oil droplet was larger than its own gravity. If the upper sheet was lifted up, the oil droplet would leave the below sheet away and rise up following the upper sheet, like being

picked up by a hand (Step 4). Compared to this "picking up" process, the oil droplet can also be put back its original location through an opposite operation. The upper sheet was lowered down again to let the hanging oil droplet just contact with the below sheet (Step 5). Next, the aqueous solution was diluted by deionized water until the density of aqueous solution switched

www.advancedsciencenews.com



www.advmatinterfaces.de

to be much smaller than that of oil (Step 6). At present, the buoyancy force was lower than the gravity of the oil droplet. If the upper sheet was lifted up, the oil droplet would detach from the upper sheet and finally stayed on the below sheet (Step 7). By switching the density of surrounding water solution, the oil droplet can even be reversibly "picked up" from the below sheet and then "put down" in a water medium (Figure 20c). Such in situ transportation of oil droplet can be repeated many cycles without any oil loss (Figure 20d). The above-mentioned methods for no-loss oil droplet transportation have many potential applications such as droplet-based microreactor, in situ chemical analysis, in situ detection, cell engineering, and so on. [99,100,199–202]

### 4.3. Oil/Water Separation

The frequency of oil-spill accidents and the increasing amounts of industrial wastewater discharges have caused severe water pollution, not only resulting in huge economic losses but also threatening the ecological system. Oil/water separation technology has become a global challenge to protect the environment and reduce economic loss. [26-30,204] Recently, various meshes or porous materials with special wettability (such as superhydrophobicity or superoleophobicity) have been successfully used in oil/water separating application owning to the different interface effect between water and oil.[80,94,129,130,188,205-215] In 2004, Feng et al. fabricated a superhydrophobic-superoleophilic mesh by coating polytetrafluoroethylene (PTFE) rough microstructures onto stainless steel mesh surface. [216] When the mixture of water and oil was poured onto the as-prepared mesh, oil could quickly permeate through the mesh for the superoleophilicity, but water was intercepted by the mesh because of the superhydrophobicity. Therefore, the oil/water mixture was separated by the superhydrophobic mesh. Similarly, Yong et al. simply created rough microstructures on PTFE sheet surface by femtosecond laser ablation.<sup>[217]</sup> The structured surface showed both superhydrophobicity and superoleophilicity. After the formation of penetrating through-microholes array by a subsequent mechanical drilling process, the as-prepared microporous PTFE sheet was endowed with great ability of oil/water separation. In 2011, Xue et al. proposed a new way to achieve oil/water separation by using underwater superoleophobic meshes.<sup>[211]</sup> After coating a porous stainless steel mesh with nanostructured hydrogel, the mesh finally showed underwater superoleophobicity. The prewetted resultant mesh was able to remove water from the mixture of water and oil.

Li et al. prepared a micropore-array-structured ultrathin aluminum foil by femtosecond laser perforating and successfully used it to achieve oil/water separation. [218] After the ultrathin aluminum foil with the thickness of  $\approx\!25~\mu m$  being irradiated by femtosecond laser pluses (pulse energy of 50  $\mu J$ , 4–5 pluses per ablated point) using the typical point-by-point process, a uniform micropores array was generated on the sample surface (**Figure 21a**). Every ablated point finally resulted in a single micropore with the diameter of  $\approx\!2.4~\mu m$ . The rim of the micropore is also dotted with rough nanostructures (Figure 21b). From the transmission microscope photograph, it is demonstrated that all of the laser-induced micropores are

through the aluminum foil because the backlight can pass through the micropores (inset of Figure 21a). Further experiment reveals that the diameter of the femtosecond-laser-induced micropores can be simply designed by using different laser pulse energy and pulse numbers, changing from 2.4 to 32 µm. The untreated flat aluminum foil is inherently hydrophilic with an intrinsic WCA of 53.9°. The sample become superhydrophilic (WCA =  $7.8^{\circ}$ ) after the formation of the microscale pores and the surrounding nanostructures by femtosecond laser perforating. When the micropore-structured foil is immersed in water, excellent underwater superoleophobicity is presented. The measured OCAs are 153.5° to an octane droplet (Figure 21c) and 153.1° to a 1,2-dichloroethane droplet (Figure 21d) on the resultant substrate. The opposite wettabilities for water and oil are able to endow the porous aluminum foil with oil/water separating function. As shown in Figure 21e, the aluminum foil with the pore diameter of 8.2 μm and the spacing of 60 μm is used as the separating membrane and is horizontally sandwiched between a glass tube and a conical flask. After the mixture of 10 mL water and 10 mL octane being poured into the upper tube, the separation process starts, which is driven by just gravity. The water can quickly permeate through the aluminum foil for the superhydrophilicity. By contrast, the underwater superoleophobicity of the aluminum foil do not allow octane to pass through, achieving oil/water separation (Figure 21e,g). This separation process can finish within 13 s. However, this kind of separator is just able to separate the mixture of water and light oils (their density is small than that of water). Regarding the mixture of water and heavy oils, another separating device is designed. A tube with a side opening is used as the skeleton, and the side opening is covered with microporestructured aluminum foil. When the oil/water mixture is poured into this tube, the water in the mixture can flow through the side foil wall but the oil is intercepted (Figure 21f,h). As a result, the mixture of water and heavy oils is separated, driven by just gravity effect. The separation efficiency of the designed device is measured up to 99% for no matter the light oils or the heavy oils.

Similar to Li et al.'s method, [218] Ye et al. prepared a microholes array on titanium foil by femtosecond laser drilling process.[219] It was found that some micro/nanoscale rough structures formed surrounding the microholes and their chemical composition was TiO2 because the Ti substrate was oxidized by laser during the formation of the microholes. Such rough porous titanium foil shows superhydrophilicity in air and excellent superoleophobicity in water. When an underwater oil droplet is placed on the structured titanium foil, the OCA of the droplet is as high as  $159.6 \pm 2.2^{\circ}$ , and the oil droplet can roll off the surface once the titanium foil is slightly tilted. By using the prewetted microholes-structured titanium foil as separating membrane, oil/water separation was successfully achieved, with a separation efficiency exceeding 99%. The high separation efficiency still kept after 40 cycles of recycling or after suffering from erosion by corrosive solutions. Furthermore, even the femtosecond-lasertreated titanium foil was polluted with oil, its underwater superoleophobicity and separating ability could be recovered by UV illumination because the degradation of intrusive organic pollutants could be catalyzed by the laser-induced TiO2 layer with UV light.[220,221]

21967350, 2018, 7, Downloaded from https://advanced.onlinelibrary.wiley.com/doi/10.1002/admi.201701370 by CAS-XIAN INSTITUTION OPTICS PRECISION MECHANICS, Wiley Online Library on [09/11/2025]. See the Terms

nditions) on Wiley Online Library for rules of use; OA articles are governed by the applicable Creative Commons

www.advmatinterfaces.de

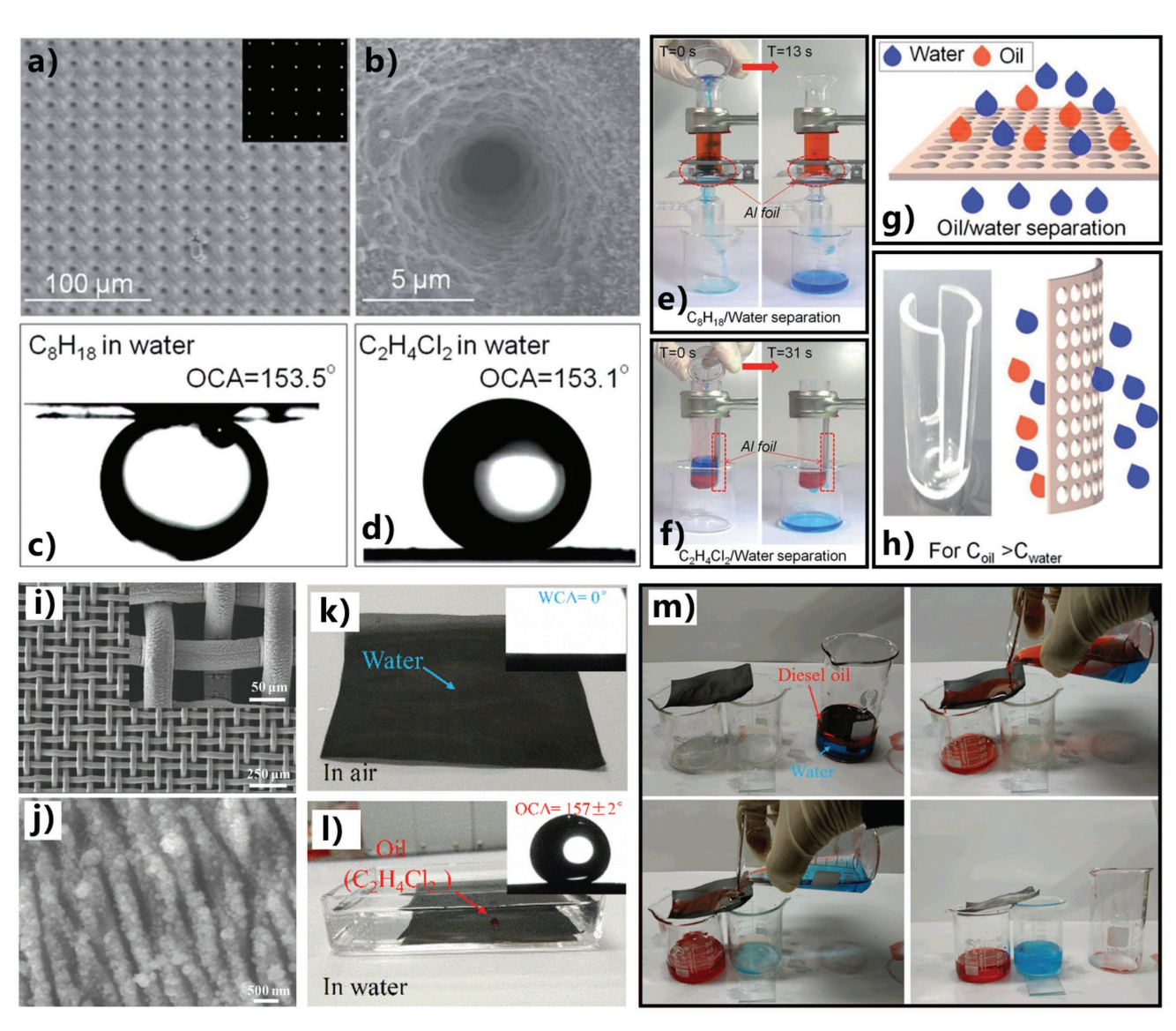


Figure 21. Oil/water separation based on the femtosecond-laser-induced a-h) micropore-structured aluminum foil and i-m) nanoripple-structured stainless steel mesh. a) SEM image of the femtosecond laser-treated aluminum foil with uniform micropores array. The inset is the transmission microscope photograph in the case of a backlight behind the micropore-structured aluminum foil. b) SEM image of a single micropore at high magnification. Shapes of c) an octane droplet and d) a 1,2-dichloroethane droplet on the resultant aluminum foil surface in a water medium. e) Separating the mixture of water and light oil (octane) by the porous aluminum foil. f) Separating the mixture of water and heavy oil (1,2-dichloroethane) by the porous aluminum foil. g) Schematic diagram of separating the mixture of water and light oils. h) Equipment and schematic diagram of separating the mixture of water and heavy oils. a-h) Reproduced with permission. [218] Copyright 2016, Royal Society of Chemistry. i,j) Surface microstructure of the femtosecond laser-treated stainless steel mesh. k) In-air superhydrophobicity of the resultant mesh. l) Underwater superoleophobicity of the resultant mesh. The insets show the shapes of the water and oil droplets. m) Process of oil/water separation by the femtosecond-laser-treated stainless steel mesh. i-m) Reproduced with permission. [198] Copyright 2017, Royal Society of Chemistry.

Yin et al. directly built periodic nanoripples on stainless steel mesh (300 mesh) surface by the one-step femtosecond laser ablation, as shown in Figure 21i,j.[198] The period of the nanoripples ranges from 500 and 800 nm and their height is about 130 nm. The surface of the uniform periodic nanoripples is further covered by abundant nanoparticles with the size of tens to hundreds nanometers (Figure 21j). Compared to the weak hydrophobicity of the bare mesh, the water wettability of the stainless steel mesh turns to superhydrophilicity with a WCA of nearly 0° after femtosecond laser treatment (Figure 21k). Figure 21l shows an oil droplet (1,2-dichloroethane) on the nanoripplestructured mesh surface in a water medium. The droplet maintains an approximately spherical shape and shows underwater superoleophobicity. The measured OCA is 157.2  $\pm$  2 $^{\circ}$  (inset of Figure 211) while the OSA is as low as 5°. The ability of the laser-ablated stainless steel mesh for separating oil/water mixtures was demonstrated, as shown in Figure 21m. The treated mesh was previously wetted by water. Then, it was placed over two breakers with different heights, ensuring an ≈25° tilted angle of the mesh. When the mixture of water (blue color, dyed



www.advmatinterfaces.de

with methylene) and diesel (red color, dyed with Sudan III) was poured onto the mesh, water could permeate through the femtosecond-laser-induced rough stainless steel mesh for the superhydrophilicity and fall into the right beaker. On the contrary, because of the excellent underwater superoleophobicity and ultralow oil adhesion of the femtosecond-laser-ablated mesh, diesel flowed over the resultant mesh and finally poured into the left beaker by gravity. Therefore, the water and oil were successfully separated. The surface microstructures, wettability, and separation effect of the as-prepared mesh showed no obvious variation even though the laser induced rough mesh suffered from repeated friction on sandpaper and the immersion in corrosive solutions (1 M HCl, 1 M NaOH, and 10 wt% NaCl). Such mechanical and chemical stability confirm that the separating function of the laser-treated mesh is valid even in harsh conditions.

Recently, Sun et al. reported the fabrication of a Janus wire mesh toward its applications in efficient oil/water separation. [222] Laser-induced periodic surface structure was first formed on both sides of a copper mesh by femtosecond laser processing. Then, one side of the mesh was modified with fluorosilane and another side was modified with graphene oxide, endowing the two sides of the Janus mesh with inverse wettabilities. That is, one side of the resultant mesh shows superhydrophobicity and superoleophilicity in air, and the other side shows in-air superhydrophilicity and underwater superoleophobicity. This Janus mesh can separate the mixture of water with not only light oil but also heavy oil.

#### 4.4. Oil Droplets Patterning

If a heterogeneous pattern composes of underwater superoleophobic area and weak oleophobic or oleophilic area, the pattern can be used to restrict oil droplets to specific area (i.e., weak oleophobic or oleophilic area) because of the strong oil-repellent ability of the superoleophobic area. Therefore, different shapes and arrays of small oil droplets can be obtained on the pattered structure in water.

Lens is one of the most basic optical components, which is widely applied in light convergence and divergence, imaging, photography, optical microscopy, and optical communication.[223-226] Femtosecond laser microfabrication has been very successful in fabricating various microlens arrays.[170,227-236] For example, Chen et al. develops a technology named "femtosecond laser wet etching" and have prepared different microlens structure on the silica glass, K9 glass, and silicon surfaces.[170,227-235] The sample surface is first irradiated by femtosecond laser pulses through a point-by-point process to generate a series of separated microholes on the surface. By the subsequent chemical etching, the microholes are further enlarged to smooth curved craters with the diameter of several tens micrometers. The resultant smooth curved craters can be acted as a concave microlens array. Wu et al. fabricated a closed-packed, high-NA microlens array with aspheric profiles by the technology of femtosecond-laser-induced two-photon polymerization.<sup>[236]</sup> Yong et al. reported a fast, low-cost strategy for obtaining high-quality and large-area concave microlens arrays by high-speed scanning of femtosecond laser pulses.<sup>[170]</sup>

Every laser pulse could generate a single concave microlens, and over 2.78 million microlenses were formed on a PDMS surface within 50 min. Compared to the above solid microlens, liquid lens is also an important type of lenses and has some crucial applications due to the advantages of economical materials, simple preparation process, and easily tunable focal length. [237–241] The formation of liquid lens is based on the surface tension of a liquid droplet (e.g., water) to form a partsphere shape on a solid substrate. The liquid droplet is used as a convex lens.

Recently, Yong et al. put forward a new strategy to fabricate a liquid lens array based on an underwater oleophobic—superoleophobic heterogeneous pattern. The design principle is shown in Figure 22a. A circle array pattern was previously created on a glass slide surface by femtosecond laser selectively ablating specific area. The rest of the ablated region forms a periodic untreated uniform circles array. As shown in Figure 22b, the as-prepared pattern is composed of untreated flat circles and surrounding laser-induced rough

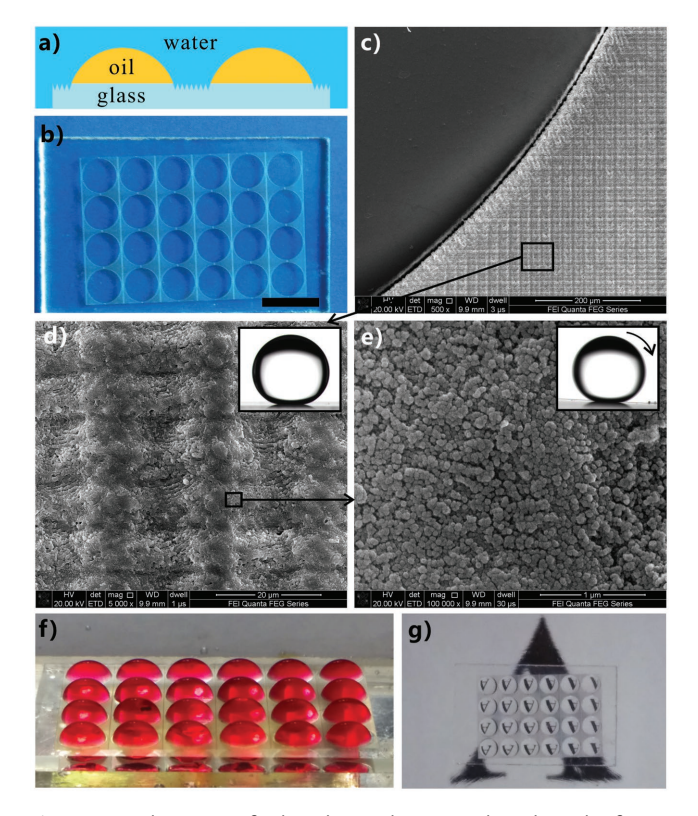


Figure 22. Fabrication of a liquid microlens array based on the femto-second-laser-induced underwater oleophobic–superoleophobic heterogeneous pattern. a) Design principle. b) Digital photograph of the as-prepared circle array pattern. The pattern is composed of two different areas: untreated circles and the surrounding femtosecond-laser-ablated area. Scale bar: 5 mm. c–e) SEM image of the patterned microstructure: c) the boundary between the flat circles and the surrounding laser-induced rough area and d,e) the microstructure of the laser-ablated area under high magnification. Inset in (d): shape of an underwater oil droplet on the entire rough glass slide surface. Inset in (e): underwater oil droplet rolling on the entire laser-ablated surface. f) Photograph of the fabricated liquid lens array. g) Imaging ability of the as-prepared microlens array. Reproduced with permission. [105] Copyright 2015, Royal Society of Chemistry.

21967350, 2018, 7, Downloaded from https://advanced.onlinelibrary.wiley.com/doi/10.1002/admi.201701370 by CAS-XIAN INSTITUTION OPTICS PRECISION MECHANICS, Wiley Online Library on [09/11/2025]. See the Terms

nditions) on Wiley Online Library for rules of use; OA articles are governed by the applicable Creative Commons

www.advmatinterfaces.de

microstructures. A sharp boundary exists between the circles and their surrounding area (Figure 22c). The flat glass surface shows inherent weak oleophobicity with OCA of  $121 \pm 3^{\circ}$  in water. The glass surface after femtosecond laser ablation is characterized as nanoparticle-coated rough ridge-like microstructure (Figure 22d,e). Underwater superoleophobicity is exhibited by the laser-generated rough microstructure. In water, oil (chloroform) droplet on the rough glass surface has an OCA of  $160.5 \pm 2^{\circ}$  (inset of Figure 22d) and an OSA of  $1^{\circ}$  (inset of Figure 22e). Therefore, the designed pattern is indeed a heterogeneous structure, which composes of both oleophobic circles and surrounding underwater superoleophobic areas. When the sample was immersed in water and oil droplets were dripped onto every circular area, the oil droplets would be locked to the circles, resulting in an oil droplets array. An energy barrier exists at the boundary between the untreated circles and surrounding laser-ablated domain because of their different wettabilities. [106,189] The oil droplets are hindered by such energy barrier from spreading to the laser-ablated area, thereby are restricted to the untreated circles (Figure 22a). The oil droplet spontaneously formed a spherical crown shape by surface tension. The curved interface between the oil and water phases can act as a liquid lens. In fact, the resultant liquid lens is a converging lens because the refractive index of the part-sphere oil (chloroform) droplet is larger than that of the surrounding water medium. The optical parameters of the liquid lens

depend on the shape of the formed oil droplets which can easily be designed by the diameter of the untreated circles and the used oil volume. Evaporation problem of common liquid lenses is avoided because the oil droplet is in a water medium.<sup>[242]</sup> In addition, the oil droplets of the lenses array can be located very close, without worrying that they merge together. This is because the underwater superoleophobic region has strong isolation effect toward the oil droplet. Figure 22f shows the photography of the as-prepared liquid lenses array. When a paper with a black letter "A" is placed below the lens plane, an array of inverted real images can be clearly observed, demonstrating that the liquid microlens array possesses excellent imaging ability (Figure 22g).

#### 4.5. Guiding the Movement of Oil droplets

Femtosecond-laser-ablated silicon surface and nickel surface shows excellent superoleophobicity in water while the bare flat surfaces generally exhibit underwater weak oleophobicity. [101,104] By utilizing the oil wettability contrast between the laser-ablated and untreated areas, some hollow pathways that are like a flat canal for guiding the movement of oil droplets were designed by Wu and co-workers, as shown in **Figure 23**.[101,104] The pathway is composed of a bare flat middle path without any treatment and two laser-induced rough thick lines on the two sides of the

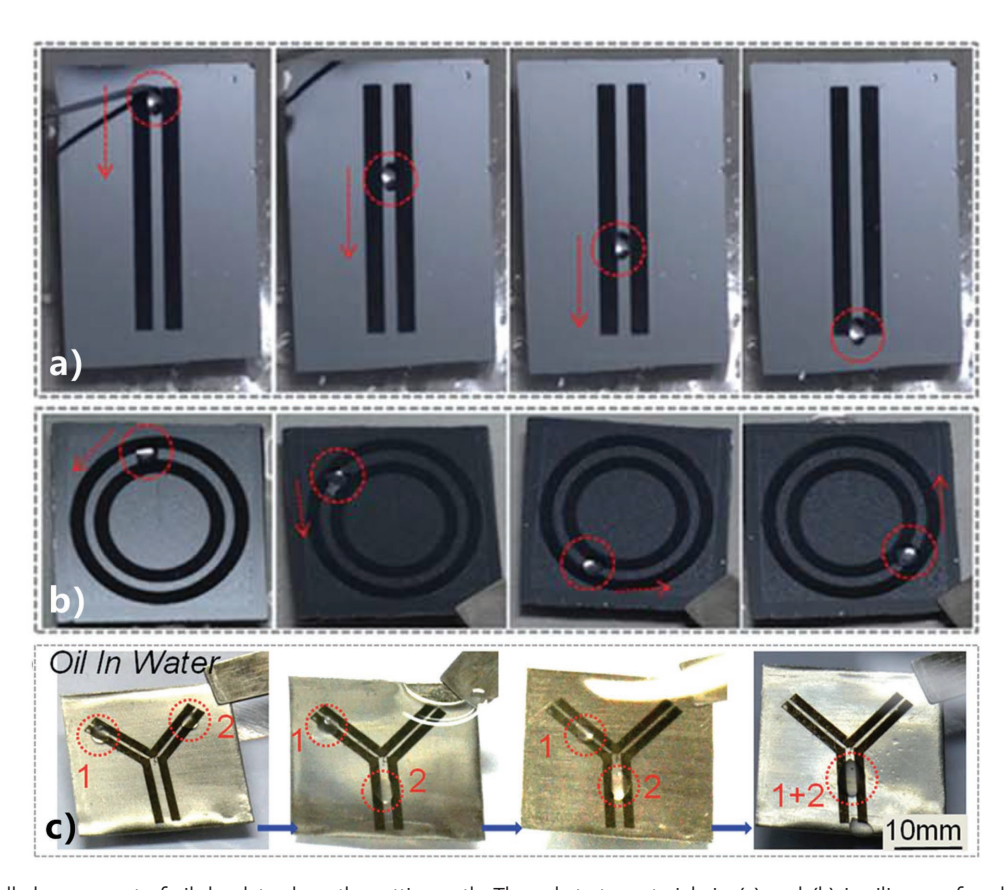


**Figure 23.** Controlled movement of oil droplets along the setting path. The substrate materials in (a) and (b) is silicon wafer while in (c) is nickel sheet. a,b) Reproduced with permission.<sup>[104]</sup> Copyright 2016, Royal Society of Chemistry. c) Reproduced with permission.<sup>[104]</sup> Copyright 2015, Royal Society of Chemistry.

ditions) on Wiley Online Library for rules of use; OA articles are governed by the applicable Creative Commons



www.advmatinterfaces.de

untreated middle path. In water, oil droplets are limited to the middle path by the energy barrier resulted from the underwater superoleophobicity of the two side structured lines. As a result, the oil droplets can only move along the setting path. For an oil droplet on a straight pathway in water, the oil droplet can move from one end to the other without loss as long as the sample surface is slightly tilted (Figure 23a). The oil droplet also can be controlled to move in circles on a circular orbit (Figure 23b). In addition, a hollow "Y"-shaped pathway is prepared. Oil droplets are put on the both ends of the "Y"-shaped path in advance. With the sheet inclined slightly, these two droplets will travel along the "Y"-shaped line and finally merge together once they contact with each other (Figure 23c).

### 4.6. Floating on Oil Surface

The microdevice that can float and move on liquid surfaces has many potential applications in aquatic microrobot and liquid environment monitoring. Zhou et al. demonstrated that the femtosecond laser-induced underwater superoleophobic metal thin sheet can steadily float on a water/oil (up/below) interface. [173] For the comparison, they fabricated three different metal sheets: sample 1 has two unprocessed surface; both side of sample 2 show in-air superhydrophilicity and underwater superoleophobicity; and sample 3 has two superhydrophobic sides. After the immersion of these three samples in water-oil solution and shaking the container, the locations of the samples were carefully monitored. As shown in Figure 24a,d, it can be seen that sample 3 could float on the water surface because

of the enhanced buoyancy resulting from "superhydrophobic edge/surface effect."<sup>[175]</sup> In contrast, sample 1 directly sank to the bottom of the beaker due the density of metal is larger than that of water and oil. Regarding the sample 2, when it was put on the water surface, it would immediately sink down but finally stop and reside at the water/oil interface for its double-faced underwater superoleophobicity. Even when shaken strongly, sample 2 still stably floated on the oil surface with unchangeable position (Figure 24b,c,e–g).

## 4.7. Underwater Military Devices

Military submarines, amphibious aircraft, and tanks are usually sent on a stealthy mission even in harsh environments, such as oil-polluted water. To be on the safe side, they must avoid contamination and be not discovered in shallow seas or in air by radar. After femtosecond laser ablation, Yin et al. formed corallike microstructures on the stainless steel surface, as shown in Figure 25a,b.[243] There are a large number of cavities with the diameter of 3-10 um randomly covering on the treated surface. The sidewalls and edges of the microcavities are also decorated with plentiful protrusions which come from the conglomeration of nanoparticles ejected from the ablated area. [244–246] The laserinduced rough stainless steel surface has remarkable underwater superoleophobicity and ultralow adhesion to oil droplets. The measured OCAs are above 150° for different oils and the OSAs are ≈1°, indicating that this surface has strong antioil ability in water environment. Figure 25c,d shows the spectral reflectance of the bare flat stainless steel and the laser-induced

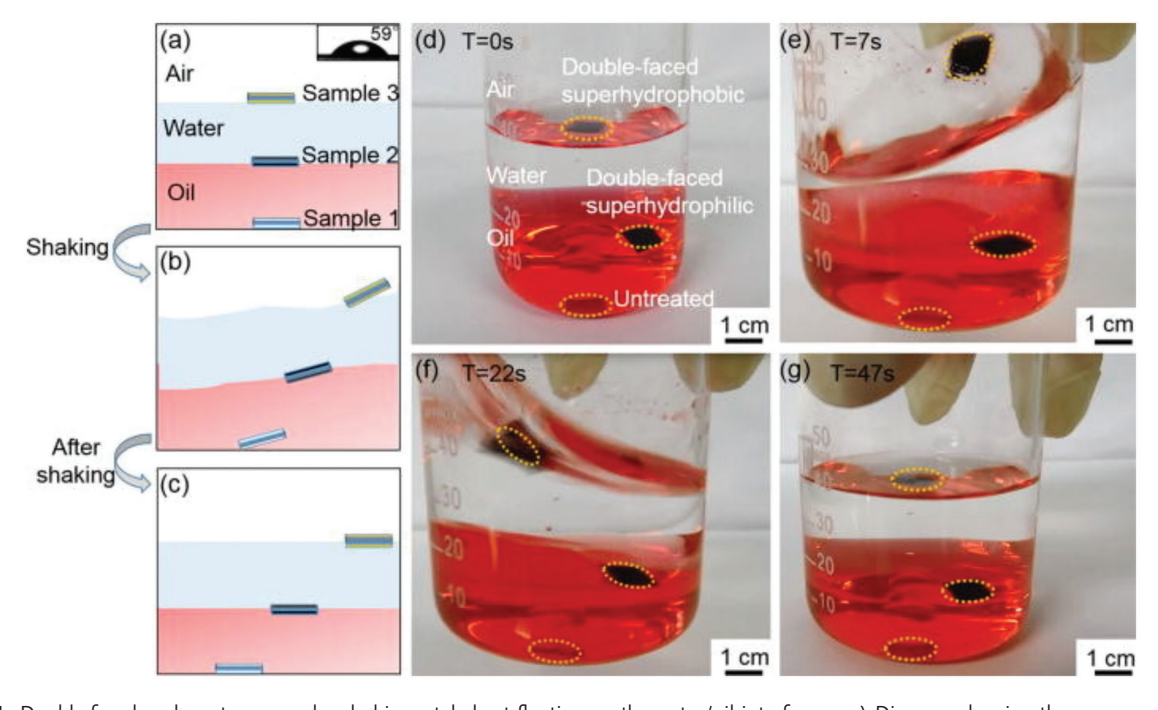


Figure 24. Double-faced underwater superoleophobic metal sheet floating on the water/oil interface. a–c) Diagram showing the process of shaking the container. d–g) Placing the unprocessed, underwater superoleophobic and superhydrophobic metal sheets in the water/oil container, respectively. It is clear to see that the three samples are located at different positions because of different wettabilities. Sample 1: Unprocessed sheet; sample 2: double-faced superhydrophobic sheet. Reproduced with permission. [173] Copyright 2017, American Institute of Physics.

21967350, 2018. 7, Downloaded from https://advanced.onlinelibrary.wiley.com/doi/10.1002/admi.201701370 by CAS-XIAN INSTITUTION OPTICS PRECISION MECHANICS, Wiley Online Library on [09/11/2025]. See the Terms and Conditions (https://onlinelibrary.com/doi/10.1002/admi.201701370 by CAS-XIAN INSTITUTION OPTICS PRECISION MECHANICS, Wiley Online Library on [09/11/2025]. See the Terms and Conditions (https://onlinelibrary.com/doi/10.1002/admi.201701370 by CAS-XIAN INSTITUTION OPTICS PRECISION MECHANICS, Wiley Online Library on [09/11/2025]. See the Terms and Conditions (https://onlinelibrary.com/doi/10.1002/admi.201701370 by CAS-XIAN INSTITUTION OPTICS PRECISION MECHANICS, Wiley Online Library on [09/11/2025]. See the Terms and Conditions (https://onlinelibrary.com/doi/10.1002/admi.201701370 by CAS-XIAN INSTITUTION OPTICS PRECISION MECHANICS, Wiley Online Library on [09/11/2025]. See the Terms and Conditions (https://onlinelibrary.com/doi/10.1002/admi.201701370 by CAS-XIAN INSTITUTION OPTICS PRECISION MECHANICS, Wiley Online Library on [09/11/2025]. See the Terms and Conditions (https://onlinelibrary.com/doi/10.1002/admi.201701370 by CAS-XIAN INSTITUTION OPTICS PRECISION MECHANICS, Wiley Online Library on [09/11/2025]. See the Terms and Conditions (https://onlinelibrary.com/doi/10.1002/admi.201701370 by CAS-XIAN INSTITUTION OPTICS PRECISION MECHANICS.

conditions) on Wiley Online Library for rules of use; OA articles are governed by the applicable Creative Commons

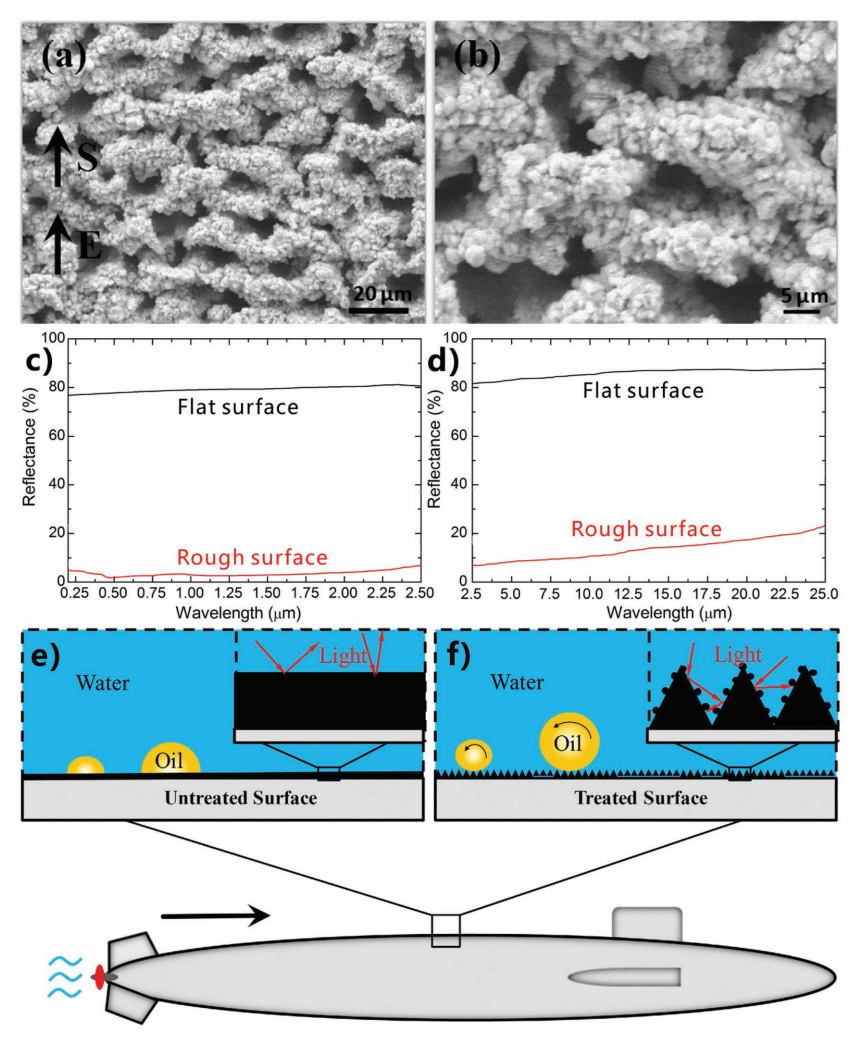


Figure 25. Enhanced absorption over a broadband wavelength of the femtosecond-laser-ablated stainless steel surface. a,b) SEM images of the laser-induced microstructure. c,d) Spectral reflectance of the bare flat surface and the laser-induced coral-like structured stainless steel surface over the broadband wavelength ranging from 0.2 to 25 μm. e,f) Schematic of the potential application of the femtosecond-laser-treated metal surface on a submarine: the effect of e) an untreated flat metal surface and f) a laser-induced rough metal surface on the oil wettability and light reflectance in a water medium. Reproduced with permission.<sup>[243]</sup> Copyright 2016, Springer Nature.

coral-like stainless steel surface over the broadband wavelength ranging from 0.2 to 25 µm. Compared to the polished flat surface (before laser treatment) with a reflectance above 80%, the femtosecond-laser-ablated surface has a very low reflectance of less than 8% in the UV-infrared range of 0.2-2.5 µm (Figure 25c) and less than 25% in the broad wavelength range of 0.2-2.5 µm (Figure 25d), respectively. The result indicates that the as-prepared stainless steel surface has strongly enhanced absorption and great antireflective performance. The properties of antioil and the enhanced absorption over a broadband wavelength allow the femtosecond-laser-induced rough metal surfaces to become a candidate for the shell of underwater military devices. Figure 25e depicts the oil wettability and light reflectance performance of an untreated flat metal surface in a water medium. Large contact area between oil and the flat

substrate surface results in a high oil adhesion, thereby oil impurities can firmly adhere to the surface of the underwater military devices, contaminating or even corroding the metal shell over time. When the flat metal surface is irradiated by external light or wave, a strong oscillation of the high free-electron density occurs. As a result, the light will be efficiently radiated back to the surrounding medium. By contrast, underwater oil droplets can maintain a spherical shape and easily roll off on the rough underwater superoleophobic metal surface, that is, the oil droplets are very difficult to stay on such metal surface (Figure 25f). Meanwhile, because of the dual effect of the laser-induced microcavities and nanoparticles, most incident light beams will be trapped by these microstructures, leading to a significant decrease in reflectance. [247-250]

## 5. Conclusions and Future Outlook

The development of superoleophobic surfaces is an area of significant academic and industrial interest because of the wide range of applications. Taking advantages of negligible heat-affected zone, no-contact process, precise ablation threshold, and high resolution, femtosecond laser microfabrication has been proven to be a powerful tool for controlling the wettability of a solid surface. Specially, this technology is better at the design of complicated and subtle wetting surfaces compared to the traditional micromachining methods. In this review, we systematically summarize the application of the technology of the femtosecond laser microfabrication in the field of preparing underwater superoleophobic materials. Based on the design principle of "from in-air superhydrophilicity to underwater superoleophobicity," various underwater superoleophobic surfaces have been fabricated by combining the femto-

second-laser-induced microstructures and a hydrophilic chemical composition. The fabrication, characteristics, functions, and important applications of these underwater superoleophobic surfaces are introduced respectively. The underwater superoleophobicity is widely achieved on the surfaces of silicon wafers, glasses, metals, and even polymers by simple femtosecond laser ablation. Different functional superoleophobic surfaces with the additional properties such as controllable oil adhesion, anisotropic oil wettability, good transparency, and durability are also developed. In addition, some examples of the early practical applications of the femtosecond-laser-induced underwater superoleophobic surfaces are illustrated in the last part.

Currently, as the research of femtosecond-laser-induced underwater superoleophobicity is still at an early stage, there still exist many development problems which worried industry.

21967350, 2018, 7, Downloaded from https://advanced.onlinelibrary.wiley.com/doi/10.1002/admi.201701370 by CAS-XIAN INSTITUTION OPTICS PRECISION MECHANICS, Wiley Online Library on [09/11/2025]. See the Terms and Conditions (https://onlinelibrary.wiley.com/terms-

and-conditions) on Wiley Online Library for rules of use; OA articles are governed by the applicable Creative Commons

www.advancedsciencenews.com



www.advmatinterfaces.de

First and foremost, the processing efficiency is required to be improved and perfected toward industrializing because the current machining process is relatively time-consuming. Highpower laser system and more efficient scanning manner (e.g., automatic parallel processing) are eagerly awaited. Second, since the single underwater superoleophobicity does not fully satisfy the needs of practical application, the preparation of the underwater superoleophobic surfaces with multiple functions and even smart properties (respond to external stimulus) will become the major trend in this research field. Last but not least, the proven applications of the as-prepared underwater superoleophobic materials are still limited since this research direction is now at the "toddler stage" of development. More potential applications should be developed in the next several years. It could be expected that the combination of the advanced features of femtosecond laser microfabrication and underwater superoleophobicity would lead to an increasing interest in this area. Overall, we believe that an exciting future in the synthesis and commercialization of underwater superoleophobic surfaces will be witnessed since an ever-increasing number of scientists and engineers have been devoted to the design and fabrication of such surfaces.

## Acknowledgements

This work was supported by the National Key Research and Development Program of China under Grant No. 2017YFB1104700, the National Science Foundation of China under Grant Nos. 51335008 and 61475124, the NSAF under Grant No. U1630111, China Postdoctoral Science Foundation under Grant No. 2016M600786, and the Collaborative Innovation Center of Suzhou Nano Science and Technology. This article is part of the *Advanced Materials Interfaces* Hall of Fame article series, which highlights the work of top interface and surface scientists.

#### **Conflict of Interest**

The authors declare no conflict of interest.

## **Keywords**

antioil, femtosecond laser microfabrication, laser ablation, superhydrophilicity, underwater superoleophobicity

Received: October 22, 2017 Revised: January 24, 2018 Published online: March 12, 2018

- [1] M. Liu, S. Wang, L. Jiang, Nat. Rev. Mater. 2017, 2, 17036.
- [2] J. L. Yong, F. Chen, Q. Yang, J. Huo, X. Hou, Chem. Soc. Rev. 2017, 46, 4168.
- [3] Y. Tian, B. Su, L. Jiang, Adv. Mater. 2014, 26, 6872.
- [4] L. Wen, Y. Tian, L. Jiang, Angew. Chem., Int. Ed. 2015, 54, 3387.
- [5] B. Su, Y. Tian, L. Jiang, J. Am. Chem. Soc. 2016, 138, 1727.
- [6] H. Bellanger, T. Darmanin, E. T. De Givenchy, F. Guittard, Chem. Rev. 2014, 114, 2694.
- [7] Y. Lee, S.-H. Park, K.-B. Kim, J.-K. Lee, Adv. Mater. 2007, 19, 2330.
- [8] F. Chen, D. Zhang, Q. Yang, J. Yong, G. Du, J. Si, F. Yun, X. Hou, ACS Appl. Mater. Interfaces 2013, 5, 6777.

- [9] J.-N. Wang, Y.-L. Zhang, Y. Liu, W. Zheng, L. P. Lee, H.-B. Sun, Nanoscale 2015, 7, 7101.
- [10] J. L. Yong, F. Chen, Q. Yang, X. Hou, Soft Matter 2015, 11, 8897.
- [11] X. Yao, Y. Song, L. Jiang, Adv. Mater. 2011, 23, 917.
- [12] K. Liu, X. Yao, L. Jiang, Chem. Soc. Rev. 2010, 39, 3240.
- [13] K. Liu, L. Jiang, Annu. Rev. Mater. Res. 2012, 42, 231.
- [14] T. Darmanin, F. Guittard, J. Mater. Chem. A 2014, 2, 16319.
- [15] P. Roach, N. J. Shirtcliffe, M. I. Newton, Soft Matter 2008, 4, 224.
- [16] Y. Shi, Z. Guo, Nanoscale 2015, 7, 5922.
- [17] G. Wen, Z. Guo, W. Liu, Nanoscale 2017, 9, 3338.
- [18] C.-H. Xue, J.-Z. Ma, J. Mater. Chem. A 2013, 1, 4146.
- [19] S. Nishimoto, B. Bhushan, RSC Adv. 2013, 3, 671.
- [20] P. Ragesh, V. A. Ganesh, S. V. Nair, A. S. Nair, J. Mater. Chem. A 2014, 2, 14773.
- [21] L. Shen, B. Wang, J. Wang, J. Fu, C. Picart, J. Ji, ACS Appl. Mater. Interfaces 2012, 4, 4476.
- [22] X. Liu, Y. Liang, F. Zhou, W. Liu, Soft Matter 2012, 8, 2070.
- [23] J. L. Yong, F. Chen, Q. Yang, D. Zhang, G. Du, J. Si, F. Yun, X. Hou, J. Phys. Chem. C 2013, 117, 24907.
- [24] M. Wang, C. Chen, J. Ma, J. Xu, J. Mater. Chem. 2011, 21, 6962.
- [25] J. Li, Z. Jing, F. Zha, Y. Yang, Q. Wang, Z. Lei, ACS Appl. Mater. Interfaces 2014, 6, 8868.
- [26] Z. Xue, Y. Cao, N. Liu, L. Feng, L. Jiang, J. Mater. Chem. A 2014, 2, 2445.
- [27] B. Wang, W. Liang, Z. Guo, W. Liu, Chem. Soc. Rev. 2015, 44, 336.
- [28] Z. Chu, Y. Feng, S. Seeger, Angew. Chem., Int. Ed. 2015, 54, 2328.
- [29] R. K. Gupta, G. J. Dunderdale, M. W. England, A. Hozumi, J. Mater. Chem. A 2017, 5, 16025.
- [30] J. L. Yong, F. Chen, Q. Yang, H. Bian, G. Du, C. Shan, J. Huo, Y. Fang, X. Hou, Adv. Mater. Interfaces 2016, 3, 1500650.
- [31] S. Pan, A. K. Kota, J. M. Mabry, A. Tuteja, J. Am. Chem. Soc. 2013, 135, 578.
- [32] X. Gao, X. Yan, X. Yao, L. Xu, K. Zhang, J. Zhang, B. Yang, L. Jiang, Adv. Mater. 2007, 19, 2213.
- [33] M. Nosonovsky, V. Hejazi, ACS Nano 2012, 6, 8488.
- [34] M. J. Kreder, J. Alvarenga, P. Kim, J. Aizenberg, Nat. Rev. Mater. 2016, 1, 15003.
- [35] J. Lv, Y. Song, L. Jiang, J. Wang, ACS Nano 2014, 8, 3152.
- [36] F. Shi, J. Niu, J. Liu, F. Liu, Z. Wang, X. Q. Feng, X. Zhang, Adv. Mater. 2007, 19, 2257.
- [37] G. McHale, N. J. Shirtcliffe, C. R. Evans, M. I. Newton, Appl. Phys. Lett. 2009, 94, 064104.
- [38] H. Dong, M. Cheng, Y. Zhang, H. Wei, F. Shi, J. Mater. Chem. A 2013, 1, 5886.
- [39] G. McHale, M. I. Newton, N. J. Shirtcliffe, Soft Matter 2010, 6, 714.
- [40] J. Genzer, K. Efimenko, Biofouling 2006, 22, 339.
- [41] E. P. Ivanova, J. Hasan, H. K. Webb, G. Gervinskas, S. Juodkazis, V. K. Truong, A. H. Wu, R. N. Lamb, V. A. Baulin, G. S. Watson, J. A. Watson, D. E. Mainwaring, R. J. Crawford, *Nat. Commun.* 2013, 4, 2838.
- [42] E. Stratakis, A. Ranella, C. Fotakis, Biomicrofluidics 2011, 5, 13411.
- [43] A. Ranella, M. Barberoglou, S. Bakogianni, C. Fotakis, E. Stratakis, *Acta Biomater.* **2010**, *6*, 2711.
- [44] R. P. Garrod, L. G. Harris, W. C. Schofield, J. Mcgettrick, L. J. Ward, D. O. Teare, J. P. Badyal, *Langmuir* 2007, 23, 689.
- [45] L. Zhai, M. C. Berg, F. C. Cebeci, Y. Kim, J. M. Milwid, M. F. Rubner, R. E. Cohen, *Nano Lett.* 2006, 6, 1213.
- [46] A. R. Parker, C. R. Lawrence, Nature 2001, 414, 33.
- [47] S. Wang, T. Wang, P. Ge, P. Xue, S. Ye, H. Chen, Z. Li, J. Zhang, B. Yang, *Langmuir* 2015, 31, 4032.
- [48] G. H. Kim, B.-H. Lee, H. Im, S.-B. Jeon, D. Kim, M.-L. Seol, H. Hwang, Y.-K. Choi, RSC Adv. 2016, 6, 41914.
- [49] J. Songok, M. Tuominen, H. Teisala, J. Haapanen, J. Makela, J. Kuusipalo, M. Toivakka, ACS Appl. Mater. Interfaces 2014, 6 20060

21967350, 2018, 7, Downloaded from https://advanc

com/doi/10.1002/admi.201701370 by CAS-XIAN INSTITUTION OPTICS PRECISION MECHANICS, Wiley Online Library on [09/11/2025]. See the Terms

applicable Creative



- [50] A. Ghosh, R. Ganguly, T. M. Schutzius, C. M. Megaridis, Lab Chip 2014. 14. 1538.
- [51] A. Vitale, M. Quaglio, S. L. Marasso, A. Chiodoni, M. Cocuzza, R. Bongiovanni, Langmuir 2013, 29, 15711.
- [52] K. W. Kwon, S. S. Choi, S. H. Lee, B. Kim, S. N. Lee, M. C. Park, P. Kim, S. Y. Hwang, K. Y. Suh, Lab Chip 2007, 7, 1461.
- [53] T. i. Kim, K. Y. Suh, Soft Matter 2009, 5, 4131.
- [54] H. X. Ren, X. Chen, X. J. Huang, M. Im, D. H. Kim, J. H. Lee, J. B. Yoon, N. Gu, J. H. Liu, Y. K. Choi, Lab Chip 2009, 9, 2140.
- [55] T. Jiang, Z. Guo, W. Liu, J. Mater. Chem. A 2015, 3, 1811.
- [56] K. Liu, Y. Tian, L. Jiang, Prog. Mater. Sci. 2013, 58, 503.
- [57] D. Tian, X. Zhang, Y. Tian, Y. Wu, X. Wang, J. Zhai, L. Jiang, J. Mater. Chem. 2012, 22, 19652.
- [58] X. Deng, L. Mammen, H. J. Butt, D. Vollmer, Science 2012, 335, 67.
- [59] K. Tsujii, T. Yamamoto, T. Onda, S. Shibuichi, Angew. Chem., Int. Ed. 1997, 36, 1011.
- [60] Y. Huang, M. Liu, J. Wang, J. Zhou, L. Wang, Y. Song, L. Jiang, Adv. Funct. Mater. 2011, 21, 4436.
- [61] Z. Chu, S. Seeger, Chem. Soc. Rev. 2014, 43, 2784.
- [62] G. Whyman, E. Bormashenko, Langmuir 2011, 27, 8171.
- [63] A. Tuteja, W. Choi, M. Ma, J. M. Mabry, S. A. Mazzella, G. C. Rutledge, G. H. Mckinley, R. E. Cohen, Science 2007, 318, 1618.
- [64] R. Hensel, C. Neinhuis, C. Werner, Chem. Soc. Rev. 2016, 45, 323.
- [65] J. L. Yong, F. Chen, Q. Yang, Y. Fang, J. Huo, X. Hou, Chem. Commun. 2015, 51, 9813.
- [66] T. Liu, C. Kim, Science 2014, 346, 1096.
- [67] A. K. Kota, Y. Li, J. M. Mabry, A. Tuteja, Adv. Mater. 2012, 24, 5838.
- [68] A. Ahuja, J. A. Taylor, V. Lifton, A. A. Sidorenko, T. R. Salamon, E. J. Lobaton, P. Kolodner, T. N. Krupenkin, Langmuir 2008, 24, 9.
- [69] A. Tuteja, W. Choi, J. M. Mabry, G. H. Mckinley, R. E. Cohen, Proc. Natl. Acad. Sci. USA 2008, 25, 18200.
- [70] L. Yuan, T. Wu, W. Zhang, S. Ling, R. Xiang, X. Gui, Y. Zhu, Z. Tang, J. Mater. Chem. A 2014, 2, 6952.
- [71] M. Im, H. Im, J. Lee, J. Yoon, Y. Choi, Soft Matter 2010, 6, 1401.
- [72] H. Zhao, K. Law, V. Sambhy, Langmuir 2011, 27, 5927.
- [73] M. Liu, S. Wang, Z. Wei, Y. Song, L. Jiang, Adv. Mater. 2009, 21, 665.
- [74] D. Wu, S. Wu, Q. Chen, S. Zhao, H. Zhang, J. Jiao, J. A. Piersol, J. Wang, H. Sun, L. Jiang, Lab Chip 2011, 11, 3873.
- [75] L. Lin, M. Liu, L. Chen, P. Chen, J. Ma, D. Han, L. Jiang, Adv. Mater. 2010, 22, 4826.
- [76] Y. Cai, L. Lin, Z. Xue, M. Liu, S. Wang, L. Jiang, Adv. Funct. Mater. 2014, 24, 809.
- [77] Q. Cheng, M. Li, Y. Zheng, B. Zheng, B. Su, S. Wang, L. Jiang, Soft Matter 2011, 7, 5948.
- [78] M. Li, B. Wang, L. Heng, L. Jiang, Adv. Mater. Interfaces 2014, 1, 1400298.
- [79] X. Liu, J. Gao, Z. Xue, L. Chen, L. Lin, L. Jiang, S. Wang, ACS Nano **2012**. *6*. 5614.
- [80] F. Zhang, W. Zhang, Z. Shi, D. Wang, J. Jin, L. Jiang, Adv. Mater. 2013, 25, 4192.
- [81] Z. Cheng, H. Lai, Y. Du, K. Fu, R. Hou, N. Zhang, K. Sun, ACS Appl. Mater. Interfaces 2013, 5, 11363.
- [82] X. Liu, J. Zhou, Z. Xue, J. Gao, J. Meng, S. Wang, L. Jiang, Adv. Mater. 2012, 24, 3401.
- [83] H. Wang, Z. Guo, Appl. Phys. Lett. 2014, 104, 183703.
- [84] Z. Cheng, H. Liu, H. Lai, Y. Du, K. Fu, C. Li, J. Yu, N. Zhang, K. Sun, ACS Appl. Mater. Interfaces 2015, 7, 20410.
- [85] Z. Cheng, C. Ding, H. Liu, Y. Zhu, L. Jiang, Nanoscale 2014, 6, 190.
- [86] Z. Wang, L. Zhu, W. Li, H. Liu, ACS Appl. Mater. Interfaces 2013, 5, 10904.
- [87] C. Ding, Y. Zhu, M. Liu, L. Feng, M. Wan, L. Jiang, Soft Matter **2012**, 8, 9064.
- [88] E. Zhang, Z. Cheng, T. Lv, L. Li, Y. Liu, Nanoscale 2015, 7, 19293.

- [89] E. Zhang, Z. Cheng, T. Lv, L. Y. Qian, Y. Liu, J. Mater. Chem. A **2015**. 3, 13411.
- [90] M. Liu, X. Liu, C. Ding, Z. Wei, Y. Zhu, L. Jiang, Soft Matter 2011, 7, 4163.
- [91] B. Wang, Z. Guo, Chem. Commun. 2013, 49, 9416.
- [92] L. Li, Z. Liu, Q. Zhang, C. Meng, T. Zhang, J. Zhai, J. Mater. Chem. A 2015, 3, 1279.
- [93] J. Li, L. Yan, H. Li, W. Li, F. Zha, Z. Lei, J. Mater. Chem. A 2015, 3. 14696.
- [94] D. Ge, L. Yang, C. Wang, E. Lee, Y. Zhang, S. Yang, Chem. Commun. 2015, 51, 6149.
- [95] M. A. Gondal, M. S. Sadullah, M. A. Dastageer, G. H. McKinley, D. Panchanathan, K. K. Varanasi, ACS Appl. Mater. Interfaces 2014, 6. 13422.
- [96] J. Li, D. Li, Y. Yang, J. Li, F. Zha, Z. Lei, Green Chem. 2016, 18, 541
- [97] Y. Liu, Y. Zhang, X. Fu, H. Sun, ACS Appl. Mater. Interfaces 2015, 7, 20980.
- [98] J. L. Yong, F. Chen, Q. Yang, U. Farooq, H. Bian, G. Du, X. Hou, Appl. Phys. A 2015, 119, 837.
- [99] J. L. Yong, Q. Yang, F. Chen, H. Bian, G. Du, U. Farooq, X. Hou, Adv. Mater. Interfaces 2015, 2, 1400388.
- [100] B. Su, S. Wang, Y. Song, L. Jiang, Soft Matter 2011, 7, 5144.
- [101] G. Li, Z. Zhang, P. Wu, S. Wu, Y. Hu, W. Zhu, J. Li, D. Wu, X. Li, J. Chu, RSC Adv. 2016, 6, 37463.
- [102] L. Chen, M. Liu, H. Bai, P. Chen, F. Xia, D. Han, L. Jiang, J. Am. Chem. Soc. 2009, 131, 10467.
- [103] J. L. Yong, F. Chen, Q. Yang, D. Zhang, U. Farooq, G. Du, X. Hou, J. Mater. Chem. A 2014, 2, 8790.
- [104] G. Li, Y. Lu, P. Wu, Z. Zhang, J. Li, W. Zhu, Y. Hu, D. Wu, J. Chu, J. Mater. Chem. A 2015, 3, 18675.
- [105] J. L. Yong, Q. Yang, F. Chen, G. Du, C. Shan, U. Farooq, J. Wang, X. Hou, RSC Adv. 2015, 5, 40907.
- [106] J. L. Yong, Q. Yang, F. Chen, D. Zhang, U. Farooq, G. Du, X. Hou, J. Mater. Chem. A 2014, 2, 5499.
- [107] J. L. Yong, F. Chen, Q. Yang, U. Farooq, X. Hou, J. Mater. Chem. A **2015**, 3, 10703.
- [108] J. L. Yong, F. Chen, Q. Yang, G. Du, C. Shan, H. Bian, U. Farooq, X. Hou, J. Mater. Chem. A 2015, 3, 9379.
- [109] D. Zhang, F. Chen, Q. Yang, J. L. Yong, H. Bian, Y. Ou, J. Si, X. Meng, X. Hou, ACS Appl. Mater. Interfaces 2012, 4, 4905.
- [110] J. L. Yong, F. Chen, Q. Yang, Y. Fang, J. Huo, J. Zhang, X. Hou, Adv. Mater. Interfaces 2017, 4, 1700552.
- [111] K. Sugioka, Y. Cheng, Appl. Phys. Rev. 2014, 1, 041303.
- [112] K. Sugioka, Y. Cheng, Light: Sci. Appl. 2014, 3, e149.
- [113] T. C. Chong, M. H. Hong, L. P. Shi, Laser Photonics Rev. 2010, 4,
- [114] A. Y. Vorobyev, C. Guo, Laser Photonics Rev. 2013, 7, 385.
- [115] T. Darmanin, F. Guittard, Mater. Today 2015, 18, 273.
- [116] M. Liu, Y. Zheng, J. Zhai, L. Jiang, Acc. Chem. Res. 2010, 3, 368.
- [117] B. Bhushan, Philos. Trans. R. Soc., A 2009, 367, 1445.
- [118] Y. Zhang, Q. Chen, Z. Jin, E. Kim, H. Sun, Nanoscale 2012, 4, 4858.
- [119] W. Barthlott, C. Neinhuis, Planta 1997, 202, 1.
- [120] V. Zorba, E. Stratakis, M. Barberoglou, E. Spanakis, P. Tzanetakis, S. H. Anastasiadis, C. Fotakis, Adv. Mater. 2008, 20, 4049.
- [121] X. Gao, L. Jiang, Nature 2004, 432, 36.
- [122] D. L. Hu, B. Chan, J. W. Bush, Nature 2003, 424, 663.
- [123] L. Feng, Y. Zhang, J. Xi, Y. Zhu, N. Wang, F. Xia, L. Jiang, Langmuir **2008**, 24, 4114.
- [124] L. Feng, S. Li, Y. Li, H. Li, L. Zhang, J. Zhai, Y. Song, B. Liu, L. Jiang, D. Zhu, Adv. Mater. 2002, 14, 1857.
- [125] D. Wu, J.-N. Wang, S.-Z. Wu, Q.-D. Chen, S. Zhao, H. Zhang, H.-B. Sun, L. Jiang, Adv. Funct. Mater. 2011, 21, 2927.
- [126] Y. Zheng, X. Guo, L. Jiang, Soft Matter 2007, 3, 178.
- [127] K. Liu, J. Du, J. Wu, L. Jiang, Nanoscale 2012, 4, 768.

21967350, 2018, 7, Downloaded from https://advanced.onlinelibrary.wiley.com/doi/10.1002/admi.201701370 by CAS-XIAN INSTITUTION OPTICS PRECISION MECHANICS, Wiley Online Library on [09/11/2025]. See the Terms

ditions) on Wiley Online Library for rules of use; OA articles are governed by the applicable Creative Commons

*A*DVANCED

- [128] Y. Cai, Q. Lu, X. Guo, S. Wang, J. Qiao, L. Jiang, Adv. Mater. 2015, 27, 4162.
- [129] X. Gao, L.-P. Xu, Z. Xue, L. Feng, J. Peng, Y. Wen, S. Wang, X. Zhang, Adv. Mater. 2014, 26, 1771.
- [130] K. He, H. Duan, G. Y. Chen, X. Liu, W. Yang, D. Wang, ACS Nano 2015, 9, 9188.
- [131] J. L. Yong, F. Chen, Q. Yang, D. Zhang, H. Bian, G. Du, J. Si, X. Meng, X. Hou, *Langmuir* 2013, 29, 3274.
- [132] J. Yang, H. Song, B. Chen, H. Tang, C. Li, RSC Adv. 2014, 4, 14227.
- [133] X. Yao, J. Guo, Y. Song, L. Jiang, Adv. Funct. Mater. 2011, 21, 4270.
- [134] S. Wang, L. Jiang, Adv. Mater. 2007, 19, 3423.
- [135] J. Li, X. Liu, Y. Ye, H. Zhou, J. Chen, J. Phys. Chem. C 2011, 115, 4726.
- [136] R. N. Wenzel, Ind. Eng. Chem. 1936, 28, 988.
- [137] A. B. D. Cassie, S. Baxter, Trans. Faraday Soc. 1994, 40, 546.
- [138] S. Tian, L. Li, W. Sun, X. Xia, D. Han, J. Li, C. Gu, Sci. Rep. 2012, 2, 511.
- [139] M. Liu, L. Jiang, Adv. Funct. Mater. 2010, 20, 3753.
- [140] K. Li, X. Zeng, H. Li, X. Lai, C. Ye, H. Xie, Appl. Surf. Sci. 2013, 279, 458
- [141] Z. Cheng, M. Du, H. Lai, N. Zhang, K. Sun, Nanoscale 2013, 5, 2776.
- [142] H. Y. Erbil, C. E. Cansoy, Langmuir 2009, 25, 14135.
- [143] D. Wu, Q.-D. Chen, L.-G. Niu, J.-N. Wang, J. Wang, R. Wang, H. Xia, H.-B. Sun, Lab Chip 2009, 9, 2391.
- [144] M. Y. Shen, C. H. Crouch, J. E. Carey, E. Mazur, Appl. Phys. Lett. 2004, 85, 5694.
- [145] J. Bonse, S. Baudach, J. Krüger, W. Kautek, M. Lenzner, Appl. Phys. A 2002, 74, 19.
- [146] D. J. Hwang, T. Y. Choi, C. P. Grigoropoulos, Appl. Phys. A 2004, 79, 605.
- [147] G. Daminelli, J. J. Krüger, W. Kautek, Thin Solid Films 2004, 467, 334.
- [148] M. Shen, J. E. Carey, C. H. Crouch, M. Kandyla, H. A. Stone, E. Mazur, *Nano Lett.* 2008, 8, 2087.
- [149] C. H. Crouch, J. E. Carey, M. Shen, E. Mazur, F. Y. Génin, Appl. Phys. A 2004, 79, 1635.
- [150] M. Y. Shen, C. H. Crouch, J. E. Carey, R. Younkin, E. Mazur, M. Sheehy, C. M. Friend, Appl. Phys. Lett. 2003, 82, 1715.
- [151] M. Zhou, H. F. Yang, B. J. Li, J. Dai, J. K. Di, E. L. Zhao, L. Cai, Appl. Phys. A 2009, 94, 571.
- [152] N. Bärsch, K. Körber, A. Ostendorf, K. H. Tönshoff, Appl. Phys. A 2003, 77, 237.
- [153] H. Imamoto, S. Kanehira, X. Wang, K. Kametani, M. Sakakura, Y. Shimotsuma, K. Miura, K. Hirao, Opt. Lett. 2011, 36, 1176.
- [154] B. C. Stuart, M. D. Feit, S. Herman, A. M. Rubenchik, B. W. Shore, M. D. Perry, Phys. Rev. B 1996, 53, 1749.
- [155] S. Baudach, J. Bonse, W. Kautek, Appl. Phys. A 1999, 69, S395.
- [156] C. B. Schaffer, A. Brodeur, J. F. García, E. Mazur, Opt. Lett. 2001, 26, 93
- [157] J. Krüger, M. Lenzner, S. Martin, M. Lenner, C. Spielmann, A. Fiedler, W. Kautek, Appl. Surf. Sci. 2003, 208–209, 233.
- [158] S. E. Kirkwood, A. C. van Popta, Y. Y. Tsui, R. Fedosejevs, Appl. Phys. A 2005, 81, 729.
- [159] A. Ben-Yakar, A. Harkin, J. Ashmore, R. L. Byer, H. A. Stone, J. Phys. D: Appl. Phys. 2007, 40, 1447.
- [160] S. H. Cho, W.-S. Chang, K.-R. Kim, J. W. Hong, Opt. Commun. 2009, 282, 1317.
- [161] K. K. Lee, P. R. Herman, T. Shoa, M. Haque, J. D. Madden, V. X. Yang, Adv. Mater. 2012, 24, 1243.
- [162] E. Fadeeva, V. K. Truong, M. Stiesch, B. N. Chichkov, R. J. Crawford, J. Wang, E. P. Ivanova, *Langmuir* 2011, 27, 3012.
- [163] K. Yin, J. A. Duan, X. Sun, C. Wang, Z. Luo, Appl. Phys. A 2015, 119, 69.

- [164] X. Zhang, H. Liu, X. Huang, H. Jiang, J. Mater. Chem. C 2015, 3, 3336.
- [165] J. L. Yong, F. Chen, M. Li, Q. Yang, Y. Fang, J. Huo, X. Hou, J. Mater. Chem. A 2017, 5, 25249.
- [166] J. L. Yong, Q. Yang, F. Chen, D. Zhang, H. Bian, Y. Ou, J. Si, G. Du, X. Hou, Appl. Phys. A 2013, 111, 243.
- [167] J. L. Yong, Q. Yang, F. Chen, D. Zhang, G. Du, H. Bian, J. Si, X. Hou, RSC Adv. 2014, 4, 8138.
- [168] J. L. Yong, Q. Yang, F. Chen, D. Zhang, G. Du, H. Bian, J. Si, F. Yun, X. Hou, Appl. Surf. Sci. 2014, 288, 579.
- [169] Y. Fang, J. Yong, F. Chen, J. Huo, Q. Yang, H. Bian, G. Du, X. Hou, Appl. Phys. A 2016, 122.
- [170] J. L. Yong, F. Chen, Q. Yang, G. Du, H. Bian, D. Zhang, J. Si, F. Yun, X. Hou, ACS Appl. Mater. Interfaces 2013, 5, 9382.
- [171] D. von der Linde, K. Sokolowski-Tinten, J. Bialkowski, *Appl. Surf. Sci.* 1997, 109, 1.
- [172] J. Huo, Q. Yang, F. Chen, J. Yong, Y. Fang, J. Zhang, L. Liu, X. Hou, Langmuir 2017, 33, 3659.
- [173] C. Zhou, G. Li, C. Li, Z. Zhang, Y. Zhang, S. Wu, Y. Hu, W. Zhu, J. Li, J. Chu, Z. Hu, D. Wu, L. Yu, Appl. Phys. Lett. 2017, 111, 141607.
- [174] J. Zhang, F. Chen, Q. Yang, J. Yong, J. Huo, Y. Fang, X. Hou, Appl. Phys. A 2017, 123, 594.
- [175] J. L. Yong, Q. Yang, F. Chen, D. Zhang, G. Du, J. Si, F. Yun, X. Hou, J. Micromech. Microeng. 2014, 24, 035006.
- [176] I. A. Larmour, S. E. J. Bell, G. C. Saunders, Angew. Chem. 2007, 119, 1740.
- [177] Y. Zhao, Y. Tang, X. Wang, T. Lin, Appl. Surf. Sci. 2010, 256, 6736
- [178] J. L. Yong, F. Chen, Y. Fang, J. Huo, Q. Yang, J. Zhang, X. Hou, Nanoscale 2018, 10, 3688.
- [179] H. Hillborg, J. F. Ankner, U. W. Gedde, G. D. Smith, H. K. Yasuda, K. Wikström, *Polymer* **2000**, *41*, 6851.
- [180] M. J. Hancock, K. Sekeroglu, M. C. Demirel, Adv. Funct. Mater. 2012, 22, 2223.
- [181] X. D. Zhao, H. M. Fan, X. Y. Liu, H. Pan, H. Y. Xu, Langmuir 2011, 27, 3224.
- [182] L. Chen, M. Liu, L. Lin, T. Zhang, J. Ma, Y. Song, L. Jiang, Soft Matter 2010, 6, 2708.
- [183] W. Li, G. Fang, Y. Li, G. Qiao, J. Phys. Chem. B 2008, 112, 7234.
- [184] F. Chen, D. Zhang, Q. Yang, X. Wang, B. Dai, X. Li, X. Hao, Y. Ding, J. Si, X. Hou, *Langmuir* 2011, 27, 359.
- [185] M. Morita, T. Koga, H. Otsuka, A. Takahara, *Langmuir* 2005, 21, 911
- [186] E. Me le, S. Girardo, D. Pisignano, Langmuir 2012, 28, 5312.
- [187] H. Zhao, K. Y. Law, Langmuir 2012, 28, 11812.
- [188] K. Li, J. Ju, Z. Xue, J. Ma, L. Feng, S. Gao, L. Jiang, *Nat. Commun.* **2013**, *4*, 2276.
- [189] J. L. Yong, F. Chen, Q. Yang, U. Farooq, H. Bian, G. Du, X. Hou, Appl. Phys. Lett. 2014, 105, 071608.
- [190] J. Y. Chung, J. P. Youngblood, C. M. Stafford, Soft Matter 2007, 3, 1163.
- [191] M. Gleiche, L. F. Chi, H. Fuchs, Nature 2000, 403, 173.
- [192] S. Neuhaus, N. D. Spencer, C. Padeste, ACS Appl. Mater. Interfaces 2012. 4, 123.
- [193] D. Zhang, F. Chen, Q. Yang, J. Si, X. Hou, Soft Matter 2011, 7, 8337.
- [194] S. Z. Wu, D. Wu, J. Yao, Q. D. Chen, J. N. Wang, L. G. Niu, H. H. Fang, H. B. Sun, *Langmuir* **2010**, *26*, 12012.
- [195] S. G. Park, J. H. Moon, H. C. Jeon, S.-M. Yang, Soft Matter 2012, 8, 4567.
- [196] S. Nishioka, M. Tenjimbayashi, K. Manabe, T. Matsubayashi, K. Suwabe, K. Tsukada, S. Shiratori, RSC Adv. 2016, 6, 47579.
- [197] P. A. Levkin, F. Svec, J. M. Frechet, Adv. Funct. Mater. 2009, 19, 1993.

21967350, 2018, 7, Downloaded from https://advanced.onlinelibrary.wiley.com/doi/10.1002/admi.201701370 by CAS-XIAN INSTITUTION OPTICS PRECISION MECHANICS, Wiley Online Library on [09/11/2025]. See the Terms

ditions) on Wiley Online Library for rules of use; OA articles are governed by the applicable Creative Commons

#### www.advmatinterfaces.de

- [198] K. Yin, D. Chu, X. Dong, C. Wang, J.-A. Duan, J. He, Nanoscale 2017, 9, 14229.
- [199] D. Wu, S. Z. Wu, Q. D. Chen, Y. L. Zhang, J. Yao, X. Yao, L. G. Niu, J. N. Wang, L. Jiang, H. B. Sun, Adv. Mater. 2011, 23, 545.
- [200] F. Xia, L. Jiang, Adv. Mater. 2008, 20, 2842.
- [201] T. Sun, G. Qing, Adv. Mater. 2011, 23, H57.
- [202] Y. L. Zhang, H. Xia, E. Kim, H.-B. Sun, Soft Matter 2012, 8, 11217.
- [203] Y. Zhao, J. Fang, H. Wang, X. Wang, T. Lin, Adv. Mater. 2010, 22, 707
- [204] C.-F. Wang, F.-S. Tzeng, H.-G. Chen, C.-J. Chang, Langmuir 2012, 28, 10015.
- [205] R. Du, Z. Zheng, N. Mao, N. Zhang, W. Hu, J. Zhang, Adv. Sci. 2015, 2, 1400006.
- [206] J. Y. Huang, S. H. Li, M. Z. Ge, L. N. Wang, T. L. Xing, G. Q. Chen, X. F. Liu, S. S. Al-Deyab, K. Q. Zhang, T. Chen, Y. K. Lai, J. Mater. Chem. A 2015, 3, 2825.
- [207] B. Li, L. Wu, L. Li, S. Seeger, J. Zhang, A. Wang, ACS Appl. Mater. Interfaces 2014, 6, 11581.
- [208] A. K. Kota, G. Kwon, W. Choi, J. M. Mabry, A. Tuteja, *Nat. Commun.* 2012, 3, 1025.
- [209] J. Song, S. Huang, Y. Lu, X. Bu, J. E. Mates, A. Ghosh, R. Ganguly, C. J. Varmalt, I. P. Parkin, W. Xu, C. M. Megaridis, ACS Appl. Mater. Interfaces 2014, 6, 19858.
- [210] C. Xue, Y. Li, J. Hou, L. Zhang, J. Ma, S. Jia, J. Mater. Chem. A 2015, 3, 10248.
- [211] Z. Xue, S. Wang, L. Lin, L. Chen, M. Liu, L. Feng, L. Jiang, Adv. Mater. 2011, 23, 4270.
- [212] Q. Wen, J. Di, L. Jiang, J. Yu, R. Xu, Chem. Sci. 2013, 4, 591.
- [213] Q. Liu, A. A. Patel, L. Liu, ACS Appl. Mater. Interfaces 2014, 6, 8996.
- [214] M. Tao, L. Xue, F. Liu, L. Jiang, Adv. Mater. 2014, 26, 2943.
- [215] S. Wang, X. Peng, L. Zhong, J. Tan, S. Jing, X. Cao, W. Chen, C. Liu, R. Sun, J. Mater. Chem. A 2015, 3, 8772.
- [216] L. Feng, Z. Zhang, Z. Mai, Y. Ma, B. Liu, L. Jiang, D. Zhu, Angew. Chem., Int. Ed. 2004, 43, 2012.
- [217] J. L. Yong, Y. Fang, F. Chen, J. Huo, Q. Yang, H. Bian, G. Du, X. Hou, Appl. Surf. Sci. 2016, 389, 1148.
- [218] G. Li, H. Fan, F. Ren, C. Zhou, Z. Zhang, B. Xu, S. Wu, Y. Hu, W. Zhu, J. Li, Y. Zeng, X. Li, J. Chu, D. Wu, J. Mater. Chem. A 2016, 4 18832
- [219] S. Ye, Q. Cao, Q. Wang, T. Wang, Q. Peng, Sci. Rep. 2016, 6, 37591.
- [220] K. Liu, M. Cao, A. Fujishima, L. Jiang, Chem. Rev. 2014, 114, 10044.
- [221] R. Wang, K. Hashimoto, A. Fujishima, M. Chikuni, E. Kojima, A. Kitamura, M. Shimohigoshi, T. Watanabe, *Nature* 1997, 388, 431.
- [222] Y.-Q. Liu, D.-D. Han, Z.-Z. Jiao, Y. Liu, H.-B. Jiang, X.-H. Wu, H. Ding, Y.-L. Zhang, H.-B. Sun, Nanoscale 2017, 9, 17933.
- [223] F. Chen, Z. Deng, Q. Yang, H. Bian, G. Du, J. Si, X. Xun, Opt. Lett. 2014, 39, 606.

- [224] Y. Sun, W. Dong, R. Yang, X. Meng, L. Zhang, Q. Chen, H. Sun, Angew. Chem., Int. Ed. 2012, 51, 1558.
- [225] X. Lee, I. Moreno, C. Sun, Opt. Express 2013, 21, 10612.
- [226] X. Li, Y. Ding, J. Shao, H. Tian, H. Liu, Adv. Mater. 2012, 24, OP165.
- [227] F. Chen, H. Liu, Q. Yang, X. Wang, C. Hou, H. Bian, W. Liang, J. Si, X. Hou, Opt. Express 2010, 18, 22334.
- [228] H. Liu, F. Chen, Q. Yang, P. Qu, S. He, X. Wang, J. Si, X. Hou, Appl. Phys. Lett. 2012, 100, 133701.
- [229] P. Qu, F. Chen, H. Liu, Q. Yang, J. Lu, J. Si, Y. Wang, X. Hou, Opt. Express 2012, 20, 5776.
- [230] B. Hao, H. Liu, F. Chen, Q. Yang, P. Qu, G. Du, J. Si, X. Wang, X. Hou, Opt. Express 2012, 20, 12939.
- [231] Y. Hu, Q. Yang, F. Chen, H. Bian, Z. Deng, G. Du, J. Si, F. Yun, X. Hou, Appl. Surf. Sci. 2014, 292, 285.
- [232] Z. Deng, Q. Yang, F. Chen, X. Meng, H. Bian, J. Yong, C. Shan, X. Hou, Opt. Lett. 2015, 40, 1928.
- [233] Q. Yang, S. Tong, F. Chen, Z. Deng, H. Bian, G. Du, J. Yong, X. Hou, Opt. Lett. 2015, 40, 5359.
- [234] H. Bian, Y. Wei, Q. Yang, F. Chen, F. Zhang, G. Du, J. Yong, X. Hou, Appl. Phys. Lett. 2016, 109, 221109.
- [235] Z. Deng, F. Chen, Q. Yang, H. Bian, G. Du, J. Yong, C. Shan, X. Hou, Adv. Funct. Mater. 2016, 26, 1995.
- [236] D. Wu, S. Wu, L. Niu, Q. Chen, R. Wang, J. Song, H. Fang, H. Sun, Appl. Phys. Lett. 2010, 97, 031109.
- [237] C. Li, H. Jiang, Appl. Phys. Lett. 2012, 100, 231105.
- [238] Y. Lu, H. Tu, Y. Xu, H. Jiang, Appl. Phys. Lett. 2013, 103, 261113.
- [239] A. O. Ashtiani, H. Jiang, Appl. Phys. Lett. 2013, 103, 111101.
- [240] Z. Ding, B. Ziaie, Appl. Phys. Lett. 2009, 94, 081111.
- [241] X. Jin, D. Guerrero, R. Klukas, J. F. Holzman, Appl. Phys. Lett. 2014, 105, 031102.
- [242] D. Kang, C. Pang, S. M. Kim, H. S. Cho, H. S. Um, Y. W. Choi, K. Y. Suh, Adv. Matter. 2012, 24, 1709.
- [243] K. Yin, Y. X. Song, X. R. Dong, C. Wang, J. A. Duan, Sci. Rep. 2016, 6, 36557.
- [244] J. L. Yong, F. Chen, Y. Fang, J. Huo, Q. Yang, J. Zhang, H. Bian, X. Hou, ACS Appl. Mater. Interfaces 2017, 9, 39863.
- [245] J. L. Yong, J. Huo, Q. Yang, F. Chen, Y. Fang, W. Xu, L. Liu, X. Lu, J. Zhang, X. Hou, Adv. Mater. Interfaces 2018, 5, 1701479.
- [246] Y. Fang, J. L. Yong, F. Chen, J. Huo, Q. Yang, J. Zhang, X. Hou, Adv. Mater. Interfaces 2018, 5, 1701245.
- [247] D. Wang, Z. Wang, Z. Zhang, Y. Yue, D. Li, R. Qiu, C. Maple, J. Appl. Phys. 2014, 115, 233101.
- [248] H. Huang, L.-M. Yang, S. Bai, J. Liu, Appl. Opt. 2015, 54, 324.
- [249] A. Y. Vorobyev, C. Guo, J. Appl. Phys. 2015, 117, 033103.
- [250] G. Li, J. Li, C. Zhang, Y. Hu, X. Li, J. Chu, W. Huang, D. Wu, ACS Appl. Mater. Interfaces 2015, 7, 383.